

Dynamic Actuation of Magnetic Beads for Immunoassays on-chip

THÈSE N° 4691 (2010)

PRÉSENTÉE LE 12 MAI 2010

À LA FACULTÉ SCIENCES ET TECHNIQUES DE L'INGÉNIEUR

LABORATOIRE DE MICROSYSTÈMES 2

PROGRAMME DOCTORAL EN MICROSYSTÈMES ET MICROÉLECTRONIQUE

ÉCOLE POLYTECHNIQUE FÉDÉRALE DE LAUSANNE

POUR L'OBTENTION DU GRADE DE DOCTEUR ÈS SCIENCES

PAR

Yves MOSER

acceptée sur proposition du jury:

Prof. H. Bleuler, président du jury

Prof. M. Gijs, Dr T. Lehnert, directeurs de thèse

Prof. J. Bibette, rapporteur

Prof. C. Guiducci, rapporteur

Dr R. Wimberger-Friedl, rapporteur



ÉCOLE POLYTECHNIQUE
FÉDÉRALE DE LAUSANNE

Suisse
2010

Abstract

This thesis was carried out in the frame of the European project *DetectHIV* aiming the development of a new biosensor platform for the highly sensitive detection of the HIV capsid protein p24. We explore the implementation of a magnetic bead-based lab-on-a-chip system, offering significant advantages compared to conventional systems, mainly through the possibility of controlled manipulation of the magnetic carriers on-chip. In particular, microfluidic immunoassays using functionalized magnetic beads raise increasing interest.

In this thesis, we present a microsystem for the magnetic manipulation of superparamagnetic beads on-chip. A highly confined and dynamically actuated plug of biochemically functionalized beads is formed in a microchannel. This plug extends over the channel cross-section, thus allowing efficient analyte capture from the flow. Subsequent immobilization of the plug for incubation modifies the colloidal state (agglutination test). Dynamic actuation of beads is enabled by superposing a static magnetic field and a time-varying magnetic field. The latter field is highly focused and concentrated across the microchannel by means of soft magnetic microtips. A new method for the fabrication of rigid monolithic SU-8 microchannels allows control and ready mechanical integration of the microtips with the microfluidic structure.

A protocol for performing magnetic bead-based immuno-agglutination assays on-chip using our system was developed. A simple detection method based on the swelling of the released plug after agglutination is presented. We demonstrate the feasibility of on-chip agglutination tests by means of a streptavidin/biotinylated-bovine serum albumin (bBSA) model assay. A detection limit of about 200 pg/mL (≈ 3 pM) was obtained.

Furthermore, the potential of the magnetic actuation method was emphasized by implementing a heterogeneous immunoassay with a dendritic amplification mechanism. Dendritic amplification aims to increase the detection sensitivity. Amplification of the detection signal is achieved by alternating exposure of the beads to a flow of fluorescently labeled streptavidin molecules and biotin conjugated anti-streptavidin, respectively.

The magnetic system developed in the frame of this thesis was integrated in the final biosensor platform of the *DetectHIV* project. This platform comprises an integrated chip cartridge with an optical detection module. This design is outlined in the last part of the thesis.

Keywords: Lab-on-a-chip, superparamagnetic beads, immunoassay, agglutination test, dendritic amplification.

Résumé

Cette thèse a été réalisée dans le cadre du projet Européen DetectHIV qui avait pour but le développement d'un nouveau type de biocapteur très sensible, permettant la détection de la capsid du virus VIH. Nous avons mis au point un système sur puce utilisant des microbilles magnétiques. Ce type de systèmes offre de nombreux avantages comparé aux méthodes traditionnelles et cela en particulier grâce à la possibilité de contrôler avec précision les billes magnétiques. C'est la raison pour laquelle on observe un intérêt croissant pour les tests immunologiques sur puce utilisant ce type de particules fonctionnalisées spécifiquement.

Dans cette thèse, nous présentons un microsystème magnétique permettant la manipulation de billes superparamagnétiques dans un micro-canal. Un paquet de billes fonctionnalisées biochimiquement est retenu et actionné dynamiquement à l'intérieur du micro-canal. Grâce à l'actionnement dynamique, le bouchon de billes s'étend au travers de la section du canal, permettant ainsi une capture efficace de l'analyte. L'actionnement des particules est rendu possible grâce à la superposition d'un champ magnétique continu et d'un champ magnétique alternatif. Le champ magnétique alternatif est focalisé à travers le canal par le biais de pointes magnétiques microstructurées. Une nouvelle méthode permettant la fabrication de canaux monolithiques en SU-8 simplifiant l'intégration de puces avec des éléments externes a également été développée dans ce cadre.

Un protocole permettant la réalisation d'un test immunologique d'agglutination utilisant notre système a été développé. Une méthode de détection simple basée sur le relâchement des particules après agglutination est présentée. Nous démontrons la faisabilité d'un test d'agglutination sur puce grâce à un modèle basé sur l'interaction streptavidin/biotine-bovine sérum albumine. Une limite de détection d'environ 200 pg/mL a été obtenue.

De plus, la flexibilité et le potentiel de notre système magnétique est mis en valeur grâce à l'implémentation d'un test immunologique hétérogène utilisant un mécanisme d'amplification dendritique. L'amplification dendritique a pour but d'augmenter la sensibilité de détection, elle est réalisée en exposant alternativement les billes à un flux de molécules de streptavidin fluorescentes et un flux de molécules d'anti-streptavidin biotinilées.

Le système magnétique développé dans le cadre de cette thèse a été intégré dans la plateforme finale du projet *DetectHIV*. Cette plateforme comprend une puce intégrée avec un système de détection optique. Le design est présenté dans la dernière partie de la thèse.

Mots-clés: Lab-on-a-chip. Billes superparamagnétiques, immunoassay, test d'agglutination, amplification dendritique.

Acknowledgments

I would like to thank my supervisor, Prof. Martin Gijs, who gave me the opportunity to carry out my thesis in his laboratory at the Swiss Federal Institute of Technology, Lausanne (Laboratory of Microsystems, EPFL-IMT-LMIS2). I appreciated the freedom he gave me during these four years and the confidence he had in my work.

I would like to thank Dr. Thomas Lehnert who supervised my thesis. I appreciated his strong physical background and all advices he gave me. It was always a pleasure working with him.

I want to thank Dr. Reinhold Wimberger-Friedl, Prof. Jérôme Bibette, Prof. Carlotta Guiducci for accepting to be members of my thesis jury and Prof. Hannes Bleuler for presiding the jury.

This thesis was carried out in the frame of the *DetectHIV* project, founded by the European Community. I would like to acknowledge all project partners: Katholieke Universiteit Leuven (KUL) (B), Ayanda Biosystems (Ayanda) (CH), Bertin Technologies (F), Ecole Supérieure de Physique et de Chimie Industrielles de la ville de Paris (ESPCI) (F), Denmark Technical University (DTU) (DK), Ademtech (F). It was great to collaborate with many scientists of different backgrounds. In particular, I want to thank Dr. Jean Baudry, Thomas Glasdam Jensen, Julie Gorge and Julien Charpentier for their help during this work.

I would like to thanks the students who contributed to various aspects of this thesis: Gabriella Sinicco, Riccardo Forti and Gilles Garcin. They all did a great job.

I wanted to thank Dr. Sebastien Jiguet for ideas and support he gave me on the SU-8 processing.

I also have a special thank for the secretaries who always helped me for the administrative work: Rose-Marie Apotheloz, Sylvie Clavel, Marie Halm and Kathlyn Mayor.

I want to thank all the CMI staff. It is a great chance to have access to a modern clean-room with a skilled staff. I also want to thank the mechanical workshop for the excellent work they did for the fabrication of the microfluidic platform.

I want to thank all my colleagues from LMIS2, LMIS4 and LMIS1. With a special thank to Jean-Baptiste, Jagoda and Hui because it was a real pleasure sharing the office with you. It was great to have always someone in front of me open for discussions. I also want to thank in particular Emile, Rana, Frédéric, Nicolas Durand, Daniel, Venkat, Elodie, Qasem, Abdeljalil and Nicolas Demierre for their help and for the good time we had. I also want to thank Cumuhr, Meena, Mina, Tuna, Meng, Josias, Ulrike, Christophe, Nicolas Abelé, Raphaël, Raphaëlle, Pierre, Sophie, Ana, Fabien, Lynda, Rob, Guillaume, Alessandro, Harsha and Oscar for all the good moments we shared.

Je tiens à remercier toute ma famille qui est toujours là pour me soutenir avec une pensée toute particulière pour ma grand-maman. Alexandra, tu m'as accompagné tout au long de cette thèse même si cela ne devait pas être facile tous les jours. Je t'en remercie et souhaite que ça continue comme ça ! J'aimerais aussi remercier toute ta famille pour m'avoir supporté pendant ces quatre ans ! Je remercie aussi tous mes amis de la Tchaux, de Lausanne, des Bioux et d'ailleurs qui ont été là pour me changer les idées.

Table of content

Abstract.....	i
Résumé	iii
Acknowledgments	v
Table of content	vii
Nomenclature.....	xi
1 Introduction	1
1.1 HIV testing and monitoring	1
1.2 The DetectHIV project.....	2
1.3 Thesis objectives and plan	3
2 Basic principles: magnetic beads and immunoassays	5
2.1 Magnetic material properties.....	6
2.1.1 Different types of magnetic materials	6
2.1.2 Ferromagnetism	9
2.1.3 Superparamagnetism	11
2.2 Magnetic beads for bio-analysis	13
2.3 Magnetophoretic forces.....	15
2.3.1 Magnetization of superparamagnetic beads	15
2.3.2 Viscous force at low Renoyld's number.....	17
2.4 Immunoassay principles.....	18
2.4.1 Heterogeneous immunoassay	19
2.4.2 Homogenous immunoassay	21
3 State of the art	23
3.1 The lab on-a-chip concept	23
3.2 On-chip particle manipulation concepts	25

3.2.1	Dynamic manipulation.....	25
3.2.2	Static and non-reversible retention of particles.....	27
3.2.3	Comparison of the manipulation methods	29
3.3	Magnetic bead concepts for bio-assays.....	30
3.3.1	Systems with external permanent magnets	30
3.3.2	Electromagnet-based systems with integrated soft magnetic poles	34
3.3.3	Comparison of magnetic bead manipulation methods	35
3.4	On-chip immunoassays	37
3.4.1	Heterogeneous magnetic bead-based immunoassays.....	37
3.4.2	Dendritic amplification method.....	39
3.4.3	Homogeneous magnetic agglutination assays	40
3.4.4	Comparison of immunoassay methods	42
3.5	Concept of our device.....	43
4	The microfluidic platform.....	47
4.1	Microfluidic design.....	47
4.1.1	Microchip design and fabrication.....	48
4.1.2	Chip holder and fluidic protocol.....	51
4.2	Electromagnetic actuation system	53
4.2.1	Core design	53
4.2.2	Coil design	55
4.2.3	Magnetic tips design	56
4.3	SU-8 monolithic microchannels.....	58
4.3.1	Motivation for the fabrication of a monolithic SU-8 channel.....	59
4.3.2	Materials and methods	60
4.3.3	Characterization of the modified SU-8 layers.....	62
4.3.4	Monolithic SU-8 microchannels.....	64
5	Kinetics of the actuated bead plug	67

5.1	Bead capture and retention.....	67
5.1.1	Forces acting on a magnetic bead in a flow.....	68
5.1.2	Bead capture optimization	70
5.2	Bead actuation principle	74
5.2.1	Bipolar configuration	74
5.2.2	Quadrupolar actuation system.....	75
5.3	Analysis of the kinetic behavior of chains and clusters.....	79
5.3.1	Dynamic properties of the actuated bead plug.....	79
5.3.2	Motion of single beads and clusters in the magnetic field	81
5.3.3	Theoretical models for chain and cluster motion.....	84
6	Agglutination assay on-chip.....	87
6.1	Evaluation of the capture efficiency by fluorescence measurements	87
6.2	Agglutination test protocol.....	89
6.2.1	On-chip immuno-agglutination assay principle	89
6.2.2	Model agglutination protocol.....	90
6.2.3	Detection principle of the immuno-agglutination	91
6.3	Dose-response curve.....	94
6.4	Enhancing the capture efficiency	96
7	Dendritic amplification on magnetic beads	101
7.1	Dendritic amplification principle	101
7.2	Chip design and fluidic protocol	103
7.2.1	Chip design	103
7.2.2	Fluidic manipulation protocol.....	104
7.3	Dendritic amplification on beads	107
7.3.1	Experimental protocols	107
7.3.2	Results of the dendritic amplification on beads	109
8	Chip integration	113

8.1	Integrated chip	113
8.1.1	Magnetic and optical module.....	113
8.1.2	Integrated chip design and fluidic manipulation.....	115
8.2	Chip and platform assembly.....	116
9	Conclusion and outlook.....	119
	References	123
	Curriculum vitae.....	137

Nomenclature

Abbreviations and Acronyms

2D	bi-dimensional
3D	tri-dimensional
Ab, Ab's	antibody, antibodies
Ag, Ag's	antigen, antigens
bAM	biotin conjugated anti-mouse
bAS	biotin conjugated anti-streptavidin
bBSA	biotin conjugated bovine serum albumin
BSA	bovine serum albumin
CCD	charge-coupled device
CD4+ T	T cells expressing CD4
CNC	Computerized Numerical Control
DA	dendritic amplification
DEP	dielectrophoresis
DNA	deoxyribonucleic acid
DTU	Danmarks Tekniske Universitet
ELISA	enzyme-linked immunosorbent assay
EOF	electroosmotic flow
EPFL	Ecole Polytechnique Fédérale de Lausanne
FEM	finite element method
FITC	fluorescein isothiocyanate
F-S	fluorescently labeled streptavidin
HIV	Human immunodeficiency virus
IgG	immunoglobulin G
LAT	latex agglutination test
LOC	lab-on-a-chip
MEMS	micro-electro-mechanical systems
MP	magnetophoresis
MR	mechanical retention
p24	component of the HIV virus particle capsid
PBS	phosphate buffered saline

PCR	polymerase chain reaction
PDF	pressure driven flow
PDMS	poly(dimethylsiloxane)
PEB	post exposure bake
pH	measure of the acidity or basicity of a solution
PMMA	poly(methylmethacrylate)
RNA	ribonucleic acid
SB	soft-bake
SEM	scanning electron microscopy
Si	silicon
s-IgA	human secretory immunoglobulin A
SP	superparamagnetic
SU-8	Epoxy based negative photoresist
TAS / μ -TAS	total analysis system / micro total analysis system
USW	ultrasonic standing-waves
UV	ultra violet

Constants

μ_0	magnetic permeability of vacuum: $\mu_0=4\pi \times 10^{-7}$ H/m
k_b	Boltzmann constant: $k_b=1.38 \times 10^{-23}$ J/K

Symbols

A	plug area [m^3] A_{ref} : reference plug area A_{bBSA} : plug area after analyte capture
B	magnetic flux density [$\text{T}=\text{Vs}/\text{m}^2$]
B_r	remanence
D	exposure dose [mJ/cm^2] D^0 : dose required to reach full polymerization of initial film thickness D^i : dose limit below which the complete layer is dissolved
E_{mag}	magnetic energy [J]
F	force [N] F_{mag} : magnetic force F_{drag} : viscous drag force

	F_g : gravitational force
	F_{bou} : buoyancy force
H	intensity of the magnetic field [A/m]
	H_c : coercive field
I	current [A]
J	magnetic exchange constant [J], current density [A/m ²]
K	magnetic anisotropy [J/m ³]
M	magnetization [A/m]
	M_r : remanent magnetization [A/m]
	M_{sat} : saturation magnetization
N_d	demagnetization factor ($N_d=1/3$ for a sphere)
R	resistance [Ω]
	R_{sw} : resistance of a single winding
	R_{tot} : total resistance of the coil
Re	Reynolds number
S	total spin quantum number, section [m ²]
T_c	Curie temperature [°K]
V	volume [m ³], voltage [V]
a	inter-atomic spacing, length of a cylinder [m]
b	radius of the cylinder [m]
d_s	superparamagnetic diameter size [m]
d_c	single domain diameter size limit [m]
l_{gap}	length of the air gap between the magnetic tips [m]
m	magnetic moment [Am ²]
r	particle or bead radius [m]
t	time [s]
v	velocity [m/s]
θ	magnetic potential [A]
χ	magnetic susceptibility
	χ_{in} : initial susceptibility
	χ_{np} : susceptibility of the nanoparticle
	χ_r : relative susceptibility
	χ_{eff} : effective relative magnetic susceptibility
Δ	difference operator, Laplace operator

∇	Nabla operator, divergence
η	dynamic viscosity [Pa·s]
λ	wavelength [nm]
μ_r	relative magnetic permeability
ρ	density [kg/m ³]
γ	contrast

1 Introduction

1.1 HIV testing and monitoring

An arsenal of laboratory methods is available to screen blood, diagnose infection, and monitor disease progression in individuals infected by HIV. These tests can be classified into those that: detect antibodies, identify antigens, a combination of these two, detect or monitor viral nucleic acids, or provide an estimate of T lymphocyte numbers. ELISA are the most commonly used tests to screen for HIV infection. Antibodies (Ab's) can be detected in a majority of individuals three to four weeks after infection with third-generation sandwich assays [1]. The window period can be shortened to about two weeks using p24 antigen (Ag) assays or reduced to one week with the implementation of nucleic acid detection assays [2]. The p24 protein is a viral capsid (core) protein that appears in blood during acute infection due to the burst of viruses during replication. The detection limit of fourth-generation combination assays is close to that of the single Ag assays [3, 4]. HIV-1 RNA detection using highly efficient amplification techniques such as polymerase chain reaction (PCR) has become the standard for monitoring antiretroviral therapies after diagnosis of the disease [5].

The p24 Ag assay sensitivity is inferior to PCR in detecting viral particles, but the presence of extraviral p24 Ag in most samples makes largely up for this. p24 Ag testing is similarly sensitive and specific in diagnosing pediatric HIV infection, in predicting CD4⁺ T cell decline and clinical progression at early and late stage of infection, and suitable for antiretroviral treatment monitoring [6].

This thesis is carried out in the frame of the European project (*DetectHIV*, #037118). The *DetectHIV* project “Sensitive nanoparticle assay for the detection of HIV” aims at developing a new platform and assay for the detection of HIV p24 proteins in serum or blood. Quantification of HIV-1 RNA remains very difficult to implement in developing countries, simple and inexpensive tests for antiretroviral treatment monitoring are therefore needed [7-9]. The advantages of a p24 test are that it can detect HIV in an early stage of the infection, before antibodies develop, and that it is quantitative. Such test can therefore be used for antiretroviral treatment monitoring. The *DetectHIV* project has the ambitious objective to detect p24 concentrations as low as 0.1 pg/ml by using nanoparticles on a microfluidic chip. This is one to two orders of magnitude more sensitive than classical p24 Enzyme Linked Immuno-Sorbent Assays (ELISA). A recent work using CD4+ T-cell counting illustrates the growing interest for quick, simple and low-cost HIV screening [10]. The main objective of the *DetectHIV* project is the development of an extremely simple viral load test with only one reactant (grafted colloids) for p24 detection.

1.2 The DetectHIV project

The feasibility and high potential of a magnetic micro or nano-particles (often called ‘beads’) agglutination assay has been recently demonstrated in the bulk format (microtiter plate) [11-13]. Immunoassays, where reactions occur both in solution and on a solid phase, offer the advantage of easy separation of chemical complexes from reactants. Biomolecule immobilization on a solid phase, such as micro-and nano-beads offers the potential to perform highly localized assays in a small volume [14, 15].

The *DetectHIV* project aims to develop an assay which consists in optically detecting the formation of a colloidal gel or aggregates of magnetic beads (agglutination test). The agglutination forms in a magnetic field under the presence of Ag’s that are able to link irreversibly two colloidal particles together. Therefore the particles are grafted with antibodies that are specific to the p24 Ag. The detection is achieved through simple optical absorbance measurements, owing to the strong optical scattering modification when passing from singlets to aggregated beads (Figure 1.1).

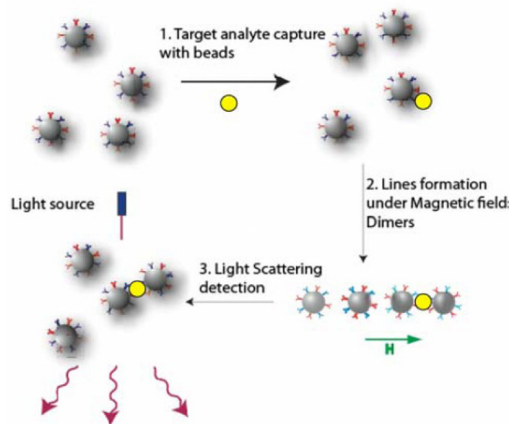


Figure 1.1: Schematic diagram of the magnetic field induced agglutination of the colloidal magnetic beads into nanoparticle doublets and their detection by optical scattering.

The main goal of the *DetectHIV* project is to develop a microfluidic chip test in which a sample solution of serum or blood is transported through a suspension of magnetic nanoparticles that are magnetically retained within the microchannel. When brought into a magnetic field, the beads are able to approach each other, form chains and are irreversibly linked if the p24 Ag is present. On-chip light scattering techniques using integrated polymer waveguides is finally used to quantify the concentration of clustered beads, which is proportional to the p24 Ag concentration. A system platform that handles all functions integrated on a disposable microfluidic chip is the ultimate goal of the collaboration. Clinical validation of the assay for the detection and quantification of p24 Ag's is an important final milestone of the DetectHIV project.

1.3 Thesis objectives and plan

We present in this work a simple method for the dynamic manipulation of magnetic beads on-chip which aims to improve the on-chip capture of Ag's at the beads surface. The principal objective of this thesis, as defined by the *DetectHIV* project, was the design of a system allowing the retention of magnetic nanoparticles in a microfluidic channel in the presence of a flow. The main function of the system is to enable the magnetic actuation of beads on a local scale in a microfluidic channel by focusing a magnetic field generated by an external electromagnet, through millimeter-size soft magnetic pole tips. This device should allow retaining magnetic beads in the channel while passing through various fluids, thereby offering a maximum exposure of the magnetic nanoparticles surface to the flow. The shape, position and

magnetic properties of magnetic tips have been optimized to provide a good magnetic bead manipulation.

An important part of the work is the characterization of the retention and handling of the magnetic nanoparticles in the microchannel. The main idea of the system is to maximize the interaction of the magnetic nanoparticles with the flow. Evaluation of the protein capture efficiency is performed using fluorescently labeled particles. This thesis presents one of the first fully integrated magnetic agglutination test on-chip, demonstrating the potential of this technique. Furthermore, a heterogeneous assay using a dendritic amplification is performed demonstrating the flexibility of the magnetic actuation system developed during this thesis and the full potential of the platform.

The thesis is divided in three main parts: theory (chapters 2-3), fabrication (chapter 4) and experimental results (chapters 5-7). Important magnetic concepts required for the manipulation of magnetic beads are given in chapter 2. An introduction to standard immunoassay test principles is also given at the end of this chapter. The state-of-the-art of bead-based microfluidic devices is discussed in chapter 3. This chapter starts with an overview of the main physical principles that may be used for the manipulation of beads on-chip. Then the main magnetic manipulation methods are reviewed. Finally, detection and immunoassay techniques are discussed. The second part of the thesis focuses on technological and fabrication aspects. The microfluidic platform developed during this thesis is presented in chapter 4, as well as a microfabrication method allowing the fabrication of monolithic SU-8 microchannels. The third part of the thesis is mainly experimental. A detailed characterization of the magnetic actuation principle is given in chapter 5. The behavior of single beads and clusters is analyzed. The efficiency of the dynamic actuation of the beads in the microchannel is highlighted. The agglutination test on-chip is demonstrated using a model based on the streptavidin-biotin interaction. The principle and results are presented in chapter 6. The feasibility to use the system to perform dendritic amplification on beads is demonstrated in chapter 7 in order to demonstrate the potential and flexibility of the system. The last chapter of the thesis is dedicated to the design of the final integrated device and fabrication of the *DetectHIV* platform in collaboration with the other partners.

2 Basic principles: magnetic beads and immunoassays

Magnetic micro- and nanoparticles are of particular interest for LOC applications. One of the main reasons is their ability to be manipulated in a fluid flow as well as the possibility to functionalize them with a large range of biomolecules. Moreover, by reducing the size of the beads, the available active surface per volume may be significantly increased. In this chapter, theoretical aspects of the main concepts behind the manipulation of magnetic beads in fluids are discussed. An introduction to basic immunoassay test principles is also given at the end of the chapter.

Magnetic beads are usually made of magnetic nanocrystals enclosed in a non-magnetic matrix of an inert and bio-compatible material such as a polymer or silicon dioxide [16]. The nanocrystals are generally composed of iron oxide such as maghemite (Fe_2O_3) or magnetite (Fe_3O_4) but they can also be made of alloys of transition metals (Ni, Fe, Co, Mg or Zn) or rare earth materials (NdFeB or SmCo). Iron oxide is preferred over pure iron due to its better stability against oxidation [16]. Magnetite and maghemite are frequently chosen because they have the highest saturation magnetization, 80 and 100 $\text{Am}^2\text{kg}^{-1}$ respectively, which is two order of

magnitude higher than the saturation magnetization of other iron oxides [17]. To understand the magnetic behavior of magnetic beads, it is important to refer to the basics of magnetism.

2.1 Magnetic material properties

2.1.1 Different types of magnetic materials

Magnetic materials can be generally classified into five types of magnetism, depending on their bulk magnetic susceptibility (see Figure 2.1 and Table 2.1).

	IA	IIA	IIIB	IVB	VB	VIB	VIIA	VIIIB	VIIIC	VIIID	IX	X	XI	XII	IIIA	IVA	VA	VIA	VIIA	0
1	1s H																			2s He
2	2s Li	2s Be													2p B	2p C	2p N	2p O	2p F	2p Ne
3	3s Na	3s Mg													3p Al	3p Si	3p P	3p S	3p Cl	3p Ar
4	4s K	4s Ca	3d Sc	3d Ti	3d V	3d Cr	3d Mn	3d Fe	3d Co	3d Ni	3d Cu	3d Zn			4p Ga	4p Ge	4p As	4p Se	4p Br	4p Kr
5	5s Rb	5s Sr	4d Y	4d Zr	4d Nb	4d Mo	4d Tc	4d Ru	4d Rh	4d Pd	4d Ag	4d Cd			5p In	5p Sn	5p Sb	5p Te	5p I	5p Xe
6	6s Cs	6s Ba	LRE	5d Hf	5d Ta	5d W	5d Re	5d Os	5d Ir	5d Pt	5d Au	5d Hg			6p Tl	6p Pb	6p Bi	6p Po	6p At	6p Rn
7	7s Fr	7s Ra	ARE	6d Rf	6d Db	6d Sg	6d Bh	6d Hs	6d Mt	6d Ds	6d Rg	6d Uuh			7p Uut	7p Uuq	7p Uup	7p Uub		

LANTHANIDE RARE EARTHES:										
LRE	5f La	5f Ce	5f Pr	5f Nd	5f Pm	5f Sm	5f Eu	5f Gd	5f Tb	5f Dy

ACTINIDE RARE EARTHES:										
ARF	5f Ac	5f Th	5f Pa	5f U	5f Np	5f Pu	5f Am	5f Cm	5f Bk	5f Cf

Figure 2.1: A periodic table showing the type of magnetic behavior of each element at room temperature [18].

Magnetism originates from the spin as well as from the orbital motion of an electron around the nucleus [19]. The circulating electron produces its own orbital magnetic moment and there is also a spin magnetic moment associated with it due to the electron itself spinning on its own axis. In most materials there are almost no resultant magnetic moments, due to the electrons being grouped in antiparallel pairs causing the magnetic moment to be cancelled (i.e. diamagnetism and paramagnetism). Diamagnetism originates from the orbital motion of electrons about the nuclei, electromagnetically induced by the application of an external magnetic field. This type of magnetism is very weak and easily overruled by paramagnetism of atoms. The paramagnetism originates from magnetic atoms or ions whose spins are isolated from their magnetic environment. This type of magnetism is also relatively weak and therefore diamagnetic and paramagnetic materials are generally referred as non-magnetic materials. In certain magnetic materials the magnetic moments of a large proportion of the electrons align, producing a

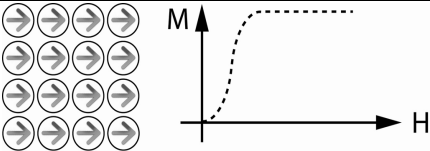
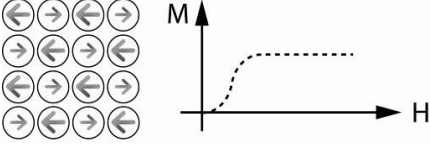
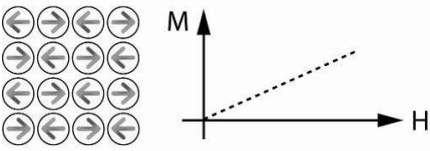
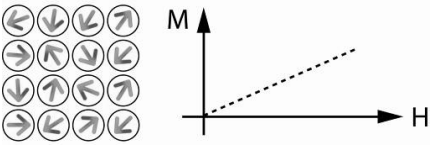
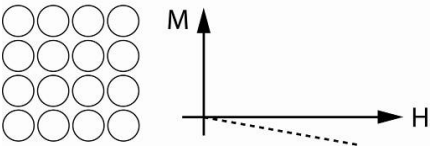
macroscopic magnetization (ferromagnetic materials). Finally, magnetic materials can also be ferrimagnetic which is generally found in compounds, such as mixed oxides, known as ferrites, from which ferrimagnetism derives its name.

Table 2.1 summarized the different types of magnetic materials in the bulk form. The first three schematic representations of the magnetic moments in Table 2.1 correspond to a temperature of 0 K (i.e. ideal alignment of the electron spins). Above this temperature, the alignment of the spins is somewhat random but keeps a preferential direction. Above the Curie temperature T_c , the thermal fluctuations are so large that the spins orientation is completely random and the total magnetic moment falls to zero. Above the Curie temperature the material behaves like a paramagnetic material. Table 2.1 shows that the magnetic character of a material may be classified using its relative magnetic susceptibility χ_r .

In order to easily manipulate a magnetic bead, the magnetic force acting on the latter has to be maximized, a high relative permeability of the material is therefore required. Consequently, the majority of the magnetic beads are made of ferro- or ferrimagnetic materials. For this reason, the following part of this section will focus on the ferromagnetic materials.

Chapter 2 - Basic principles: magnetic beads and immunoassays

Table 2.1: Overview and comparison of different types of magnetism. The two first types (ferromagnetism and ferrimagnetism) form the strongest magnetic materials. (adapted from [20])

Magnetism Type	Atomic and Magnetic Behavior		Susceptibility (χ_r)
Ferromagnetism		Atoms have parallel aligned magnetic moments within domain	- large $ \chi_r \gg 1$ - positive Fe, $\chi_r \approx 100'000$
Ferrimagnetism		Anti-parallel aligned magnetic moments of different types of atom do not cancel completely	- large $ \chi_r \gg 1$ - positive ferrite, $\chi_r \approx 1'000$
Antiferromagnetism		Atoms have parallel and anti-parallel magnetic moments aligned in a regular pattern	- small $ \chi_r \ll 1$ - positive Cr, $\chi_r = 3.6 \cdot 10^{-6}$
Paramagnetism		Atoms have randomly oriented magnetic moments Negligible interaction between atomic magnetic moments	- small $ \chi_r \ll 1$ - positive Mn, $\chi_r = 66.1 \cdot 10^{-6}$
Diamagnetism		Atoms have no magnetic moments	- small $ \chi_r \ll 1$ - negative Au, $\chi_r = -2.74 \cdot 10^{-6}$

The magnetization \vec{M} of a magnetic material under an external magnetic field \vec{H} is given by:

$$\vec{M} = \chi_r \cdot \vec{H} \quad (2.1)$$

with χ_r the relative susceptibility of the material.

The induced magnetic flux density $\vec{B} = \mu_0 \vec{H}$ is increased by the magnetization \vec{M} of the material by $\mu_0 \vec{M}$ resulting in:

$$\vec{B} = \mu_0 (\vec{H} + \vec{M}) \quad (2.2)$$

where $\mu_0 = 4\pi \cdot 10^{-7}$ Vs/Am is the permeability constant of vacuum. Combining equation 2.1 and 2.2 gives:

$$\vec{B} = \mu_0 (1 + \chi_r) \vec{H} = \mu_0 \mu_r \vec{H} \quad (2.3)$$

μ_r is the relative permeability of the material. The relative permeability is dependent upon the temperature and the frequency of the applied external magnetic field \vec{H} .

2.1.2 Ferromagnetism

In ferromagnetic materials, the relationship between the three vector fields (\vec{H} , \vec{B} and \vec{M}) is generally non-linear and history-dependent. Therefore, eqn (2.3) does not generally apply for a magnetic material, except for the initial magnetization of the material (see Figure 2.2). Ferromagnetic materials are characterized by a *hysteresis loop* as schematically shown in Figure 2.2. A hysteresis loop is defined by the saturation magnetization, the coercive field H_c and the remanent magnetization M_r . If the ferromagnetic material is magnetized up to its saturation from the initial state and then the magnetic field is switched off, a remanent magnetization M_r is observed. A negative coercive field H_c has to be applied to cancel the magnetization of the material. The three parameters (H_c , B_r and M_{sat}) allow describing the non-linear response of a ferromagnetic material to an external magnetic field. When a ferromagnetic material is subject to an external field, domains, having a magnetization parallel to the field, grow until reaching full magnetization (saturation) [21]. The initial permeability μ_{in} and susceptibility χ_{in} is defined by the initial induction B produced in response to an external field H :

$$\mu_{in} = 1 + \chi_{in} = \left. \frac{\delta B}{\delta H} \right|_{H \approx 0} \quad (2.4)$$

The hysteresis in the magnetization process of ferromagnetic materials can be explained by pinning of magnetic domains at impurities or grain boundaries within the material and the anisotropy of the crystalline lattice [22].

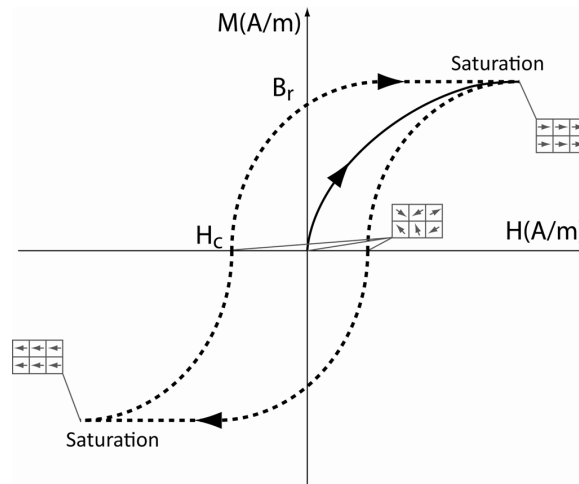


Figure 2.2: Magnetic hysteresis loop (dashed line) of a ferromagnetic material. The full line represents the first magnetization of the material from an unordered multidomain state. After saturation, the material retains a magnetization called remanence M_r at zero field. The magnetization of the material is cancelled only after application of the coercive field H_c .

In practice, almost complete demagnetization of a ferromagnetic material may be obtained by applying a damped sinusoidal external magnetic field as shown in Figure 2.3. Using this method, the remanent magnetic field is cyclically decreased until it reaches a negligible value. The sinusoidal external field may for example be applied using an external electromagnet.

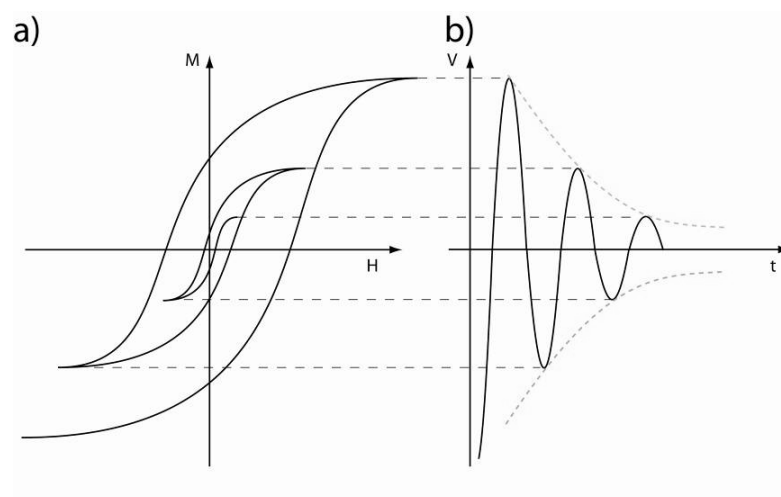


Figure 2.3: (a) Demagnetization of a ferromagnetic material. (b) A damped sinusoidal external magnetic field is applied to cyclically decrease the remanent magnetic field.

2.1.3 Superparamagnetism

A magnetic domain is a microscopic region in which the magnetic moments of atoms are grouped together and aligned. Figure 2.4 shows a picture of the magnetic domains in an iron whisker and in a thin NiFe element taken using a magneto-optical method [21]. The magnetic domain size may vary from less than ten nanometers to a few hundreds of micrometers depending on the magnetic anisotropy of the material (see below). Prior to the exposure to an external magnetic field, a ferromagnetic material is usually unmagnetized, reflecting the randomization of the distribution of the magnetic domains.

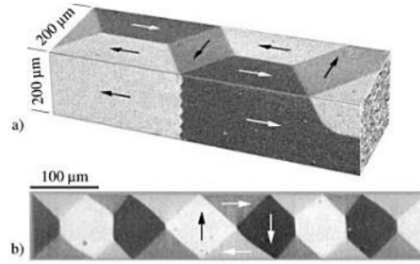


Figure 2.4: Domains observed with magneto-optical methods on homogenous magnetic samples. (a) Images from two sides of an iron whisker. (b) Thin film NiFe element [21].

Mono-domain nanoparticles are of particular interest for LOC applications. They are single domain because they have a dimension that is typically of the order or smaller than the typical thickness of a magnetic domain wall given by:

$$\delta = \sqrt{\frac{JS^2\pi^2}{Ka}} \quad (2.6)$$

with J being the magnetic exchange constant, S the total spin quantum number of each atom, K the magnetic anisotropy constant of the magnetic material, and a the inter-atomic spacing. For iron, assuming that $S=1$, and with $J=2.16 \cdot 10^{-21}$ J, $a=2.86 \cdot 10^{-10}$ m and $K=4.2 \cdot 10^4$ J/m³, the domain wall thickness is about 40 nm.

The magnetic energy E_{mag} of a particle is given by:

$$E_{mag} = K \frac{4}{3} \pi r^3 \quad (2.7)$$

with r being the radius of the spherical particle. Mono-domain magnetic particles become superparamagnetic, i.e. their time-averaged magnetization without external magnetic field is zero when their magnetic energy is lower than about ten times the thermal energy $k_B T$, with k_B the Boltzmann constant. At room temperature, $k_B T = 4.0 \cdot 10^{-21}$ J and $K = 13.4$ kJ/m³ for maghemite (Fe₂O₃) nanoparticles [23, 24]. Therefore, using eqn (2.7) one finds a maximum diameter $d_s = 18$ nm for a superparamagnetic spherical particle of maghemite.

The time over which the magnetization of a particle is stable and remains in a certain state is of importance for probing the fundamental mechanism of magnetization reversal. The relaxation time τ of the moment of a particle is given by the Néel-Brown expression.

$$\tau = \tau_0 \exp\left(\frac{K \cdot V}{k_B T}\right) \quad (2.8)$$

where V is the volume of the particle and $\tau_0 \approx 10^{-9}$ s. If the particle magnetic moment reverses at times shorter than the experimental time scales, the system is in a superparamagnetic state, if not, it is in the so-called blocked state [25].

Figure 2.5 gives a qualitative illustration of the behavior of the coercive field of magnetic nanoparticles as a function of their size. Particles are superparamagnetic below the critical superparamagnetic size d_s (i.e. $H_c = 0$). Below d_s the thermal energy is larger than the magnetic energy and therefore the spin of the particle is free to rotate in response to the thermal energy. For particles larger than d_s , the coercive field increases to maximum at the single domain size limit d_c . Above d_c , the formation of domain walls becomes energetically favorable which results in a multi-domain structure of the particle and a decrease of the coercive field H_c .

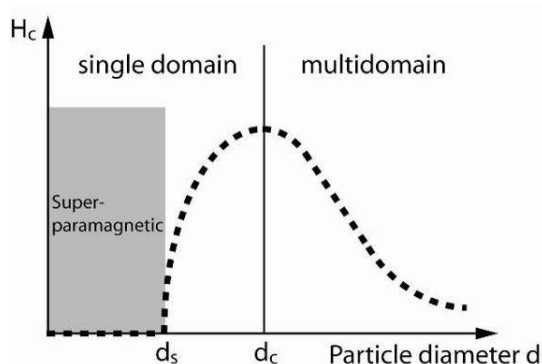


Figure 2.5: Qualitative illustration of the behavior of the coercivity as the particle size increases [23]. The coercive field of the particle is zero below d_s ($d_s=18$ nm for maghemite) and then increases to reach its maximum value for the single domain particle size limit d_c .

2.2 Magnetic beads for bio-analysis

The majority of the magnetic beads consist of superparamagnetic nanocrystal embedded in a polymer matrix protecting the analyte from a direct contact with the metal oxide. Figure 2.6 illustrates the behavior of such multi-core superparamagnetic bead. Without an external magnetic field the magnetic moments of the iron oxide nanocrystals are randomly oriented (Figure 2.6 a). Under the application of an external magnetic field, all moments align in a preferential direction (Figure 2.6 b). After switching off the external field, the bead returns to its initial state (Figure 2.6 a) without keeping any remanence. A schematic hysteresis-free magnetization curve of a superparamagnetic bead is shown in Figure 2.6 c.

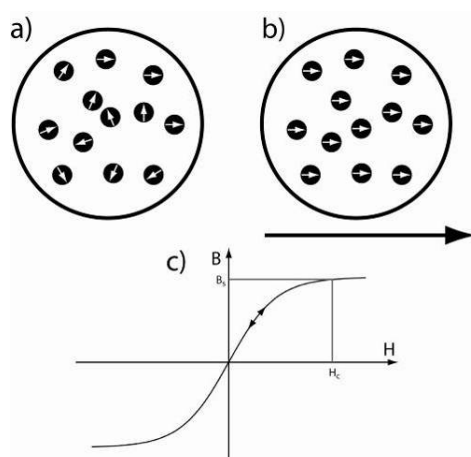


Figure 2.6: (a) Schematic representation of superparamagnetic bead at zero field. Random orientation of the nanoparticle moments. (b) Under the presence of an external magnetic field, the nanoparticles moments align in a preferential direction. (c) Hysteresis-free variation of B with changing H for superparamagnetic beads.

The advantage of using a polymer shell consists in the possibility of surface functionalization and subsequent immobilization of a target molecule [25, 26]. Figure 2.7 shows the three main morphologies of composite magnetic polymer microspheres commonly used for LOC applications. The magnetic bead may be composed of a single magnetic core surrounded by an inert and preferably biocompatible material. This method is generally used for nanometer-sized superparamagnetic beads with diameters in the range of 5 – 100 nm (Figure 2.7 a). For the synthesis of larger superparamagnetic beads (in the range 300 nm – 10 μm), nanoparticles (generally $r < 10$ nm) are embedded in a non-magnetic polymer matrix (Figure 2.7b) [23, 26]. An alternative method called “strawberry type” consists in assembling the magnetic nanoparticles around a polymer core and then passivating the surface using a surrounding inert polymer (Figure 2.7 c). Figure 2.7 d is a Scanning Electron Microscope (SEM) photograph of monodisperse magnetic beads (2.8 μm Dynabeads). Different procedures are available for the preparation of nanocomposite microspheres [26].

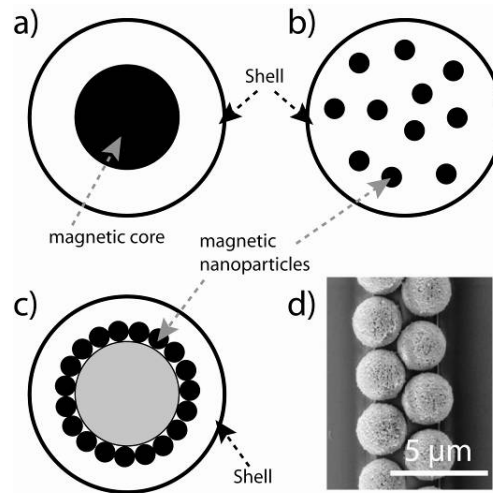


Figure 2.7: Three main methods of synthesizing magnetic beads for LOC applications: (a) Single magnetic core bead embedded in a non-magnetic shell or matrix. (b) Multi-core magnetic bead composed of magnetic nanocrystals (generally $r < 10$ nm) in a non-magnetic matrix. (c) Magnetic nanoparticles assembled around a polymer core and passivated using a surrounding inert polymer (strawberry). (d) SEM photograph of monodisperse magnetic beads (2.8 μm Dynabeads) (courtesy of V. Sivagnanam).

In general the magnetic moment \vec{m} of a bead with negligible interaction between the nanoparticles is given by the sum of the moments of all individual nanocrystals enclosed in the polymer shell. The magnetic moment of the composite microsphere is therefore directly related to the amount of magnetic nanocrystals in the matrix. Current techniques allow a filling factor up

to ~ 70 % (w/w) of Fe_3O_4 and a high saturation magnetization of $40 \text{ Am}^2\text{kg}^{-1}$ while keeping a superparamagnetic behavior [27].

The choice of the bead is finally dependent upon the final applications. The size of the bead is a critical parameter and may lead to the choice of a specific type of magnetic bead (i.e. single core, multicore or strawberry). The magnetic force F_{mag} is proportional to r^3 ($F_{mag} \sim r^3$) while the viscous drag force on the bead is directly proportional to its radius ($F_d \sim r$) (see section 2.3). Therefore decreasing the size of the bead decreases the ratio between the magnetic force and the viscous drag force, thus reducing the capacity to manipulate the bead in a liquid. Bigger beads can be manipulated easier but increasing the size reduces the surface-to-volume ratio resulting in a decrease of the specific surface available for the attachment of functional groups. The choice of the bead size is often a compromise between the biological and magnetic response.

2.3 Magnetophoretic forces

2.3.1 Magnetization of superparamagnetic beads

The force \vec{F}_{mag} acting on a single superparamagnetic bead, when it has acquired a magnetic moment m in an external magnetic induction \vec{B} , is given by [28, 29]

$$\vec{F}_{mag} = (\vec{m} \cdot \nabla) \vec{B} \quad (2.9)$$

Sometimes equation $\vec{F}_{mag} = \nabla(\vec{m} \cdot \vec{B})$ is taken as the basic equation for the calculation of the magnetic force, instead of equation (2.9) [16, 30-32]. This is correct when \vec{m} is constant and has no spatial dependence [28, 29] Figure 2.8 shows the magnetization curve of Dynabeads MyOne. Three typical regions may be distinguished. The first region is typically between 0 mT up to 10 mT, when the magnetization of the bead is proportional to the applied magnetic flux (Figure 2.8 a). In the second region the variation of magnetization of the bead is not linear with the applied magnetic flux (Figure 2.8 b). The last region corresponds to saturation and therefore the magnetization of the bead is almost constant (Figure 2.8 c)

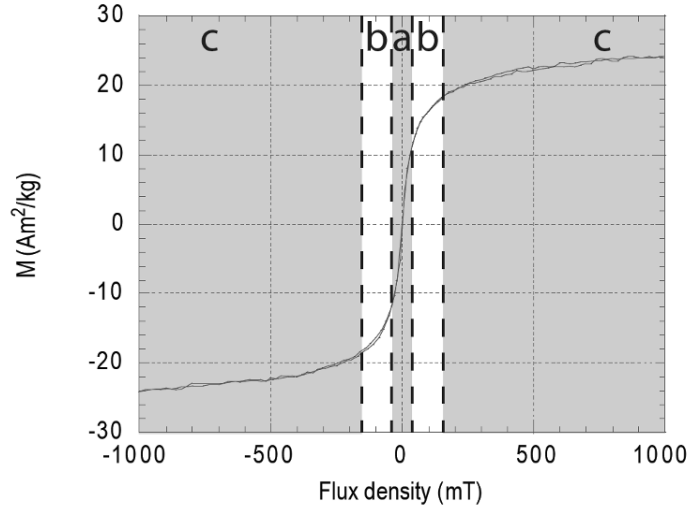


Figure 2.8: Magnetization curve of a Dynabead MyOne. Three typical regions can be approximately differentiated: a) Linear variation between the flux density B and the bead magnetization M , b) Non-linear variation between the flux density B and the bead magnetization M and c) Saturation (constant magnetization).

In general, the magnetization \vec{m} of the bead moving in the field is varying due to a spatially non-uniform magnetic field \vec{B} and an analytical solution of equation (2.9) is non-trivial. Discussions of the force on magnetic dipoles or particles have been reported [16, 33, 34], but, for our case, it is sufficient to consider two approximations: (i) weak magnetic fields where the size of the magnetic moment m of the bead is proportional to the size of the magnetic induction B (Figure 2.8 a) and (ii) stronger fields where the bead moments are saturated (Figure 2.8 c).

In the linear region (i) of the magnetization curve, the magnetic moment of a bead in a liquid medium can be written in the following form:

$$\vec{m} = V \frac{\Delta\chi}{\mu_0} \vec{B} \quad (2.10)$$

where $\Delta\chi$ is the difference in susceptibility between the bead and the medium, V is the bead volume and μ_0 is the vacuum permeability. The magnetic moment \vec{m} of a non-saturated bead freely moving in a non-uniform field has the same spatial dependence as \vec{B} . Using standard vector calculation¹, we can write equation (2.9) in the following form

¹ $\nabla(\vec{B} \cdot \vec{B}) = 2\vec{B} \times (\nabla \times \vec{B}) + 2(\vec{B} \cdot \nabla)\vec{B} = 2(\vec{B} \cdot \nabla)\vec{B}$, with the Maxwell equation $\nabla \times \vec{B} = 0$

$$\vec{F}_{mag} = (\vec{m} \cdot \nabla) \vec{B} = V \frac{\Delta \chi}{2\mu_0} \nabla \vec{B}^2 \quad (2.11)$$

In the saturated case (ii), the magnetic moment of the bead $\vec{m} = \vec{m}_{sat}$ is constant and equation (2.9) becomes

$$\vec{F}_{mag} = (\vec{m}_{sat} \cdot \nabla) \vec{B} \quad (2.12)$$

The magnetic force acting on a saturated bead is therefore directly proportional to the gradient of the magnetic flux density.

The relative susceptibility of a single bead is influenced by the demagnetization factor and is therefore given by:

$$\chi_{eff} = \frac{\chi_{np}}{1 + N_d \chi_{np}} \quad (2.13)$$

where χ_{np} is the magnetic susceptibility of the nanoparticles material and N_d the demagnetization factor. The demagnetization factor is 1/3 for a spherical bead ($N_d = 1/3$).

2.3.2 Viscous force at low Renoyld's number

The concept of manipulating magnetic beads for LOC applications consists in using magnetic forces to transport or simply retain a magnetic bead in a flow by overcoming the viscous drag force acting on the bead. Four main forces act on a magnetic bead suspended in a liquid medium, the magnetic force \vec{F}_{mag} , the viscous drag force \vec{F}_d , the gravity force \vec{F}_g and the buoyancy force \vec{F}_{buo} , as schematically shown in Figure 2.9. In general, due to the small size of the magnetic bead, the gravity force and buoyancy force may be neglected [35, 36].

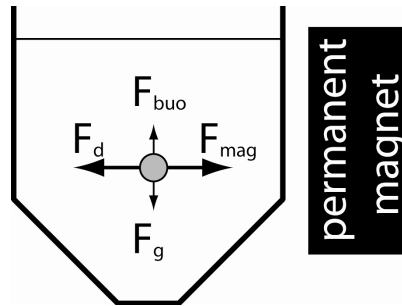


Figure 2.9: Schematic illustration of the forces acting on a magnetic bead when exposed to an horizontal magnetic force F_{mag} . F_d is the drag force which is opposed to the magnetic force. F_g corresponds to the gravity force and F_{buo} to the buoyancy force.

Therefore, the behavior of a magnetic bead in a liquid is mainly driven by the two opposite forces \vec{F}_{mag} and \vec{F}_d . In equilibrium, i.e. at constant speed, we find:

$$\vec{F}_{mag} = -\vec{F}_d \quad (2.14)$$

The drag force exerted on a bead is directly related to the flow conditions and the size of the bead. The flow conditions are linked to the Reynold's number Re , a dimensionless parameter, defined as the ratio between inertial and viscous forces [37],

$$Re = \frac{\text{inertial force}}{\text{viscous force}} = \frac{a\rho v}{\eta} \quad (2.15)$$

where a is a characteristic dimension, which may be the radius of a bead or the radius of a pipe and $\rho/\eta = 1.004 \cdot 10^{-6} \text{m}^2/\text{s}$. The flow is laminar for $Re < 2100$, where viscous forces dominate upon inertial forces. In this regime, all fluid elements move deterministically along distinct and traceable stream lines, while the turbulent regime, occurring at higher Reynolds numbers, is characterized by a random transverse motion of fluid with respect to the flow direction. The transition from one regime to the other is progressive and not clearly defined, creating a zone corresponding to a transitional regime. The Stokes flow is a particular regime of laminar flows for $Re \ll 1$. For this type of flow, the inertial forces can be neglected compared to the viscous forces, simplifying in this way the Navier-Stokes equation. As an example, a bead with a diameter of 1 μm moving at 10 mm/s using eqn (2.15) has a Reynold's number $Re = 0.5 \cdot 10^{-2}$. In these particular conditions, the viscous force on a spherical bead is given by the following equation:

$$\vec{F}_{drag} = 6\pi\eta r \Delta\vec{v} \quad (2.16)$$

where $\Delta\vec{v}$ is the velocity of the bead with respect to the liquid medium, η is the viscosity of the medium and r the radius of the bead.

2.4 Immunoassay principles

The purpose of an immunoassay is to measure the concentration of a protein in a biological liquid such as serum, blood or urine. The assay takes advantage of the specific binding of an antibody (Ab) to its Ag.

One of the most known and used methods is the Enzyme-linked immunosorbent assay (ELISA) [38]. Immunoassays may be classified into two main categories, heterogeneous and homogeneous assays. A heterogeneous assay requires a step to remove unbound Ab or Ag from the reaction site, whereas a homogeneous assay does not require this additional step. Therefore a heterogeneous immunoassay generally requires several washing steps to separate a solid phase from a liquid phase.

2.4.1 Heterogeneous immunoassay

Figure 2.10 is an illustration of a sandwich immunoassay which is one of the most used heterogeneous methods [39]. A sandwich immunoassay starts with the introduction and immobilization of the capture Ab at the surface of a solid phase (generally on the walls of the reaction chamber). Following a washing step, the sample containing the target Ag is then introduced in the chamber and binds to the capture Ab. In order to detect the presence of the target Ag, a labeled detection Ab is finally introduced in the chamber after a second washing step. Many methods exist and use different label types. In the case of an ELISA, the label is an Enzyme. Nanoparticles of gold are also used as label in *lateral flow assays*. Well-known examples of lateral flow tests are home pregnancy tests. Fluorescent dyes are also very popular labels. Magnetic beads start to be more intensively used as labels (magnetic immunoassay) to be detected by a magnetic sensor.

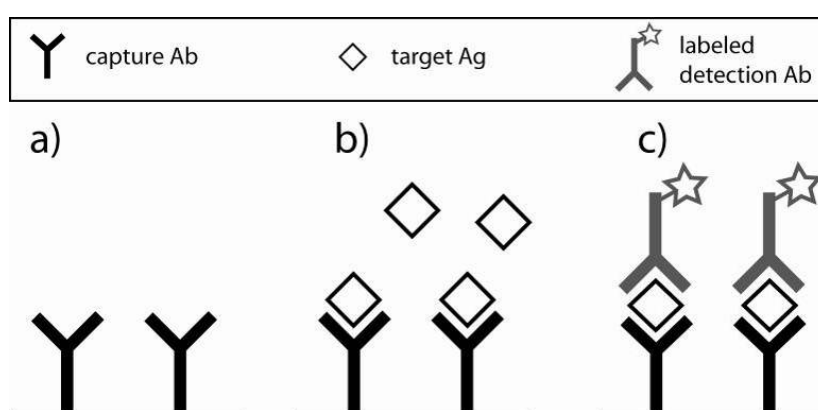


Figure 2.10: Schematic principle of a sandwich immunoassay. (a) A capture Ab is immobilized on the surface of a reservoir. (b) Buffer liquid is then replaced by sample solution containing the target Ag and immunocomplexes form. (c) Detection Ab's are introduced in the reaction chamber and bind to the target Ag. The detection Ab is labeled to allow detection (e.g. fluorescence).

Heterogeneous immunoassays can be competitive or non-competitive. The principle of a competitive immunoassay is that target Ag's in the unknown sample compete with labeled Ag's to bind with the capture Ab's. The amount of labeled Ag's bound is finally measured. Therefore, the response is inversely proportional to the Ag concentration in the sample. This is because the greater the response, the less Ag in the sample was available to compete with the labeled Ag [40]. In noncompetitive immunoassays, Ag's in the sample are bound to the capture Ab and detected using a labeled detection Ab. The amount of labeled Ab on the site is then measured. The result of the noncompetitive method is directly proportional to the Ag concentration. The detection limit of a noncompetitive immunoassay is lower than that of a competitive assay and this is why only the noncompetitive method will be considered in the present thesis [40].

One of the most known and used immunoassay methods is the enzyme-linked immunosorbent assay (ELISA). For ELISA, the detection Ab is linked to an enzyme, and in the final step a substrate is added in the detection chamber that is converted by the enzyme to become fluorescent. The main advantage of an ELISA compared to a sandwich immunoassay using a fluorescent dye is that the enzyme acts as an amplifier. Even if only few enzyme-linked Ag's remain in the solution, the enzyme molecules will produce a large amount of signal molecules. Different types of ELISA exist and are commonly used [41]. Figure 2.11 shows some of the possible configurations used in a standard ELISA. The first approach is a direct ELISA where the Ag's attached to the surface are directly detected using labeled Ab's (Figure 2.11 a). This is a relatively poor method to detect a low Ag concentration in a "raw" sample as many contaminants may bind to the surface preventing the target Ag's to find a free site. In a direct-labeled Ag assay, Ab's are immobilized on the surface of the chamber. A sample with labeled-Ag's is then introduced and bind to the capture Ab's (Figure 2.11 b). This has a relatively poor utility in practice, Ag's are in general not labeled.

The most commonly used methods are the sandwich ELISA (Figure 2.11 c) and the indirect sandwich ELISA (Figure 2.11 d). A capture Ab is first immobilized at the surface of the chamber and washed. The sample containing the target Ag is then introduced and reacts with the capture Ab. In the sandwich ELISA, target Ag is detected using a labeled detection Ab while in the indirect sandwich ELISA the detection Ab binds to a second capture Ab (Figure 2.11d) [41]. An advantage of this technique is the enhanced specificity originating from two separate recognition steps provided by the two Ab's that are generally selected to recognize two different epitopes on the Ag [39]. Low limits of detection are possible with enzyme labels, which can provide amplification by a factor larger than 10^5 . A limitation of the sandwich assay is the

requirement that the analyte should be able to bind to two Ab's simultaneously, which generally restricts its use to molecules with a certain molecular weight [42]. A major drawback of heterogeneous ELISA's is that they require several washing steps, resulting in relatively complex, time-consuming and resource-demanding protocols.

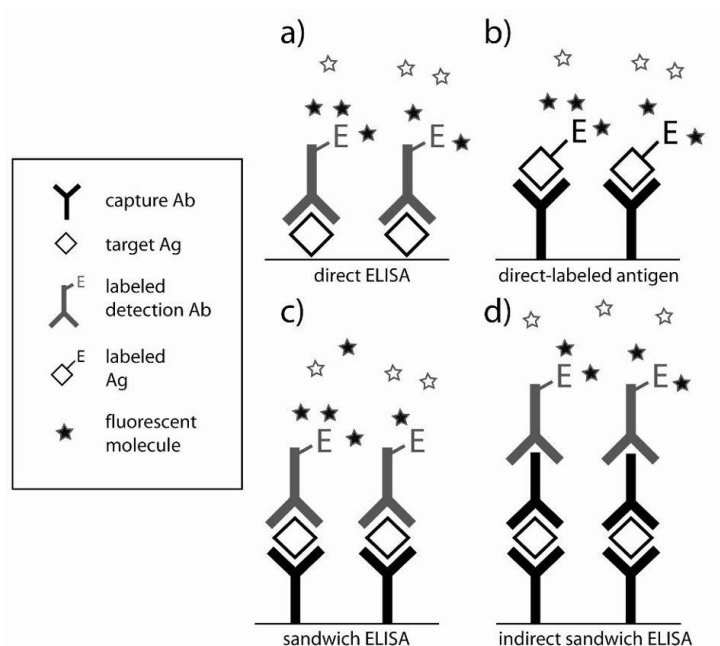


Figure 2.11: Illustration of five different types of ELISA. (a) direct ELISA, (b) direct-labeled Ag, (c) sandwich ELISA, (d) indirect sandwich ELISA.

2.4.2 Homogenous immunoassay

Homogeneous immunoassays rely on the formation of the Ag-Ab complex in solution causing a change in the intensity of a detection signal. Distinguishing between the bound and unbound states allows an immunoassay without washing or separation steps. This simplifies the assay, avoiding Ab's immobilization and rinsing steps. An advantage is that there is no solid phase that can be affected by non-specific binding. Homogeneous assays are more difficult to develop and generally have poorer limits of detection and selectivity than heterogeneous assays. They are commonly used for detecting therapeutic drugs that have a relatively high concentration in blood. They are more effective in partially purified samples, since matrices such as blood, environmental water samples and food can contain contaminants that reduce the sensitivity of the assay [42].

The latex agglutination test (LAT) is one of the most used homogenous assays. The first LAT was proposed in the 1950s by Singer and Plotz [43]. In a LAT, the analyte's Ag binds to

colloidal particles (e.g. latex particles) grafted with an Ab by forming a sandwich-like structure (Ab-Ag-Ab). Detection and quantification of particle agglutination is performed by optical methods, in particular by turbidimetry or nephelometry [44].

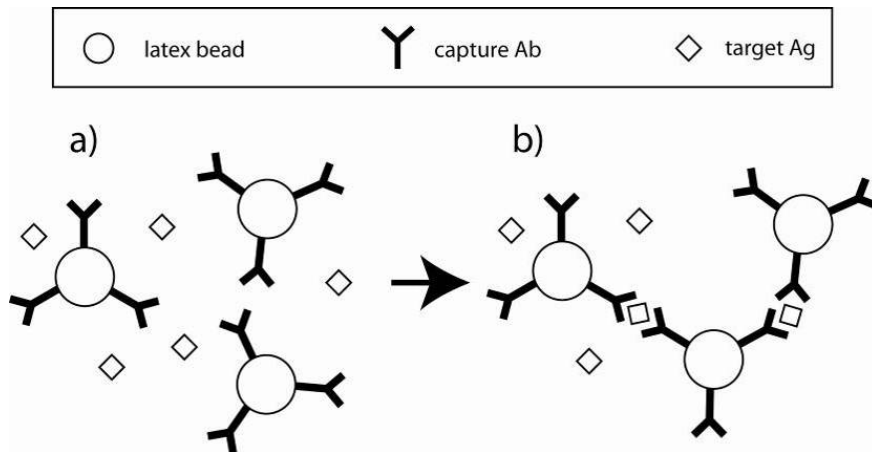


Figure 2.12: Schematic illustration of a latex agglutination test. (a) The sample containing the target Ag are mixed with a solution of latex particles coated with the capture Ab. (b) The target Ag binds to capture Ab and a lattice of particles forms.

Latex immuno-agglutination assays represent a simple and cost-efficient alternative method to ELISA [43]. LAT is very popular in point-of-care tests for diagnostic purposes due to its simplicity. More than 300 different biomolecules can now be detected using LAT [45]. A large number of tests and assays, e.g., for probing the viral or bacterial load of infectious diseases, is available on the market [46]. The intrinsic simplicity of these tests results in robust protocols. The major drawback, however, is the relatively poor detection limit of standard immuno-agglutination assays, compared to ELISA (typically 1 nM compared to 1 pM, respectively) [12, 38].

3 State of the art

3.1 The lab on-a-chip concept

The “Lab-on-a-chip (LOC)” or “micro total analysis systems (μ TAS)” concept was introduced by Manz *et al.* at the beginning of the nineties [47]. The main idea is the miniaturization of standard human sized-laboratories down to the dimension of a credit card. All the necessary handling, analysis and detections steps involved to make a chemical or biological analysis are performed on-chip. Since this date, a huge variety of miniaturized fluidic systems has been proposed, reflecting the interest of miniaturizing bioanalytical systems [48-52].

During the past two decades, specific micromachining technologies have been developed to fabricate deep structures in silicon or glass with small lateral dimensions (typically below 100 μ m) [50, 53]. This opened the way for the fabrication of new and highly integrated microfluidic systems. Furthermore, polydimethylsiloxane (PDMS) combined with molds made of the thick SU-8 photoresist has become a very popular and low-cost material for the fabrication of microchips. Microfluidic biochemical systems take advantage of small reaction volumes and short diffusion lengths, thus reducing assay times and analyte consumption and potentially results in a high detection sensitivity in the case of immunoassays [52, 54]. Microfluidic LOC devices have been developed for a broad range of biomedical and bio-analytical applications and the major part of these microfluidic systems is based on the application of continuous flow using for example external syringe pumps or capillary driven flows [55]. Already in 1997, a microfluidic H-filter was proposed as a simple device that filters particles by size without the need of a membrane [56].

The same group also proposed a T-sensor that may be used to measure analyte concentrations, diffusivities of molecules or reaction kinetics [57, 58]. A diffusion immunoassay based on a T-sensor was reported by Hatch *et al.* in 2001 [59]. This competitive assay is based on the measurement of the distribution of a labeled probe molecule diffusing into a region containing capture Ab's. The polymerase chain reaction (PCR) was one of the first diagnostic techniques to be successfully implemented on a chip [60, 61]. PCR is a technique used to amplify a few copies of a DNA fragment by several orders of magnitude. The method relies on thermal cycling, consisting of cycles of repeated heating and cooling of the sample. On-chip PCR decreases the cycle time due to better and faster control of the fluid temperature. On-chip microfluidic capillary electrophoresis using a glass microchip was also demonstrated at the beginning of the nineties [62, 63]. Capillary electrophoresis is one of the most common methods for the analysis of proteins and DNA in medicine. More recently, Sato *et al.* presented one of the first bead-based immunoassay systems. This multichannel system was able to process four samples in parallel with one pump unit and to complete the assay in 50 minutes [14, 64]. Bead-based systems present the additional benefit of a large surface-to-volume ratio and flexible surface functionalization on the bead surface [65, 66]. The following Section 3.2 will focus on systems and techniques using micro and nanoparticles to perform on-chip immunoassays.

One important parameter in microfluidic applications is the method used to drive the liquids through the microchannels. Three main techniques for liquid manipulation on-chip may be distinguished [67]. The most evident actuation technique is the pressure driven-flow. A pressure difference between the inlet and the outlet forces the liquid to flow through the channel. The flow rate and velocity are defined by the fluidic resistance of the channel and the pressure difference. An efficient way to control the liquid velocity is using a syringe pump that imposes a constant flow rate. According to the Poiseuille's law, the no-slip condition at the channel walls induces a parabolic velocity profile. Electro-osmotic flow (EOF) is an electrical method to move liquids in capillaries or microchannels using based on the displacement of ions. When an electrolytic solution is introduced in a glass microchannel or a capillary, an accumulation of mobile charges occurs close to the surfaces. By applying an electric field along the channel, these charges start moving and may drag the whole liquid due to viscous forces. EOF is characterized by a flat velocity profile. A liquid in a hydrophilic microchannel may also moves by capillary forces. This flow actuation does not required external sources, but allows less flexible control of the flows.

3.2 On-chip particle manipulation concepts

In this section, the main physical principles for the manipulations of particles in a fluid are briefly reviewed. The purpose of this section is to give an overview of existing methods taking advantage of different physical principles and forces. A qualitative comparison of the different techniques justifies the choice of the magnetophoretic manipulation to meet the requirements of an agglutination test or a dendritic amplification method on-chip.

3.2.1 Dynamic manipulation

Magnetophoresis

Magnetic micro- and nanoparticles are of particular interest as solid carriers in a large variety of bioanalytical and biomedical applications. Considerable advance has been achieved in recent years to incorporate magnetic structures and bead handling on-chip [16, 33, 68]. Magnetophoresis is the motion of magnetic beads in a liquid induced by magnetic forces. Magnetophoresis is probably the most versatile method for the manipulation of beads on-chip due to the relatively large force range that may be exerted on the bead and its simple implementation. Indeed, beads may be manipulated with passive elements (i.e. permanent magnets) or active elements (i.e. electromagnets) giving a relatively high degree of flexibility [16]. Magnetophoresis is the fundamental principle for the application developed in this thesis and will be discussed in more detailed further.

Electrophoresis

Electrophoresis is the motion of a charged particle in an electric field. The electrophoretic force is directly proportional to the charge of the particle. Gel electrophoresis and capillary electrophoresis are now commonly used to analyze proteins or DNA sequences.

Dielectrophoresis

A dielectric particle subjected to an electric field, accumulates charge on either side and forms an electric dipole. In a homogenous field, the particle simply aligns with the field. No net translational force is exerted on the particle. In a non-homogenous field, the particle experiences a force called the dielectrophoretic force. The concept of dielectrophoretic force in an inhomogeneous electrical field may be compared to the magnetophoretic force in a non-uniform magnetic field. Manipulation of polystyrene microparticles was previously demonstrated by Chiou *et al.* [69]. More recently, on-chip manipulation of microparticles using dielectrophoresis for the functionalization of particles was successfully demonstrated by Tornay *et al.* [70]. A flow

sandwich immunoassay on 6 μm polystyrene particles using negative dielectrophoresis was also reported by Yasukawa *et al.* [71]. In this example, particles are statically retained in the fluid flow by means a dielectrophoretic force.

Optical forces

Light can also exert a force on a particle [72]. This force may be used to trap particles, the particle being pulled by the optical pressure in the direction of the focused light beam. It was demonstrated that optical tweezers may be used to capture particles ranging from 25 nm to 10 μm [73]. Eriksson *et al.* have used an optical tweezer to move a cell across a microchannel [74] (see Figure 3.1). The basic idea behind this work is to address the need to transfer rapidly a cell or a particle from one fluidic environment to another.

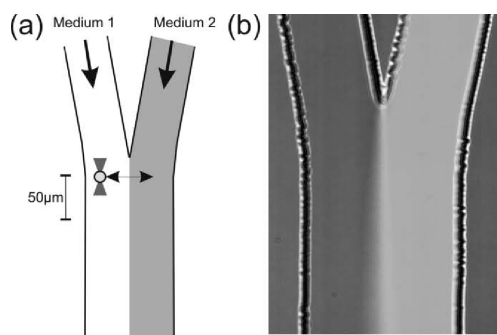


Figure 3.1: (a) Schematic drawing of a microfluidic system showing how a trapped cell can be reversibly moved between two different media. (b) A microscopic image showing the microfluidic system with a parallel flow of two different media. Fluorescein has been added to the medium in the right channel.

Acoustic waves

Exciting a liquid with standing acoustic waves creates a force on an immersed particle that is proportional to its volume. The force is function of the frequency and intensity of the sound wave, as well as the compressibility of the particle. Trapping of micrometer-sized particles was demonstrated by Hertz *et al.* [75]. Ultrasonic standing-waves (USW) have been used for the enhancement of agglutination by increasing the interaction between particles [76, 77]. Figure 3.2 a shows a typical example of such a device. The sample and the particles in a capillary tube are placed along the axis of a cylindrical USW resonator. Subsequently, the reactor is sonicated in order to concentrate the particles for the agglutination test. After aggregation, particles naturally sediment at the bottom of the capillary tube. An increase in speed and sensitivity of an agglutination test was reported with this method [78, 79]. On-chip USW manipulation of

microparticles was also reported by Wiklung *et al.* [80-84]. Figure 3.2 b shows a photograph of trapped microparticles in capillaries or microfluidic channels. The acoustic wave force was also used by Hawkes *et al.* to filter [85] and to separate different kind of particles [86].

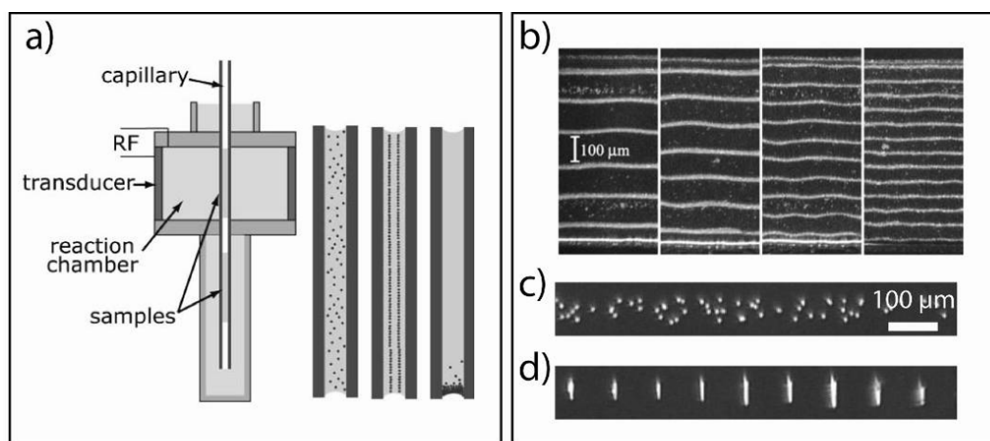


Figure 3.2: (a) Typical device used for USW enhancement of particle-based agglutination assays. The sample of analyte and particles is placed in a capillary tube along the axis of a cylindrical USW resonator, in order to concentrate the particles. After the agglutination phase, aggregated particles sediment at the bottom of the capillary and are detected (adapted from ref. [87]). (b) Multiplexed alignment of 2 μm particles in a microchannel with chains oriented along the flow direction. Increasing the frequency of acoustic waves results in an increase of the chain numbers (adapted from ref. [84]). (c) A microchannel is shown without (c) and with (d) an acoustic wave excitation. Formation of particle chains is observed perpendicular to the flow direction (adapted from ref [83]).

3.2.2 Static and non-reversible retention of particles

Mechanical trapping of particles

An important requirement for the use of micro- and nanoparticles for LOC applications is the development of efficient retention systems. About ten years ago, when the use of magnetic particles was less developed, several works were carried out in order to provide efficient passive retention system for non-magnetic particles. The main idea of this method is to trap particles mechanically with dedicated structures patterned in a microchannel. A system for particle trapping in a flow-through device was designed by Andersson *et al.* The former consists of a grid of small pillars where particles can be collected (Figure 3.3 a) [88]. A chromatographic bed was fabricated on a glass substrate as part of an electroosmotically pumped microfluidic system by Oleschuk *et al* [89]. Two weirs within a sample channel formed a cavity in which silica particles were trapped. The stationary phase was used for the separation of fluorescent dyes. Sato *et al* have developed an immunosorbent assay system integrated into a glass microchip. Polystyrene particles were introduced into a microchannel and trapped (Figure 3.3 c), subsequently human secretory

immunoglobulin A (s-IgA) adsorbed on the bead surface was reacted with colloidal gold conjugated anti-s-IgA Ab and detected by a thermal lens microscope [14].

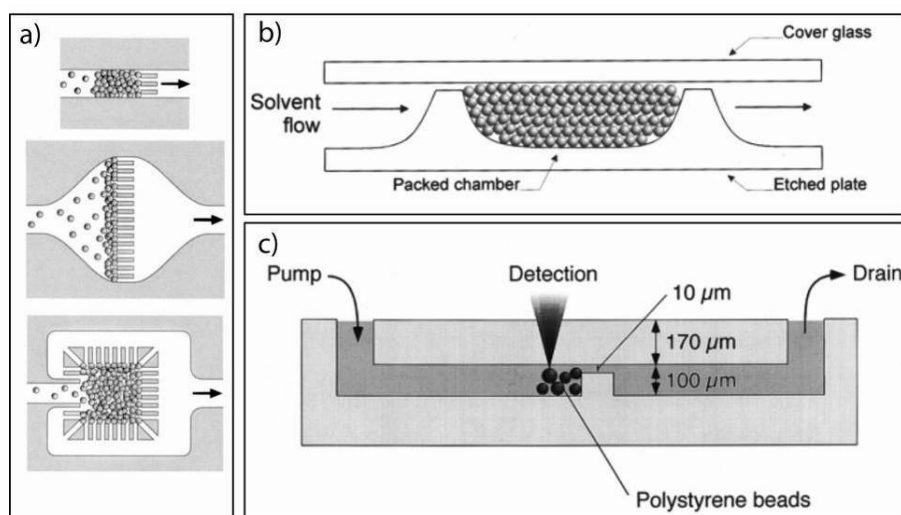


Figure 3.3: (a) Reaction chamber using micropillars where the beads may be collected to form a packed bed (adapted from [88]). Cross-sectional view of a packed chamber showing the physical retention of the beads (adapted from [89]). (c) Cross-section of the glass microchip used for an immunosorbent assay (adapted from [14]).

Physico-chemical retention of particles

Physico-chemical interactions were also used for the retention and immobilization of beads. Andersson *et al.* proposed self-assembly of the beads using surface modification by microcontact printing of polymers [90]. A polymer patterned at the surface of a microchannel is used to define the immobilization sites of the beads. Subsequently, functionalized beads are introduced in the microchannel and specifically attached to the patterned polymer (Figure 3.4 a). The dots were separated by a lithographically defined hydrophobic teflon-like film, preventing cross-contamination between the dots. The dots were subsequently chemically modified by parallel microcontact printing, enabling different chemical modification of the dots. More recently, Sivagnanam *et al.* proposed a sandwich immunoassay using streptavidin-coated beads as substrate. The latter were electrostatically self-assembled on aminosilane micropatterns at the bottom of a microfluidic channel (Figure 3.4 b) [91, 92].

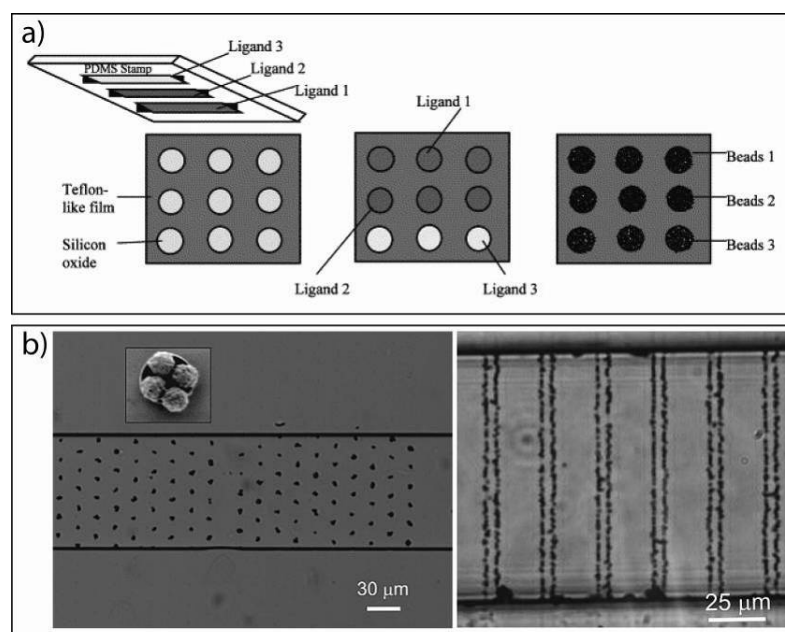


Figure 3.4: (a) Drawing showing the different steps involved in generating a bead dot array using a PDMS stamp. The dots are first defined within a Teflon-like film using standard photolithography. Different ligands are then deposited by microcontact printing and beads may finally bind specifically (adapted from [90]). (b) Optical micrographs of beads (dots and double lines) electrostatically immobilized on micropatterns. The inset in (b) is a SEM photograph of beads attached to a single dot (adapted from [92]).

3.2.3 Comparison of the manipulation methods

All the above mentioned methods are extensively used in LOC systems. To perform an efficient immunoassay or, more specifically, an agglutination test on-chip, several aspects have to be taken into account. Table 3.1 shows a comparison of the different methods considering important aspects that are required to perform an efficient immunoassay on-chip using microparticles. A high force on the particle is needed for retention and fast actuation of the particles. The maximum possible distance range between the actuator and the particles is of importance to allow convenient integration into the microchip. For example, if particles have to be in direct contact with an electrode, the later has to be directly integrated into the microchip. This results in a more complex fabrication process compared to a system where the actuator can be placed externally in proximity of the channel.

Release of the particles after an experiment for subsequent detection is a very important aspect in bioanalytical LOC systems and is therefore the main limitation preventing the use of non-reversible retention systems. The ability to concentrate the particles in a restricted volume is

generally an advantage for controlling the incubation process of a bioassay as well as to increase the particles interaction and the detection signal.

Table 3.1: Comparison of the different particle manipulation methods. Abbreviations: MP = magnetophoresis, DEP = dielectrophoresis, MR = mechanical retention and SP = superparamagnetic

Methods	Force strength	Force range in space	Possible release after experiment	Particle concentration in a restricted volume
MP	++	++	Yes (if beads are SP)	+++
DEP	+	+	Yes	+
Optical force	-	+++	Yes	-
Acoustic wave	+	++	Yes	++
MR	+++	---	No	+++

From Table 3.1, it is clear that the magnetophoresis method is one of the most competitive actuation tools for immunoassays on-chip. One of the reasons is the relatively high force that may be exerted on magnetic beads in a very simple manner, for instance by using a passive element (like a permanent magnet). This explains the increasing interest and number of publications related to the use of magnetic beads on-chip [16, 93].

3.3 Magnetic bead concepts for bio-assays

Maximizing the exposure of the bead surface to a microfluidic flow for Ag capture is an issue of primary importance [16, 33]. For that purpose, manipulation of magnetic beads on-chip is often used for the retention of beads from flow [68] or the transport of biological molecules [20, 94]. We propose here a distinction of the manipulation methods by the type of actuators that are used (i.e. permanent magnets or electromagnets).

3.3.1 Systems with external permanent magnets

A simple approach consists in passively trapping the magnetic beads in a microchannel by using external permanent magnets allowing the formation of a dense and static bead plug [95, 96]. Using this method, a small-volume heterogeneous immunoassay system was demonstrated in microchannels with small paramagnetic beads (1–2- μm diameter) [96]. The assay was demonstrated with a direct interaction of fluorescein isothiocyanate (FITC) with an immobilized anti-FITC conjugated. Heterogeneous sandwich assays were also carried out with parathyroid

hormone and interleukin-5 (Figure 3.5 a) [96]. Bronzeau *et al.* demonstrated how several assays can be performed simultaneously by flushing a sample solution over several plugs of magnetic beads with different surface coatings. Three plugs of magnetic beads were immobilized in a microchannel with external magnets. The beads featured surface coatings of glycine, streptavidin and protein A, respectively. Reagents were then flushed through the three plugs. Molecular binding occurred between matching Ag's and Ab's in continuous flow and was detected by fluorescence (Figure 3.5 b) [95]. Sensitivity of such systems using mm-sized external permanent magnets is however limited due to the high density of beads captured in the plug and the relatively poor perfusability of the plug.

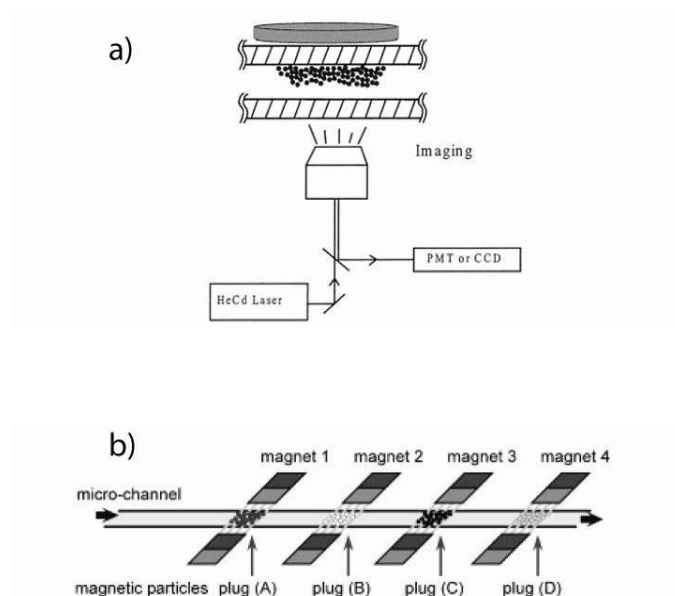


Figure 3.5: (a) Schematic representation of a flow-based micro-immunoassay system using permanent magnets. Magnetic beads are collected near a rare earth magnet to form a packed bed within a capillary or a channel (adapted from ref [96]). (b) Magnetic beads coated with different biomolecules are trapped by individual external magnets; sample or reagents can then be flushed through the different plugs and several assays can be performed simultaneously (adapted from ref [95]).

An alternative method uses geometrically trapped self-assembled chains composed of a relatively low number of magnetic nanoparticles [68]. This original concept to perform a complete on-chip sandwich immunoassay in chains was proposed by Lacharme *et al.* The magnetic chains are retained over periodically enlarged cross sections of a microfluidic channel (Figure 3.6). Thereby they strongly interact with the flow and rapidly capture the total of a low number of target molecules. As an example, the detection of murine monoclonal Ab's with a detection limit of 1 ng mL^{-1} was demonstrated. This work shows that an optimal interaction

between the analyte flow and the magnetic beads is of importance for effective capture of the target Ag's.

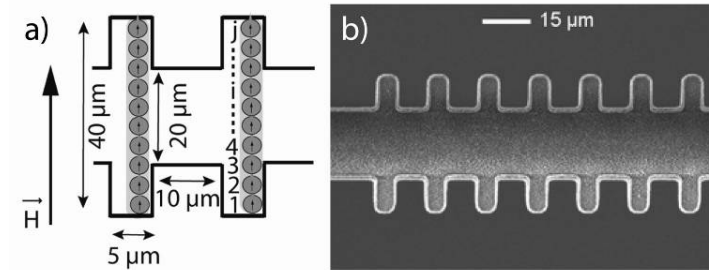


Figure 3.6: (a) Microchannel with periodically varying channel width of 20 and 40 μm . In a magnetic field \vec{H} , the magnetic nanoparticle chains are trapped in the large cross sections. (b) SEM picture of the microchannel showing the periodically varying channel width (adapted from ref [68]).

Le Nel *et al.* described a system for the detection of pathological prion protein [97, 98]. A microreactor for proteinase K-mediated protein digestion is formed in a dense arrangement of parallel bead chains by positioning strong permanent magnets in the vicinity of the microchannel. PK-grafted magnetic beads are immobilized inside a microchannel using a longitudinal magnetic field parallel to the flow direction forming a “multi-open-tubular” like column on-chip (Figure 3.7).

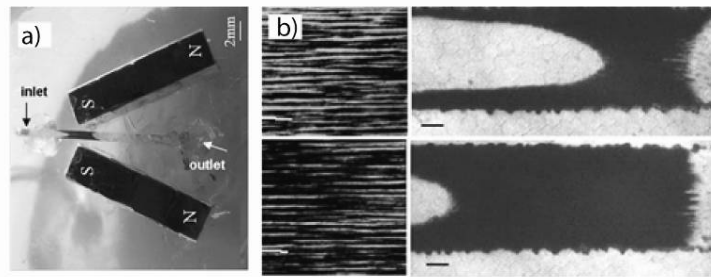


Figure 3.7: (a) Experimental setup with two magnets. (b, left) Expanded view of magnetic beads immobilized between the two magnets in a microchannel. Magnetic bead chain arrangement at an early and late stage of the magnetic microstructure formation. The orientation of the bead arrays parallel to the channel axis provides a low flow resistance and uniform pore size (black scale bar, 5 μm). (b, right) View of the whole plug at the beginning and end of the plug formation at a lower magnification (black scale bar, 200 μm) (adapted from ref [98]).

Another simple and elegant concept using a permanent magnet for the continuous flow separation of magnetic beads was proposed by Pamme *et al.* [99]. This method uses a permanent

magnet placed on one side of a microfluidic chamber. Beads are then introduced on the opposite side of the chamber and are then deflected towards the magnet (see Figure 3.8). Using this method, separation of non-magnetic beads and magnetic beads was first demonstrated in a free-flow device. Magnetic beads were also separated as a function of their sizes. More recently, this concept was used to perform a continuous flow immunoassay by Peyman *et al.* [100, 101]. The concept of the immunoassay using a continuous flow reactor is depicted in Figure 3.8. Magnetic beads are introduced on one side of a microfluidic chamber and are then deflected towards the permanent magnet on the opposite side. During the deflection, beads cross parallel reagents streams in which several binding and washing steps are performed. Using this method, a sandwich immunoassay was demonstrated. The main limitation of such approach comes from the short time during which a bead is immersed in each reagent resulting in a relatively high detection limit. Moreover, beads are moved in a unique direction (i.e. towards the permanent magnet) and therefore may not come back to the original liquid. A similar concept was presented by Sasso *et al.* [102]. In this case, a first permanent magnet is used to deflect paramagnetic beads from a buffer solution to a sample solution. Further downstream, another permanent magnet is used to move the beads back in the buffer solution.

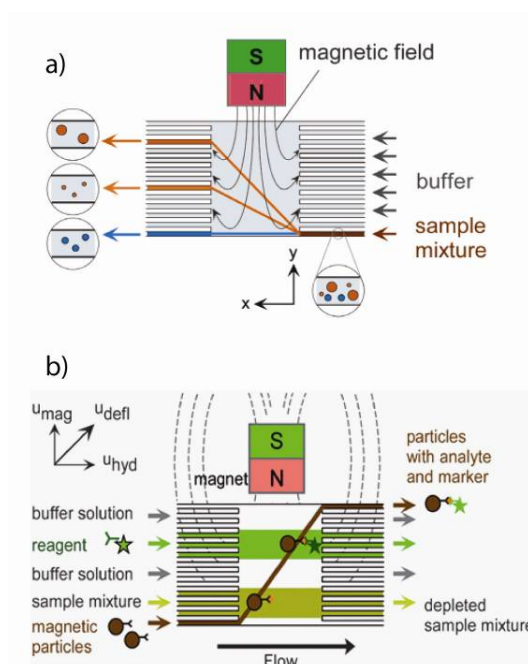


Figure 3.8: (a) Concept of the free-flow magnetophoresis. A magnetic field is applied perpendicular to the direction of the liquid flow. Beads deviate perpendicular to the flow according to their size and magnetic susceptibility and are thus separated (adapted from ref. [99]). (b) The principle of the continuous flow reactor: magnetic beads are deflected through multi-laminar reagent streams across the

reaction chamber and consecutive binding and washing steps are performed on their surface in continuous flow. The example shown above depicts a typical sandwich assay. Deflection of magnetic beads across the reaction chamber (adapted from ref [101]).

3.3.2 Electromagnet-based systems with integrated soft magnetic poles

The possibility to actively manipulate magnetic carriers in microfluidic channels opens the way to explore new opportunities for on-chip bioassays with enhanced performance [103, 104]. An approach has been the use of ferrimagnetic beads that form stable rotating chains in an alternating magnetic field [105, 106]. A magnetic core is used to guide the magnetic field generated by an external electromagnet and two microstructured soft magnetic tips are used to focus the magnetic field across a microchannel (Figure 3.9). This approach demonstrated a good mixing efficiency of two parallel flows in a microchannel and provided evidence of enhanced interaction between the magnetic beads and the fluid flow. Unfortunately, such type of ferrimagnetic particles stay agglomerated in bead clusters after field removal. In many bio-analytical applications, individual beads should be released from the plug after analyte capture for further processing. The previous technique cannot be readily applied to superparamagnetic or low-coercivity beads, as these change their magnetic state by Néel relaxation and therefore cannot be directly applied for immunoassays.

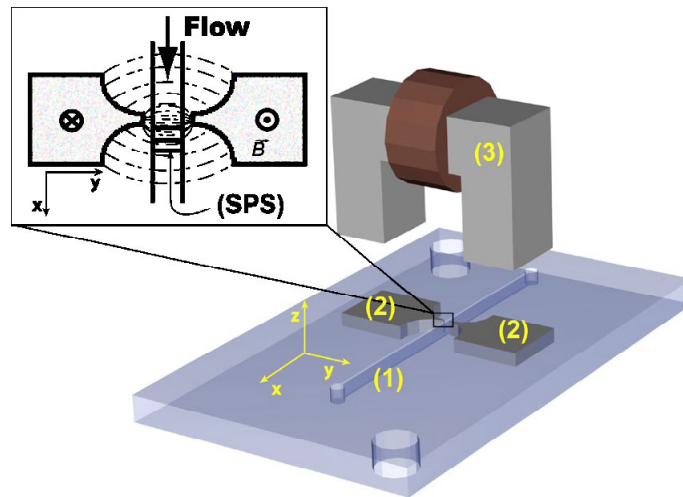


Figure 3.9: Schematic view of a magnetic actuation system for the manipulation of ferrimagnetic particles: (1) PMMA chip; (2) soft magnetic parts used for magnetic field focusing; (3) electromagnet. The insert shows a schematic view of the magnetic field distribution between the soft magnetic tips (adapted from ref [105])

An array of needle-shaped planar elements aligned on each side of a channel was also used for the capture of two differently functionalized beads [107]. The system is designed to

perform a selective on-chip DNA hybridization assay but does not allow for a dynamic actuation of the beads (Figure 3.10).

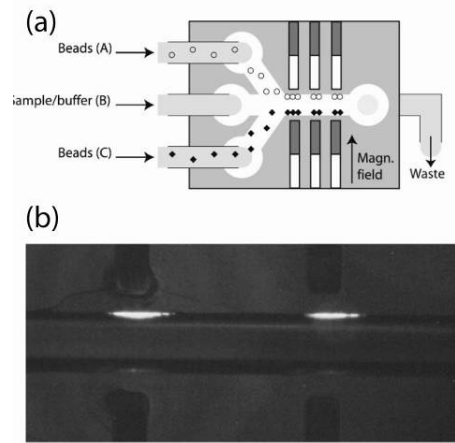


Figure 3.10: (a) Schematic illustration of the microsystem and the fluid microchip with the three inlets A–C. The two types of beads are introduced through inlets A and C, respectively, and separated by a buffer flow applied through inlet B. The captured magnetic beads close to the magnetic elements are shown. (b) Fluorescence micrograph of a section showing the beads immobilized on the side walls, a fluorescence signal is observed at the top.

Long range transport of magnetic beads using planar integrated coils was demonstrated by Rida *et al.* [94]; also a wire-based system for the displacement of clouds of magnetic beads was presented [108, 109]. Manipulation of microdroplets using magnetic beads was presented by Lehmann *et al.* [110] and this concept was used for the purification of DNA [111]. These systems are generally used to dynamically manipulate (i.e. displace) the beads in channels, capillaries or microchambers. Due to the relatively low magnetic field produced by the integrated wires or coils, the retention of beads in a flow using this principle is limited and the actuation speed is low. The combination of permanent magnets with electromagnets (coils) is only rarely applied for the manipulation of magnetic beads on-chip. The combination of integrated coils with a homogenous field produced by permanent magnets was proposed by Lehmann *et al.* to increase the moment of the magnetic bead [112]. It is clear that the combination of permanent magnets with electromagnet may still improve the efficiency of on-chip manipulation of beads.

3.3.3 Comparison of magnetic bead manipulation methods

Methods using passive elements (i.e. permanent magnets) [95] and active electromagnets [94, 106] are often reported in the literature. A qualitative comparison of the different methods is summarized in Table 3.2. The combination of active and passive elements for the manipulation of magnetic beads on-chip is still not fully explored. Indeed, the main limitation for electromagnet-based manipulation comes from the relatively low magnetic field produced by an external

electromagnet or an integrated coil and thus the low magnetic force acting on the bead. Therefore, combination of electromagnets with permanent magnets might offer a good compromise between magnetic force and ability to dynamically actuate the beads.

Table 3.2: Comparison of magnetic bead manipulation methods

Methods	Force	Dynamic actuation	Bead release
Permanent magnet	+++	-	++
External electromagnet	+	++	++
Integrated electromagnet	-	+	+++
Permanent magnets + electromagnets	+++	+++	++

Rotation of chains of superparamagnetic beads was so far achieved using a macroscopic rotating magnetic field [113-116]. Figure 3.11 shows two examples of macroscopic magnetic bead manipulators using a four-coil configuration to generate a rotating or a modulated magnetic field. Both systems are able to create highly tunable magnetic fields at the millimeter scale. Nevertheless, this approach is based on complex systems with several coils and complex magnetic cores making microfluidic integration difficult. Moreover, such a system is not ideal for bead retention in a microchannel, as the magnetic field gradients are weak. Dynamic retention of a low number of superparamagnetic beads in a flow for a bio-assay on-chip is one of the major objectives of this thesis and will be discussed in detail in Chapter 5.

A *dynamic* plug of moving beads, induced by time-varying and localized magnetic actuation fields in a restricted reaction volume is clearly of interest to increase the interaction between the beads and the analyte. A strong magnetic force has to be applied on the beads to increase the actuation speed and improve the retention of the latter in a flow.

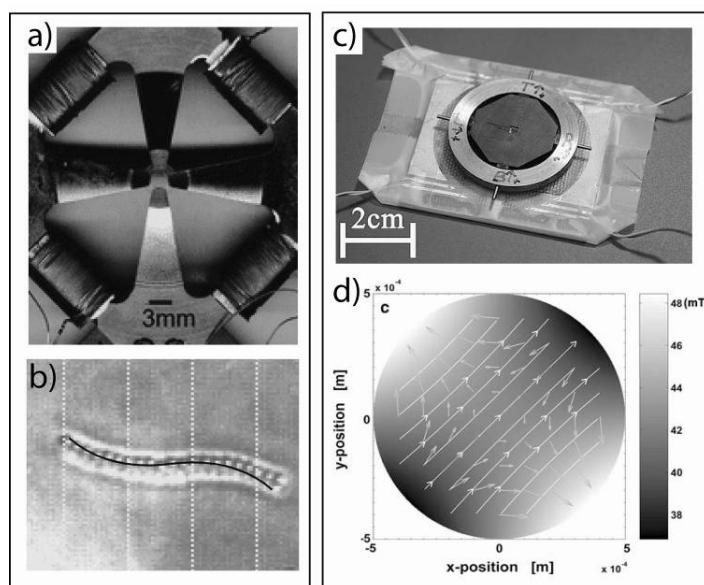


Figure 3.11: (a) Photograph of a quadrupolar coil configuration system used to generate a rotating magnetic field. (b) The system serves for the study of rotating magnetic bead chains. (c) Photograph of the magnetic bead manipulator containing a sub-microliter fluid volume surrounded by four miniaturized coils, capable to create a large variety of magnetic field shapes. (d) FEM simulation of the magnetic flux density using the same current in all the four coils [117].

3.4 On-chip immunoassays

3.4.1 Heterogeneous magnetic bead-based immunoassays

A large majority of immunoassays on-chip using magnetic beads are heterogeneous sandwich-type assays [68, 118-121]. This may be explained by the possibility to simplify standard heterogeneous protocols. Indeed, in a heterogeneous protocol, separation of the solid phase (in this case the magnetic beads) and the liquid phase has to be performed several times with additional washing steps. A LOC based system may accelerate and simplify these fluid exchanges. A standard on-chip sandwich immunoassay on magnetic beads is carried out as shown in Figure 3.12. Functionalized beads are first immobilized and then, the sample containing the target Ag's is introduced in the microchannel and binds to the capture Ab's on the magnetic beads. Finally, the labeled detection Ab's are flushed through the beads and the detection is performed. In the particular case of Figure 3.12, enzyme substrate has to be added before the electro-chemical detection.

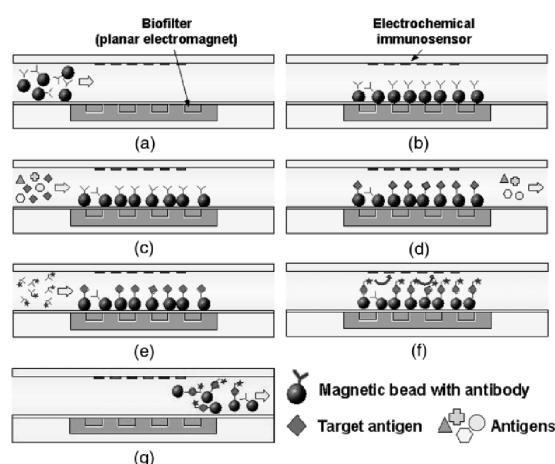


Figure 3.12: Illustration of bio-sampling and immunoassay protocols using magnetic beads. (a) injection of magnetic beads; (b) separation and retention of beads; (c) flowing sample; (d) immobilization of target Ag; (e) flowing labeled Ab; (f) electrochemical detection after adding enzyme substrate; and (g) flushing of magnetic beads (adapted from ref [122])

Fluorescent detection is a standard method in biology because it is sensitive and it can be easily performed under a microscope. The biochemistry for the labeling of proteins with enzymes or fluorescent dyes is also well established. On-chip detection sandwich immunoassays using a fluorescently labeled detection Ab were demonstrated frequently. The method is a relatively simple and straightforward one as the fluorescent signal may directly be detected on the beads and the background noise induced by non-specific adsorption of proteins at the surface of the channel is generally low [68, 118, 119]. Lowering of the detection limit using an on-chip protocol was for example demonstrated by Lacharme *et al.* [119]. The main limitation of the present method is the lack of amplification of the signal. Indeed, a relatively low number of fluorescent dyes can be attached to the detection Ab, thus inducing a weak signal when the number of target Ag's is low. Amplification of the signal is generally performed using ELISA, but implementation of the method is more difficult (see below).

ELISA tests have the advantage to amplify the signal when only a few target Ag's are captured. A single enzyme-labeled detection Ab induces the fluorescence of many surrounding substrate molecules. The main limitation for the implementation of an on-chip ELISA using magnetic beads is the non-specific adsorption of the labeled detection Ab's at the surface of the channel walls. Indeed, due to the amplification, the unwanted adsorption of only a low quantity of detection Ab's is sufficient to generate a high background signal. Herrmann *et al.* proposed two solutions to overcome this problem. The first approach is to form the immunocomplex off-chip and then to introduce the beads in the chip for detection (Figure 3.13 a). Later, Herrmann *et al.*

proposed a full on-chip ELISA using two different chambers, one for the formation of the immunocomplex and another for the detection of the fluorescent signal (Figure 3.13 b-e). Using this method a detection limit in the range of few hundreds of pg/mL was successfully demonstrated.

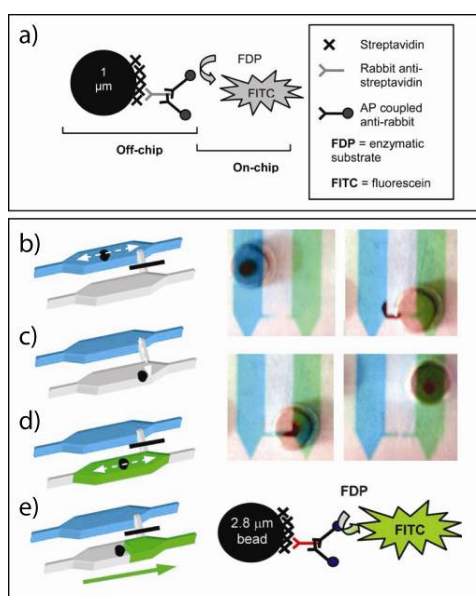


Figure 3.13: (a) First approach proposed by Herrmann *et al.* for an on-chip ELISA: the formation of the immune complex is performed off-chip in order to avoid unspecific adsorption of the detection Ab on the channel walls. Signal generation and detection are performed on-chip (adapted from ref [123]). Second approach proposed by Herrmann *et al.* for an on-chip ELISA: (b) streptavidin-coated magnetic beads are trapped inside the complexation chamber with an external permanent magnet. The anti-streptavidin Ab binds specifically to the streptavidin. Similarly, the AP-coupled secondary Ab is added to form the reactive immune complex. (c) The reactive beads are magnetically transferred into the reaction chamber. (d) The enzyme processes the FDP substrate into the fluorescent molecule FITC. (e) The reacted solution is then pushed into the detection area (adapted from ref [103]).

3.4.2 Dendritic amplification method

An alternative to ELISA is the dendritic amplification (DA) which has been developed by several groups for DNA sensors [124-126] and immunoassays [127-129]. The DA methods employ a pair of multivalent building blocks (molecules or particles) which can bind to each other. One of the building blocks also binds, directly or indirectly, to the captured analyte molecule. The amplification is performed by supplying the building blocks alternately onto the solid surface capturing the analyte. A certain number of reaction cycles build a large dendritic structure which can easily be detected on the analyte molecule. So far, the DA methods have not become as popular as the traditional enzyme-based methods, probably because of the iterative incubation steps for the layer-by-layer growth of the dendritic structure [130].

Hosokawa *et al.* proposed an original method to perform DA on-chip using the intersection of two laminar flows (Figure 3.14) [130, 131]. The dendritic structure is built at the interface of the two laminar flows avoiding the need to perform iterative steps. To our knowledge, dendritic amplification on magnetic beads was not demonstrated until now. We present a method for the use of DA on mobile magnetic beads in chapter 7.

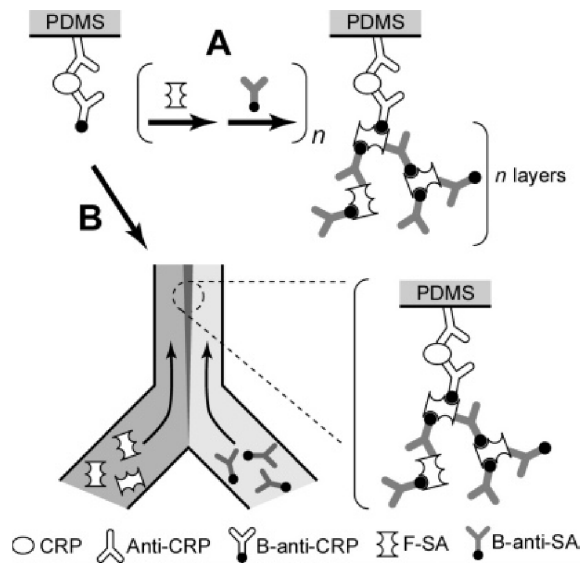


Figure 3.14: Schematic representation of the two modes of Dendritic Amplification. (A) Layer by layer mode. Fluorescently labeled-streptavidin (F-SA) and biotinylated-anti-streptavidin (B-anti-SA) are alternately supplied to the initial sandwich immunocomplex. (B) Continuous mode F-SA and B-anti-SA are simultaneously and continuously supplied from the two laminar streams formed by the Y-shaped channel. Abbreviations: CRP, C-reactive protein; B-anti-CRP, biotinylated anti-CRP; F-SA, FITC-labeled streptavidin; B-anti-SA, biotinylated anti-streptavidin (adapted from ref [130]).

3.4.3 Homogeneous magnetic agglutination assays

Standard homogeneous assays, such as the latex agglutination test have a relatively poor detection limit. It has been shown that an enhanced interaction between the beads using USW reduces the assay time and detection limit. A new approach using magnetic beads for agglutination assays was investigated by Baudry *et al.* [12, 13]. It has been demonstrated that the detection limit can be reduced down to 1 pM in the bulk format by introducing immuno-agglutination with superparamagnetic nanoparticles. This significant improvement is based on a strong increase of the colliding frequency between the magnetic carriers in the presence of a magnetic field leading to the formation of magnetic chains (Figure 3.15).

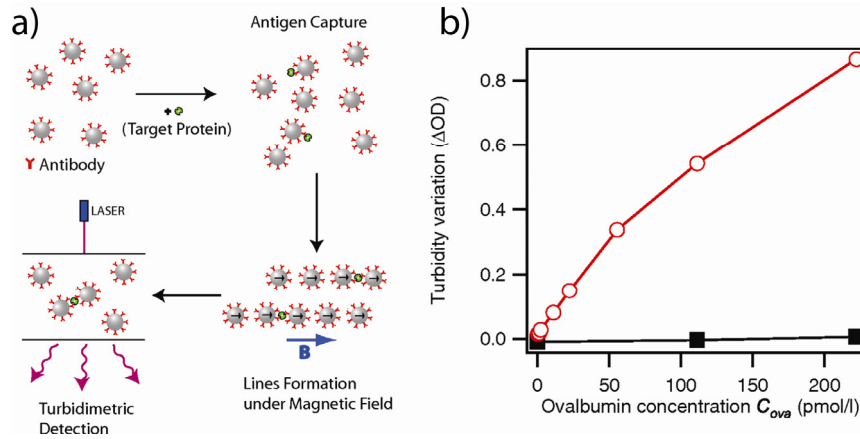


Figure 3.15: (a) The magnetic agglutination assay method: Magnetic beads grafted with antibodies are mixed with the sample containing the Ag's. Ag's are first captured on the beads. The application of a magnetic field allows the formation of bead chains. Beads that have captured an Ag will form a link with their neighbor. After a few minutes, the magnetic field is switched off and doublets are detected by a turbidimetric measurement. (b) Optical density difference measured before and after the application of the magnetic field (circles: $B = 20$ mT and squares: $B = 0$ mT).

A first approach for a chip-based agglutination test with magnetic beads was presented by Degré *et al.* [132]. Agglutination of beads was observed after placing the channel in between two permanent magnets (Figure 3.13). The high potential of the on-chip agglutination assay principle could be demonstrated by the sensitive detection of biotinylated Protein A.

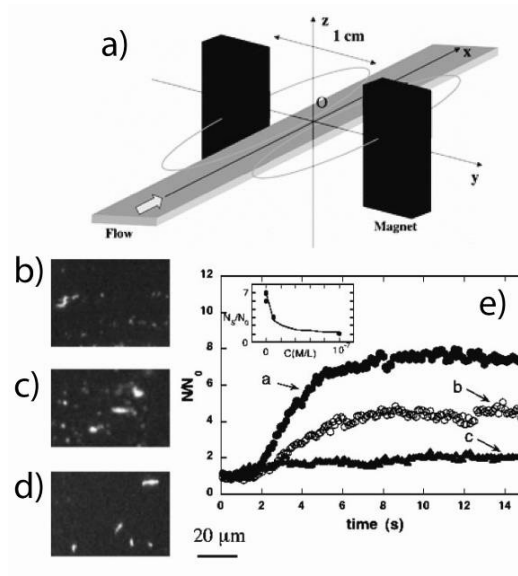


Figure 3.16: (a) Configuration of the system with the two permanent magnets positioned beside the microchannel. Images (b)–(d) show the beads, after the magnets removal, for different concentrations of biotinylated protein A. (b) $t = 4$ s, $C = 10^{-14}$ mol l^{-1} ; (c) $t = 13$ s ; $C = 10^{-8}$ mol l^{-1} ; (d) $t = 13$ s ; $C = 10^{-7}$ mol l^{-1} . Plot (e) shows the temporal evolution of the ratio of counted beads with time $N(t)/N(0)$.

3.4.4 Comparison of immunoassay methods

Electrochemical detection was previously proposed by Choi *et al.* as shown in Figure 3.12 [122]. This method has the advantage to avoid a complex optical detection system. The detection limit of such type of system still remains relatively limited compared to optical methods, while integration of electrical detectors on-chip increase the fabrication process complexity.

Non-fluorescent optical detection is generally performed for agglutination assays. Detection of aggregates for agglutination tests using small beads (typical below 500 nm) is usually performed using a turbidimetric measurement [12]. This method is in general not readily applicable on-chip after retention of the magnetic beads, as the beads have to be uniformly suspended in the medium. Moreover, for beads typically larger than 500 nm, this method does not apply as the diameter of the bead is larger than the wavelength of the light. On-chip agglutination was already detected using image treatment by counting the number of beads after field removal [132]. This approach is mainly restricted to a lab environment because an automation of this protocol remains critical as a relatively large number of images have to be taken and analyzed to obtain valuable statistical results. The implementation of a simple method for on-chip agglutination detection is therefore of interest.

The integration of heterogeneous assays on-chip has lead to a shortening in the assay time and improvement of the detection limit compared to standard off-chip assays [68, 119]. Nevertheless, commercialization of such systems remains difficult. One reason for that is the need of a high number of different liquids (sample, washing buffer, detection buffer, etc.) to perform the assay on-chip, which involves complex handling of the fluids during experiment. On-chip integration of a homogeneous assay is therefore a good alternative to reduce the complexity of an on-chip protocol. Table 3.3 gives an idea of the reduction in complexity of a homogeneous assay compared to a heterogeneous assay on-chip.

Table 3.3: Comparison of homogenous and heterogeneous on-chip assays using magnetic beads in terms of protocol complexity

Methods	Need of an additional detection Ab's	Minimum washing steps needed	Typical standard on-chip detection limit
Heterogeneous	Yes	2	Good, 1 ng/mL [68]
Homogenous	No	0	N.A.

Table 3.4 gives an overview of the possibilities given for the different detection methods. In this work, an optical detection will be used for the detection of aggregations and fluorescent dendritic amplification on-beads will be also investigated.

Table 3.4: Comparison of the different on-chip detection methods.

Methods	Assay type	Amplification	On-chip integration	Typical on-chip detection limit
Fluorescent detection	Heterogeneous	dendritic amplification	++	1 ng/ml [68]
ELISA	Heterogeneous	Yes	-	0.1 ng/ml [103]
Electrochemical detection	Heterogeneous	Possible	+	50 ng/ml [122]
Optical detection of aggregates (agglutination test)	Homogeneous	No	+++	N.A.

3.5 Concept of our device

The development of magnetic bead-based systems is gaining interest and a simple dynamic actuation system for superparamagnetic beads in a flow is clearly of interest.

The importance to simplify on-chip protocols is important to reach the goal of simple devices for point-of-care testing. The large majority of immunoassays on-chip is nowadays based on heterogeneous assays requiring iterative separation and washing steps. Implementing an agglutination test on-chip is of interest especially for the simplification of the chip integration and the test protocol. An on-chip agglutination test is discussed in the second part of the thesis and a model assay using streptavidin-biotin affinity will be used to demonstrate the feasibility of this approach.

The main concept of our device is summarized in Figure 3.17. First of all, our system has to provide a fast and efficient separation method to extract the magnetic beads ($\sim 1 \mu\text{m}$) from the buffer solution. A low number of beads has then to be confined in a restricted volume (ideally $< 1 \text{ nL}$) in order to precisely control their number (Figure 3.17 a). In a second step, beads have to be actuated in order to avoid the formation of a dense and badly perfusable plug of beads. The actuation has to be perpendicular to the flow direction in order to increase the probability for an Ag to encounter a magnetic bead (Figure 3.17 a). Finally the beads have to be released for optical detection. An efficient retention system coupled with fast dynamic actuation of superparamagnetic beads on-chip is of primary interest for many kinds of immunoassays on-chip.

Optimization of the retention and actuation of the beads is therefore an important part of the thesis.

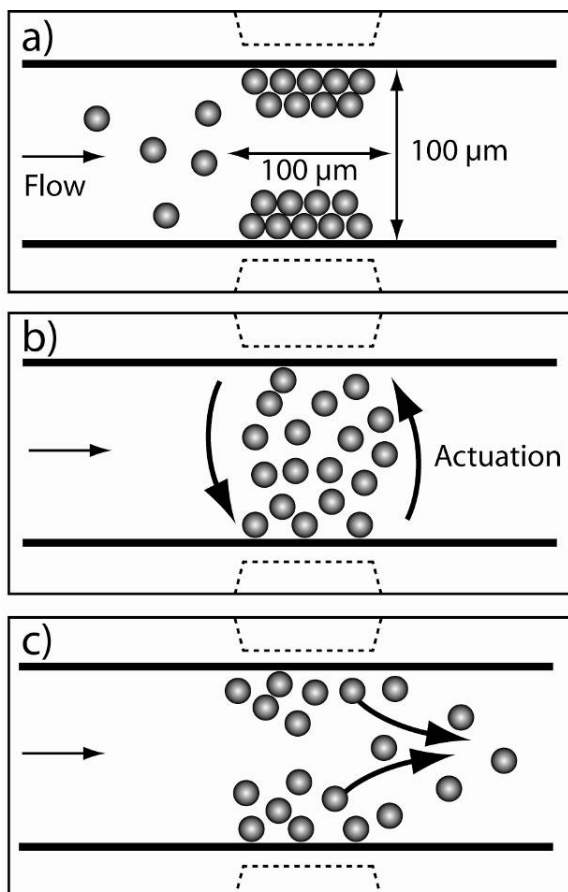


Figure 3.17: Our concept for the manipulation of magnetic beads on-chip. (a) Separation of the magnetic beads from the sample with retention of the beads in a restricted volume ($100 \times 100 \times 100 \mu\text{m}^3$). (b) Actuation of the beads perpendicular to the fluid flow. (c) Release of the beads for subsequent analysis.

Our device was designed to address the needs of an on-chip magnetic bead-based agglutination assay (Chapter 6). Nevertheless, another interesting and promising feature is the possibility to rapidly move magnetic beads through different parallel reagent flows as shown in Figure 3.18 (Chapter 7). For example, a plug of magnetic beads immobilized on the channel wall in a liquid A may be attracted towards the liquid C at the opposite channel wall after crossing an intermediate liquid B (see Figure 3.18). This method opens new perspectives for immunoassays requiring a cyclic fluidic exchange, as is the case for the dendritic amplification (see chapter 7).

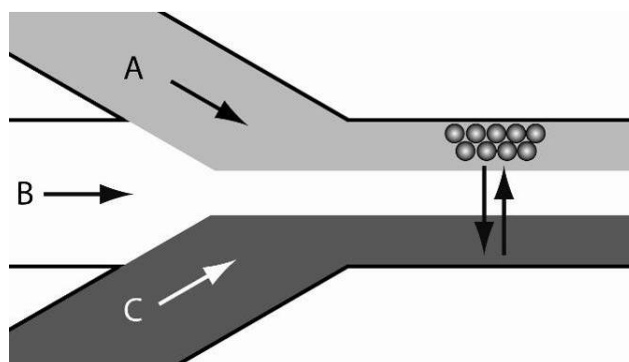


Figure 3.18: Schematic illustration of the rapid and cyclic fluidic exchange within our device. Magnetic beads rapidly move through different reagents (A-B-C) and then come back crossing the reagents in the opposite direction (C-B-A).

4 The microfluidic platform

In this chapter, the fabrication of the microchips and the microfluidic platform is discussed. The microchip used during this work is made of PDMS and glass. Fabrication of the chips is based on standard PDMS replication methods. A microfluidic set-up was designed to provide a platform for LOC devices requiring magnetic actuation with an external electromagnet. This set-up was used for several applications such as actuation of magnetic beads [133], magnetic agglutination test on-chip [134], separation of magnetic beads [135], dendritic amplification on-chip and magnetic 3D focusing. Moreover, the platform has been used as a basis for the development of the final integrated chip in the *DetectHIV* project (see chapter 8). The second part of this chapter demonstrates the feasibility of an innovative method for the fabrication of SU-8 monolithic channels in a simple and reliable manner, aiming to simplify the integration of magnetic parts on-chips and thus the handling of the whole system.

4.1 Microfluidic design

An exploded view of the set-up is shown in Figure 4.1. The magnetic and microfluidic set-up may be divided in three main components: the microchip, the chip-holder and the electromagnet (Figure 4.1). Design and fabrication of these three components are discussed in this section

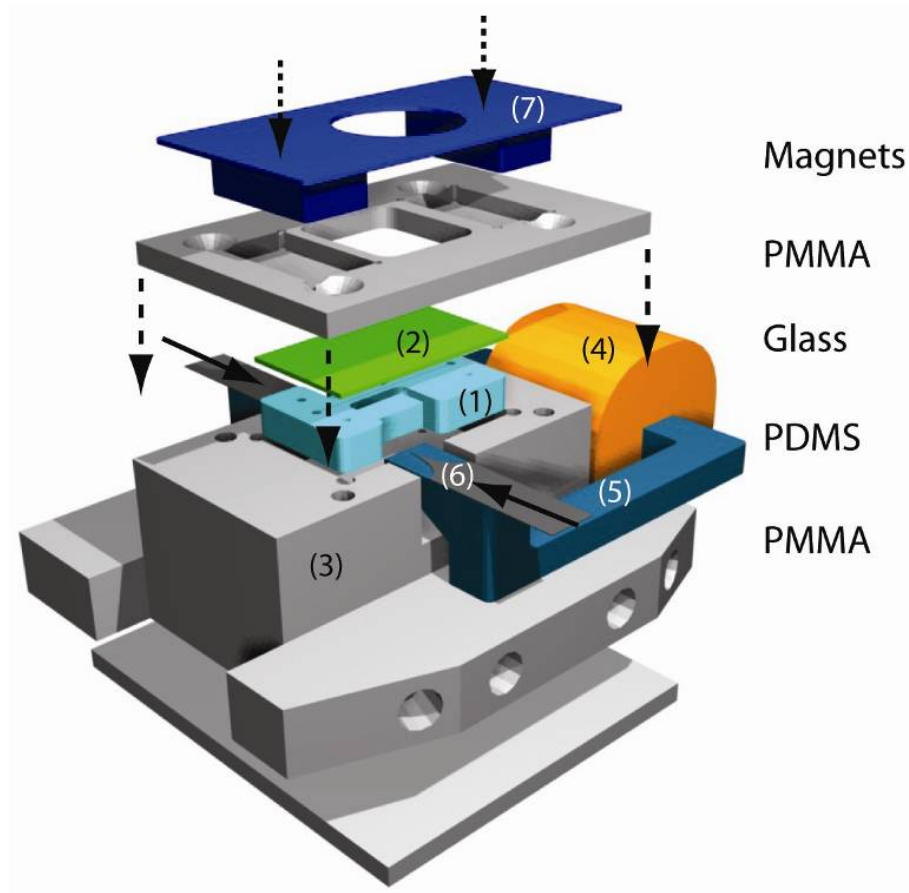


Figure 4.1: Exploded view of the magnetic actuation system. The microchip is made of a PDMS molded part (1) and a glass slide (2). The microfluidic set-up is made of three PMMA parts (3) and the electromagnet is made of a copper coil (4), a magnetic core (5), two micromachined magnetic tips (6) and two permanent magnets (7).

4.1.1 Microchip design and fabrication

The microchip for the retention and manipulation of magnetic beads in a sample flow relies on a simple and robust design. A unique microfluidic channel including a single inlet and a single outlet will be sufficient to perform the agglutination assay on-chip. Two recesses on the channel side allow the insertion of planar magnetic elements in close vicinity of the channel (Figure 4.2).

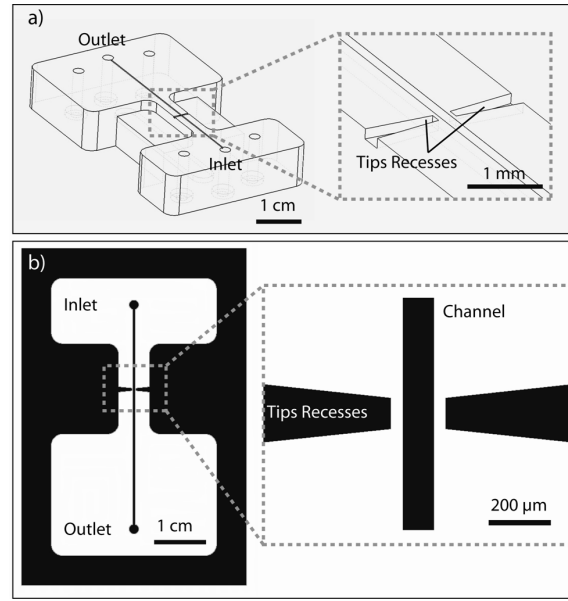


Figure 4.2. Schematic view of the microfluidic chip. The chip is made of a single microfluidic channel with one inlet and one outlet. (a) 3D view of the PDMS chip, microchannel and tip recesses allowing the positioning of two magnetic tips on the side of the channel, (b) 2D view of the chip design.

A standard molding process is used for the fabrication of the microfluidic chip. A SU-8/silicon master is employed for molding of the polydimethylsiloxane (PDMS) chip. The fabrication starts with the patterning of a 100 μm thick SU-8 layer on a silicon wafer (Figure 4.3 (a and b)). The PDMS is then molded using the SU-8/silicon master. The PDMS is baked during 12 hours at 65°C for complete polymerization. The cured PDMS part is placed on a glass slide and the magnetic tips are inserted manually from the side of the chip (Figure 4.3 d).

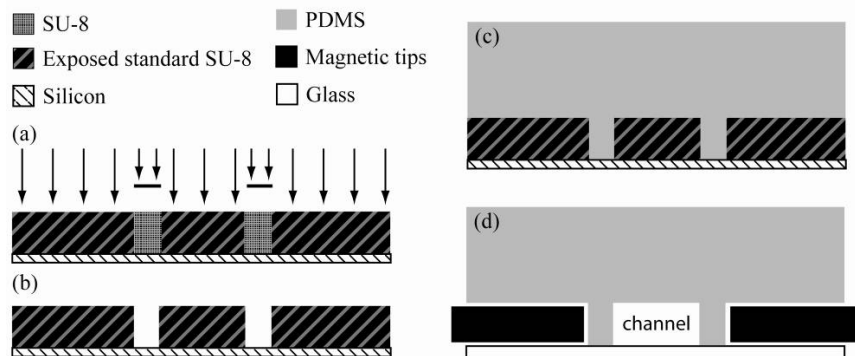


Figure 4.3: PDMS chip fabrication. (a) A 100 μm thick SU-8 layer is deposited on a silicon wafer and patterned to define the channel and the recesses for the magnetic tips. (b) The SU-8 master is developed. (c) PDMS is molded using the SU-8/silicon master. (d) The PDMS part is then positioned on a glass slide to form the microchannel. Two magnetic tips are inserted from the side of the chip.

In practice, molding of the chip starts with the positioning of the SU-8 master on an aluminum support (Figure 4.4 a). A PMMA piece serves to define the outer shape of the chip. Using this method, it is possible to precisely control the outer shape of the chip. Brass pins are used to define holes for the fluidic connections and reservoirs (Figure 4.4 b). The mould is finally filled with PDMS in a vertical position using a venting hole to remove trapped air bubbles (see Figure 4.4 c). PDMS is manually injected through the PMMA inlet using a disposable syringe and the device is cured as mentioned before.

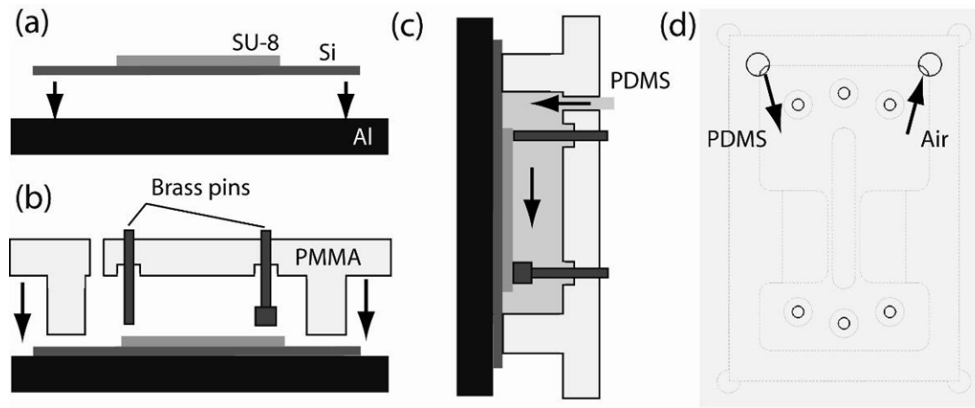


Figure 4.4: Molding of the PDMS chip. (a) Positioning of the SU-8/silicon master on the aluminum support, (b) positioning of the PMMA case and insertion of the brass pins, (c) Injection of the PDMS and expulsion of the air bubbles (d) front view of the mold showing the PDMS inlet and the air outlet.

Figure 4.5 shows the device used for molding of the PDMS chip. The mold is made of three distinct components to allow easy unmolding of the chip (see Figure 4.5).

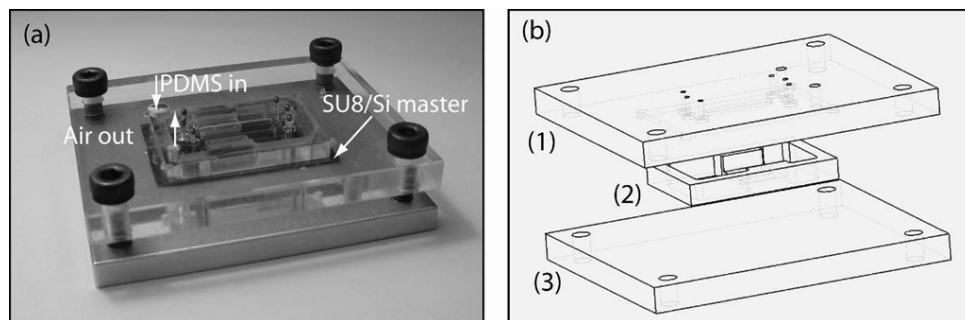


Figure 4.5 : (a) Photograph of the mold used for the fabrication of the PDMS chip. PDMS is injected in the mold using a disposable syringe from the PDMS inlet while the air outlet is used to remove eventual bubbles trapped in the PDMS. (b) Exploded view of the mold with the cap (1), the frame (2) and the base (3).

Using this method, reproducible PDMS chips are fabricated (Figure 4.6 a). The outer shape of these chips is well defined and can therefore easily fit into a chip holder. A photograph taken with an optical microscope of the channel and the magnetic tips is shown in Figure 4.6. Moreover, this method allows changing the microfluidic design of the chip without affecting the rest of the microfluidic platform.

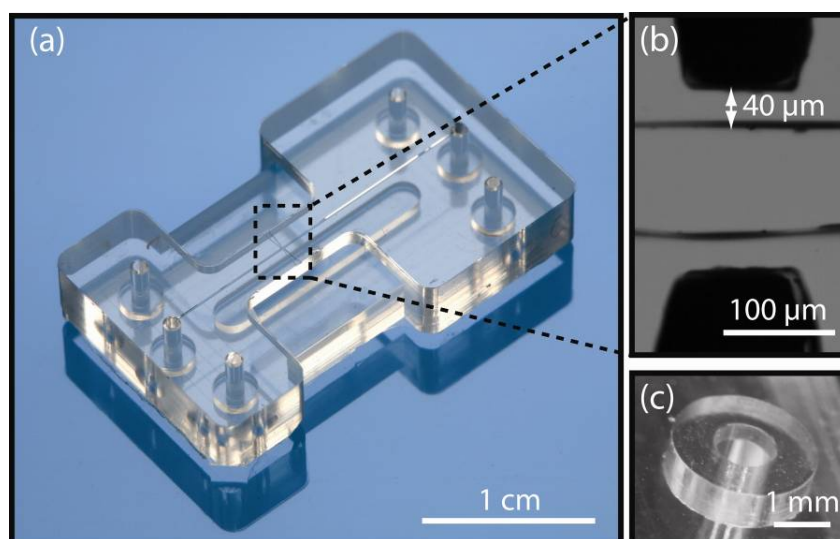


Figure 4.6: (a) PDMS chip with the single microchannel and the two recesses for the magnetic tips. (b) Photograph of the microchannel with the inserted magnetic elements showing the critical dimension of 40 μm between the magnetic tip and the microchannel wall. (c) An O-ring like structure directly molded in PDMS is used to obtain a leakage free connection between the chip and the chip holder.

4.1.2 Chip holder and fluidic protocol

The chip holder was designed to be flexible and to address the needs of a maximum of different applications involving magnetic actuation. Six microfluidic outlets have been included in the platform (see Figure 4.7 a). For each connection, a direct access to the chip is possible using a pipette and a micro-loader or via an external flexible tube. A photograph of the whole magnetic platform is shown in Figure 4.7 b. In this example three inlets (I-1,I-2,I-3) and one outlet (O-1) are connected. “Up-church®” connectors are used for secure connections between the flexible tubes and the PMMA chip holder.

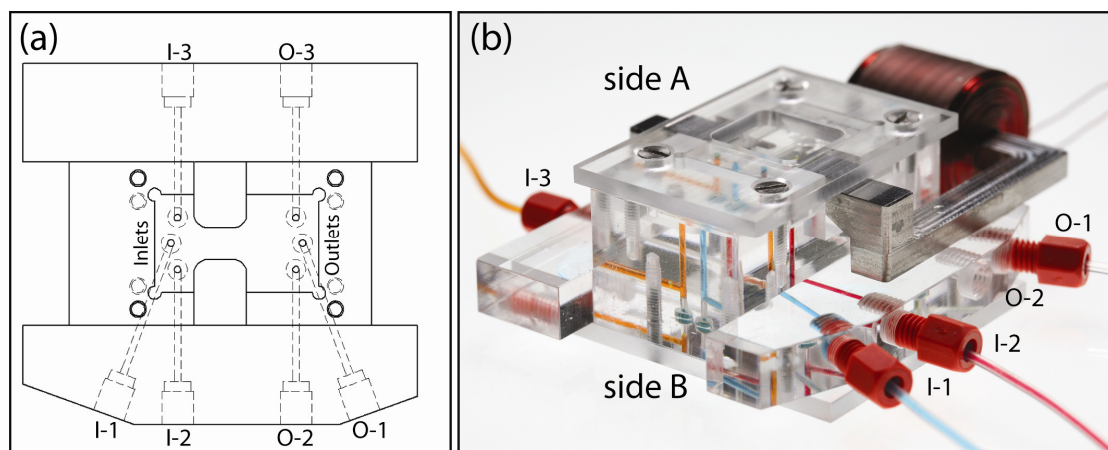


Figure 4.7: (a) Schematic view of the chip holder (from the top), three inlets and three outlets may be connected to external tubes. (b) Photograph of the magnetic retention system with three inlets (I-1, I-2, I-3) and one outlet (O-1) connected to external tubes.

Assembling of the system starts with the insertion of the PDMS/glass chip in the PMMA holder. The PDMS chip is self-aligned in the chip-holder and secure fluidic connections between the PDMS and the PMMA are established by “O-ring like” structures molded into the PDMS chip (Figure 4.6 c). A PMMA cap tightly clamps the chip into the holder. The two magnetic poles are inserted from the sides into the PDMS recesses prior to final clamping. Two movable permanent magnets required for the plug actuation can be easily placed on the PMMA cap.

The microfluidic setup is schematically shown in Figure 4.8 (a). We have chosen to drive the liquid in the microchannel by connecting a syringe pump to the outlet (O-1) of the chip in order to have access to an open reservoir. This simple method allows for a good control of the flow in the channel in suction mode. An open reservoir is essential to introduce fresh and well suspended bead solution before each experiment. Moreover, a single inlet is enough to introduce different liquid (i.e. beads, sample or washing solution).

Before starting an experiment, the microfluidic setup is manually prefilled with buffer solution using a prefilling syringe (see Figure 4.8 a). Buffer solution is injected through the outlet (O-1) to fill the chip holder and microchannel (Figure 4.8 b). Bubbles trapped in tubes and fluidic connections are removed through a venting bypass in the chip holder (Figure 4.8 c). The system has to be completely bubble-free to enable control of flow rates down to 1 nl/s in a reliable manner, i.e. without any hydraulic compliance effect. Subsequent flow control is done using an automated precision syringe pump (Figure 4.8 a). The small on-chip reservoir in the PDMS chip is then emptied using a pipette and refilled with beads or sample solution (Figure 4.8 c).

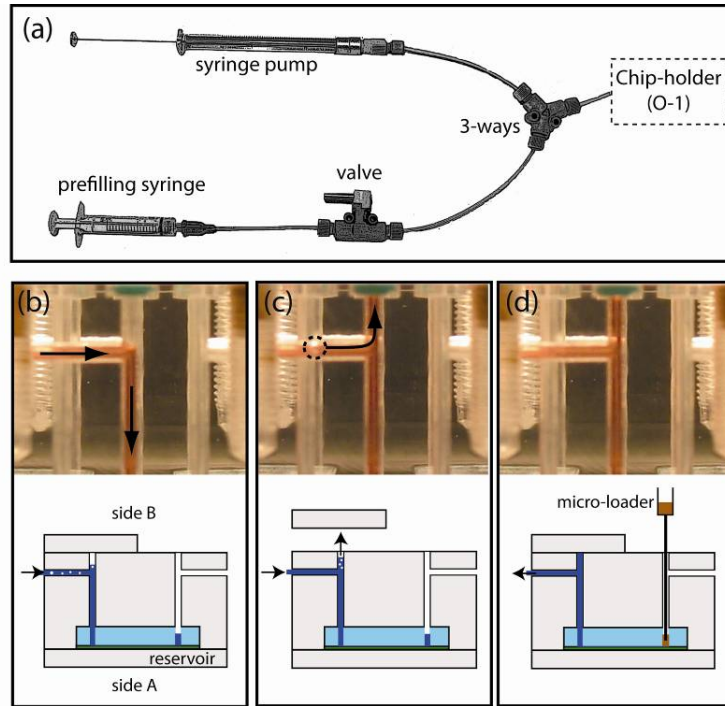


Figure 4.8: Microfluidic platform. (a) Schematic view of the fluidic setup used to control the flow in the microchannel from the outlet (O-1). (b-d) Prefilling of the device with buffer from the outlet (O-1): (b) cap closed for initial filling; (c) Cap open for releasing the bubbles (dashed circle) trapped in the tubes and connectors; (d) the on-chip reservoir in the PDMS chip is manually emptied and refilled with beads or sample using a pipette with a microloader tip.

4.2 Electromagnetic actuation system

4.2.1 Core design

An external coil is used to generate a time-varying magnetic flux which is guided through a magnetic core and by the micromachined magnetic tips to focus the magnetic field across the microchannel. The electromagnet core is positioned around the microfluidic chip holder (see Figure 4.9). The whole system is designed to fit under an upright or an inverted microscope. In this study, an inverted microscope was preferred to simplify the access to the open reservoir. Observation of the microchannel is always performed through the glass slide. The electromagnet is placed horizontally in order to allow illumination from the top of the system while observing the channel from below. The optical transmission mode is used to improve the image contrast when observing the beads in the microchannel. By applying an AC current decreasing in time through the coil, the magnetic core may be magnetized and demagnetized. The residual field should be small in order to allow the magnetic beads to flow away in the microfluidic chip for

Chapter 4 - The microfluidic platform

further analysis. Materials exhibiting this characteristic are called soft magnetic materials. The magnetic core and magnetic plates require different characteristics which are discussed in this section.

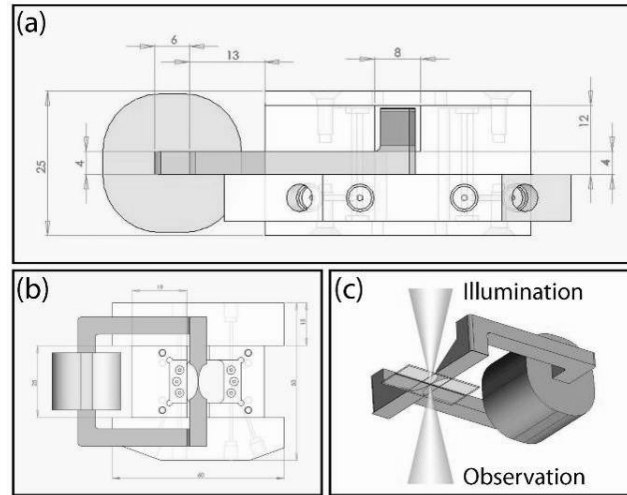


Figure 4.9: Side (a) and top (b) view of the magnetic system. A transmission mode optical set-up is used to improve the image contrast of the beads in the microchannel (c).

The role of the magnetic core is to guide the magnetic flux from the middle of the coil to the focusing magnetic tips. The relative permeability of the material has therefore to be high. It has also to have a sufficient saturation magnetic induction, to avoid saturation. The materials listed below match these requirements and are compared in Table 4.1. Parameters to consider the best choice are: ease to process the material and the relevant magnetic characteristics (B_{sat} and μ_R).

Table 4.1: Comparison of soft magnetic materials in terms of magnetic characteristics and ease of machining for the magnetic core

Material	Relative permeability μ_R	Saturation induction B_{sat}	Machining
Soft ferrite	+	-/+	---
Pure Iron	+	+++	--
PERMENORM	+++	++	++

The PERMENORM material is the best option according to the above table. The magnetic core has millimeter size features. The machining technique was determined according

to the dimensions and to the material. PERMENORM with such dimensions may be easily machined using Computerized Numerical Control (CNC) machining.

4.2.2 Coil design

Figure 4.10 shows the maximum coil size that can fit into the system under a standard optical microscope. From these dimensions, it is possible to estimate the maximum magnetic potential that can be produced with the coil while avoiding overheating of the system. The magnetic potential produced by a coil is given by:

$$\theta = N \cdot I = N \cdot S \cdot J \quad (4.1)$$

with S the section of the coil and J the current density. The equivalent system to determine the magnetic potential is a single wire filling a section of $20 \times 10 \text{ mm}^2$ with about 50% filling factor. The filling factor is the percentage of the cross section of the coil which is filled by copper.

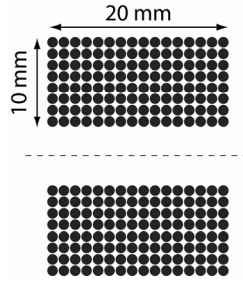


Figure 4.10. Cross-section of the maximum coil size allowed to fit into the system under the microscope.

The maximum current density in a copper wire to avoid overheating is estimated to be around 7 A/mm^2 . Using eqn (4.1) and considering the filling factor of 50%, the maximum magnetic potential is 700 A using the given coil.

For a good control of the magnetic potential, a maximum current of 0.5 A with an operation voltage below 12 V was chosen. The number of windings using the chosen maximum current is calculated using eqn (4.1) as $N=1400$. The maximum area for a single winding according to the 100 mm^2 available is thus $S_{sw} = 0.07 \text{ mm}^2$ which correspond to a diameter of 0.3 mm. The electrical resistance for one average winding is given by:

$$R_{sw} = \frac{\rho \cdot l}{S} \quad (4.2)$$

with ρ being the resistivity of the copper, $l = 7.5$ mm being the perimeter of the winding and S the section of the wire. The total resistance of the coil is finally:

$$R_{tot} = N \cdot R_{sw} \quad (4.3)$$

In consequence, the voltage needed to obtain a 0.5 A current is 8 V and may therefore be applied with a standard power supply. An experiment was performed in order to measure the temperature rise of the coil generated by the current. Figure 4.11 shows that using a current of 0.5 A, the outer part of the coil is heated up to 60°C. To prevent any damage of the system, the upper current limit was set to 0.3 A corresponding to a temperature of 40°C in use.

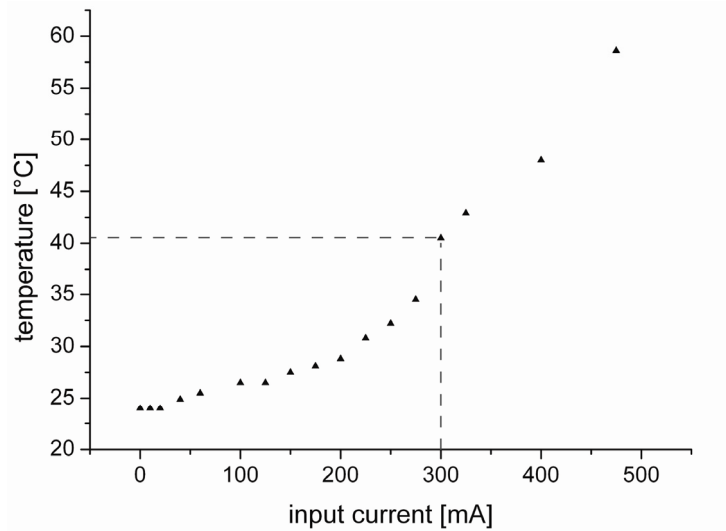


Figure 4.11. Temperature rise measured at the surface of the coil as a function of the current applied. An upper limit of 0.3 A was defined to prevent any damage of the system.

4.2.3 Magnetic tips design

The magnetic tips are one of the most critical parts of the system as their function is to focus the magnetic field and create the highest possible gradient across the channel in order to retain the magnetic beads in the flow. The thin and sharp focusing tips are the part of the magnetic circuit that saturate first. Hence, the foremost parameter to maximize is the saturation magnetic induction of the material to be used. Low coercivity is needed to demagnetize readily the device once the current in the electromagnet is switched off. A satisfying relative permeability is also needed to minimize the magnetic reluctance of the focusing plates. The first approach would be to integrate the magnetic tips directly on the chip. Electroplating would be required for

the deposition of thick metal layer in the range of 50 to 100 μm . However, the only available material type that could be easily deposited, permalloys (NiFe alloys), has much poorer magnetic properties than permalloy thin foils (clean room processing would also be required to implement this method). Laser cutting of a thin magnetic foil (50 or 100 μm in thickness) is a versatile and simple option offering sufficiently high precision for our application.

Different materials commercially available fulfill the application requirements. Figure 4.12 reports soft magnetic materials from Vacuumschmelze. Those in the highlighted region meet our specifications (i.e. high saturation potential and low coercivity).

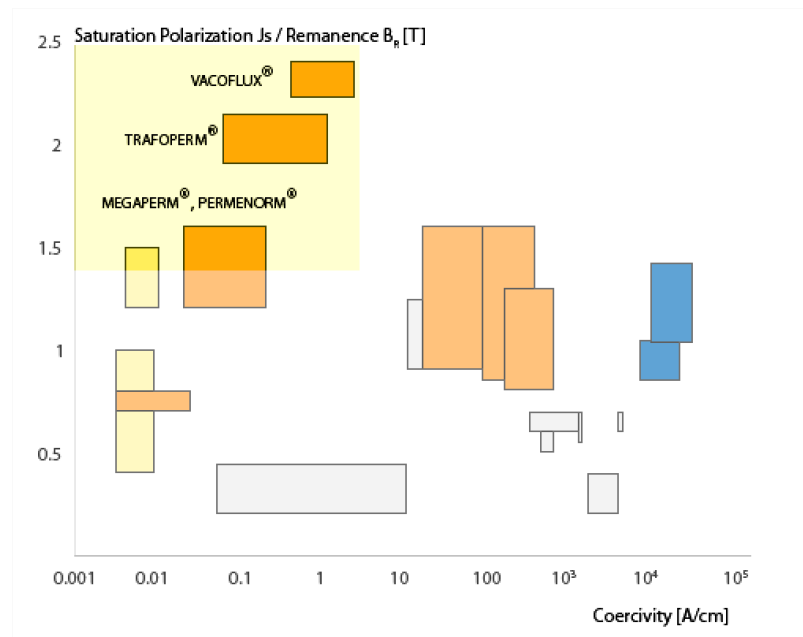


Figure 4.12: Vacuumschmelze's soft magnetic material product catalog displayed in terms of saturation magnetic induction as function of the coercivity (adapted from [136])

For our application, VACOFLUX 50 was chosen. The latter has the best saturation potential and good magnetic properties which make this material well appropriate for the present application. Properties of the VACOFLUX 50 are reported in the Table 4.2 below:

Table 4.2: Magnetic properties of the Vacoflux 50 which is used for the fabrication of the magnetic tips

VAC-product	Saturation Induction, B_{sat} [T]	Coercivity, H_c [A/m]	Relative Permeability, μ_r
Vacoflux 50	2.35	<0.8	13 000

The fabrication process of the magnetic tips has to be precise (resolution < 20 μm) and cost-effective. For this purpose, this was done by laser cutting using an Nd-YAG laser, with 1024 nm wavelength. This method is well adapted to cut metal sheet from 10 μm up to 1 mm. The cutting speed is typically 1.6 mm/s thus allowing the fabrication of more than 30 tips per hour. The heat affected zone is estimated to about 2-to 3 μm which is acceptable on a 100 μm wide tip.

4.3 SU-8 monolithic microchannels

As described, our microfluidic chip is made of PDMS and a glass slide. In this case, the magnetic parts have to be inserted from the side of the chip in between the glass and the PDMS part which is well appropriate for lab work [133, 137]. Nevertheless, this operation is not suitable for reproducible and automated positioning of the magnetic tips. Furthermore, the distance of the tips from the magnetic bead suspension in the channel is a critical parameter. It is defined by the sidewall thickness of the microchannel. However, thin PDMS sidewalls may be easily deformed when inserting the magnetic tips, resulting in inaccurate positioning and, in the worst case, in leaking microchannels. Here, we demonstrate the feasibility of a new fabrication technique used to make monolithic SU-8 structures providing a reliable solution for these issues. It provides an efficient design for the chip open recesses and sealed microfluidic structures, which are in close proximity on the same chip. The magnetic tips are typically 100 μm wide and the channel sidewall thickness is 40 μm . A schematic 3D view of the device is presented in Figure 4.13.

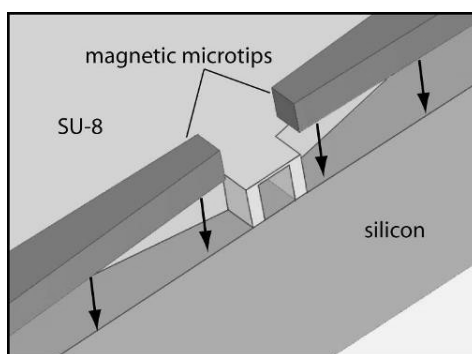


Figure 4.13: Schematic view of the microfluidic device for magnetic bead handling on-chip implementing a new fabrication process. This device requires, on the same chip, a monolithic sealed SU-8 channel and open recesses for easy insertion from the top and accurate positioning of the magnetic microtips in close contact with the rigid channel sidewalls. A high-UV absorption SU-8 layer is used to define the channel top membrane.

4.3.1 Motivation for the fabrication of a monolithic SU-8 channel

SU-8 photoresist is commonly used in the field of microfabrication as structural material or for molding of microfluidic devices as discussed above. One major limitation, however, is the difficulty to process partially freestanding SU-8 structures or monolithic closed cavities and channels on-chip. We propose here a simple method for the fabrication of suspended structures, in particular of monolithic SU-8 microchannels. The method is based on the processing of a SU-8 double-layer. Appropriate modification of the optical properties of the upper layer allows for selective crosslinking in the layer sandwich. This process is suitable for versatile layouts comprising open and hollow SU-8 structures on the same chip.

The negative epoxy-based photoresist SU-8 has a wide range of applications in the field of microfabrication. The possibility to process up to several 100 μm thick layers with high aspect ratio, as well as its optical transparency and chemical inertness explain the popularity of this material [138]. SU-8 masters are frequently used for molding of PDMS microfluidic channels as it is the case for our PDMS chip [139]. Even if standard SU-8 processing is routinely implemented in most microfabrication laboratories, a particular challenge consists in fabricating SU-8 structures with free-standing or suspended parts [138]. Here, we propose a new and robust technique to fabricate monolithic suspended SU-8 structures. In particular, we demonstrate the feasibility of creating closed SU-8 microfluidic channels on-chip, side-by-side with open structures. This degree of flexibility in SU-8 processing could not be achieved with other techniques presented so far.

Different approaches have been proposed in literature to fabricate SU-8 structures that are dissociated from the substrate. A positive photoresist (AZ-1518) was used as sacrificial layer for the fabrication of a SU-8 rotor for piezoelectric motors [140]. This method, however, may not be generally applicable, as the thickness of the sacrificial layer does not exceed a few micrometers. Furthermore, it has been observed that solvent diffusion at the interface strongly alters the SU-8 properties [141]. Bonding of two SU-8 layers was successfully implemented for the fabrication of SU-8 microchannels [142, 143]. With this technique patterned SU-8 films on two distinct wafers are brought in close contact and bonded by thermal treatment. This approach also allows for the fabrication of multilayer structures. Lamination of a dry film photoresist (Riston®)[144] or uncrosslinked SU-8 layers[145] was also reported to cover microchannels, but applying pressure on the substrate may make this process prone to failure.

Free-standing SU-8 structures can be obtained by selective polymerization of a top layer without affecting the underlying unexposed layer. The latter layer has the function of a sacrificial layer and can be dissolved to release the suspended part. Selective exposure of SU-8 is possible

using e-beam lithography [146], laser writing [147] or deep-UV lithography [148]. These approaches offer good results, but require particularly sophisticated equipments. Another successful method was the deposition of a thin aluminum film in between two SU-8 layers to stop light propagation during exposure of the top SU-8 layer [148]. Partial exposure of SU-8 was also achieved by using substrates coated with an antireflection layer [149] or by adding a positive resist (SC1827) to the SU-8 to increase UV absorption [150]. The latter method is comparable to our approach but addition of SC1827 may negatively affect the material properties of the SU-8.

In this work, we present and demonstrate a new approach for the fabrication of SU-8 monolithic suspended structures by using standard photolithography. Our method is based on the selective enhancement of the UV-absorption in the modified top layer of a SU-8 double-layer structure. This simple approach allows the fabrication of both long monolithic closed SU-8 microchannels and large suspended membranes.

4.3.2 Materials and methods

Our fabrication process is based on a SU-8 double-layer structure. Figure 4.14 schematically shows the process flow. Two SU-8 layers featuring different UV absorption spectra are superposed and processed. First, a standard SU-8 layer (GM 1070, Gersteltec, Switzerland) is spin-coated on a silicon wafer and processed (thickness 50 μm , 2000 rpm for 30 s, 400 mJ/cm^2 , mask 1). For microfluidic applications, this layer will define the height of the microchannel (Figure 4.14 a). Parameters for soft and post-exposure bake are indicated in table 1. The layer is not developed at this stage. Subsequently, the second SU-8 layer (GM 1060, Gersteltec) is spin-coated on top of the first one (20 μm , 1000 rpm for 30 s), soft-baked and exposed (Fig 1b, mask 2, 44 mJ/cm^2).

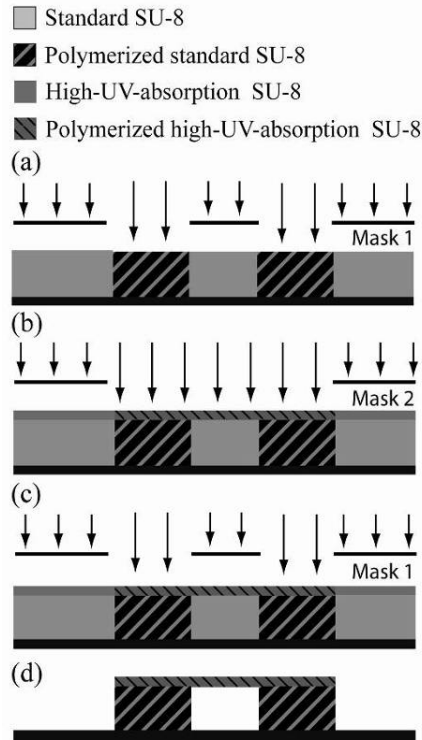


Figure 4.14: Fabrication process of a suspended SU-8 structure for a monolithic closed SU-8 microchannel. (a) A standard SU-8 layer is spin-coated on a silicon wafer, followed by a soft-bake, exposure to define the channel walls (mask 1) and a post-bake. (b) A second layer using a modified high-UV-absorption SU-8 is spin-coated, soft-baked and exposed to define the roof of the microchannel (mask 2). (c) Subsequent exposure through mask 1 improves the adhesion between the two SU-8 layers. (d) The SU-8 double layer is developed to release the microchannel.

The second SU-8 layer defines the thickness and shape of the suspended membrane in the final monolithic device. In order to fabricate the suspended structure, the optical properties of the second SU-8 layer have been modified. Exposure of the top layer must not affect underlying unexposed parts. We solved this issue by using a SU-8 film with enhanced UV-absorption, as is shown schematically in Figure 4.14 b. Enhanced UV-absorption is achieved by increasing the photoinitiator concentration of the standard SU-8 (GM 1060) by a factor k ($k=5$ or $k=10$; $k=1$ refers to the unmodified commercial resist). Different concentrations were prepared by mixing corresponding quantities of dissolved triarylsulfonium salt with SU-8.

To ensure good adhesion between the two superposed patterned SU-8 layers in the final structure and full crosslinking of the top SU-8 layer is required at the interfaces. This is achieved

by an additional exposure step through the first mask (Figure 4.14 c, mask 1, 30 mJ/cm²). After a final post-exposure bake, the wafer is developed in propylene glycol monomethyl ether acetate (PGMEA) for 16 minutes to release the microchannels and to remove encapsulated unpolymerized SU-8 (Figure 4.14 d). Soft-bake and post exposure bake temperatures and ramps are adjusted experimentally and are summarized in Table 4.3. The soft-bake parameters of the second layer are most critical as they affect also the properties of the underlying first layer. In order to avoid overheating of the first layer, the maximum temperature of the post-exposure bake is reduced from 130°C (value recommended by the supplier) to 80°C and the time was increased from 5 min to 120 min.

Table 4.3: Parameters for soft-bake (SB) and post exposure bake (PEB) of the first SU-8 layer and the two superposed layers for the fabrication of suspended structures

	1st layer Resist type: GM 1070		1st+2nd layer Resist type: GM 1070/modified GM 1060	
SB	30 \Rightarrow 130°C	50 min	30 \Rightarrow 80°C	25 min
	130°C	5 min	80°C	120 min
	130 \Rightarrow 30°C	50 min	80 \Rightarrow 30°C	25 min
PEB	30 \Rightarrow 80°C	30 min	30 \Rightarrow 90°C	20 min
	80°C	20 min	90°C	50 min
	80 \Rightarrow 30°C	90 min	90 \Rightarrow 30°C	90 min

4.3.3 Characterization of the modified SU-8 layers

Increasing the photoinitiator concentration in the upper SU-8 layer enhances absorption of UV-light. We take advantage of this property to minimize cross-linking of the underlying SU-8 in the double-layer during exposure. Figure 4.15 shows measurements of the transmitted light through a 20 μ m thick SU-8 layer (GM 1060) on quartz in the range of 280 to 420 nm. Transmission curves have been recorded for three different photoinitiator concentrations ($k=1$, 5 and 10) using a Lambda 900 spectrophotometer (Perkin Elmer, USA). For the wavelength of interest (Hg I-line, 365nm), the transmitted light for a standard SU-8 film ($k=1$) is 87% of the incident light. A fivefold increase of the photoinitiator concentration ($k=5$) results in a strong reduction of the transmitted light intensity to 69%. Further increase of the photoinitiator concentration still reduces the transmitted intensity, but the effect is less pronounced (59% for $k=10$).

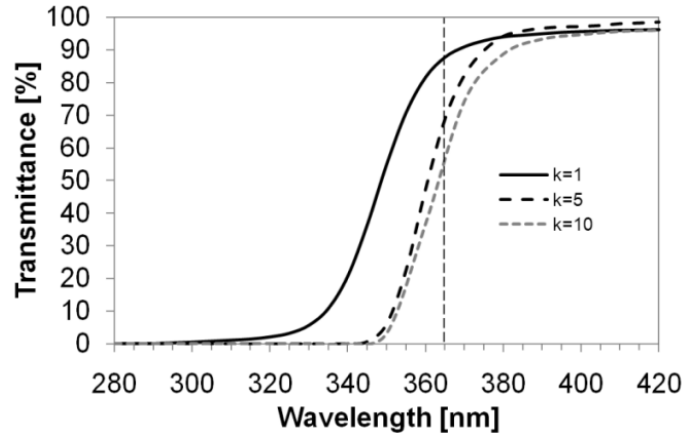


Figure 4.15: Transmittance of 20 μm thick SU-8 films (GM 1060) on quartz at different wavelengths as a function of the relative photoinitiator concentration k ($k=1$ refers to the standard concentration). In the modified films with 5 or 10 fold increase of the photoinitiator concentration a clear reduction of the transmittance from 87% to 59% is observed for the I line of the Hg spectrum (≈ 365 nm).

It is important for the fabrication of suspended SU-8 structures to control precisely the thickness of polymerization when exposing the upper layer of the sandwich. The latter was determined by backside exposure of a 20 μm thick single SU-8 film through a quartz wafer. Exposure at various doses results in polymerization of the film on the side in contact with the wafer, leaving an unpolymerized portion on top of it. After development, only the polymerized film remains on the wafer. Figure 4.16 shows the polymerization thickness as a function of exposure dose for two different photoinitiator concentrations (GM 1060, $k=1$ and $k=5$). Films with higher photoinitiator concentration ($k=10$) show bad uniformity, most likely due to an excessive amount of solvent.

The polymerization thickness as a function of the exposure dose is related to the contrast γ of the resist,

$$\gamma = \left[\log \frac{D^0}{D^i} \right]^{-1} \quad (4.4)$$

where D^0 is the dose required to reach full polymerization of initial film thickness. The critical dose D^i corresponds to the dose limit below which the complete SU-8 layer is dissolved during development (i.e. no polymerization occurred). In general, standard SU-8 formulations have high contrast, as is required for patterning thick layers with high aspect ratio. In our case, it is important to reduce the contrast of the top SU-8 layer in order to increase the window between

the critical exposure dose D^i and the exposure dose D^o that leads to complete polymerization of the layer. The corresponding values can be derived from Fig. 4 (D^o for a normalized film thickness of 1 and D^i for a normalized thickness of 0). We find $D^i=15$ mJ/cm² and $D^o=150$ mJ/cm² for the standard SU-8 film ($k=1$), and $D^i=9$ mJ/cm² and $D^o=250$ mJ/cm² for the modified SU-8 film (5 fold increased photoinitiator concentration, $k=5$), respectively. Using eqn. (1), we derive a contrast of 0.7 for the modified film, compared to 1.0 for the standard film. Increasing the photoinitiator concentration thus decreases the slope of the dose-thickness curve in Figure 4.16, allowing more precise control of the exposure of the modified top layer. As a consequence, residual polymerization of the underlying unexposed SU-8 can be efficiently avoided.

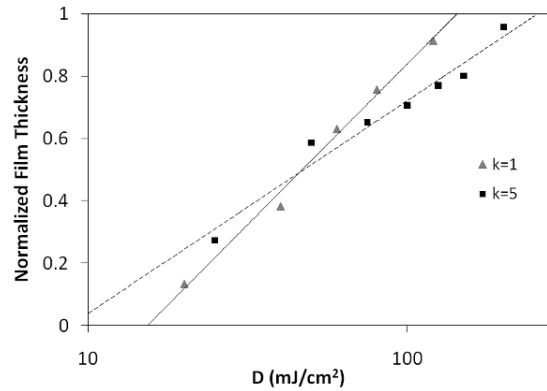


Figure 4.16: Polymerized SU-8 film thickness as a function of the exposure dose D , as obtained by backside exposure after development ($\lambda = 365$ nm, normalized with respect to the initial film thickness of 20 μm). Standard SU-8 ($k=1$, GM 1060) and SU-8 with a 5 fold increased photoinitiator concentration ($k=5$) are compared.

4.3.4 Monolithic SU-8 microchannels

Double layer sandwiches comprising a standard SU-8 film ($k=1$) and a modified SU-8 film ($k=5$) are processed as shown in Figure 4.13 to fabricate monolithic closed microfluidic channels on silicon substrates. The thickness of the lower layer, i.e. the channel height, is 50 μm and the thickness of the top layer is 20 μm , respectively. The exposure dose of the modified film is adjusted experimentally to 44 mJ/cm². According to Figure 4.16, this dose is sufficient to trigger crosslinking in about 10 μm of the modified upper SU-8 layer. Cross-linking of underlying unexposed structures may therefore be securely avoided. These “sacrificial” parts are fully dissolved during development, which is done after an additional exposure step (Figure 4.14 c) that allows to fully polymerize the 20 μm top layer at areas that are attached to the underlying SU8 structures.

Figure 4.17 shows scanning electron microscope (SEM) pictures of the cross-section of three monolithic SU-8 microchannels that have been fabricated with the new method. The

channel width is in the range of 50 to 200 μm with a length of 3 cm. Pictures of the cross-sections are taken in the middle of the channel and show the complete dissolution and removal of encapsulated unpolymerized SU-8 in the channel. Due to the choice of the exposure dose, the resulting final thickness of the suspended structure, i.e. the roof of the microchannel, is about 10 μm . The required fine adjustment of the polymerized layer thickness is only possible with the modified SU-8. Similar experiments using a SU-8 top layer with standard properties were not successful.

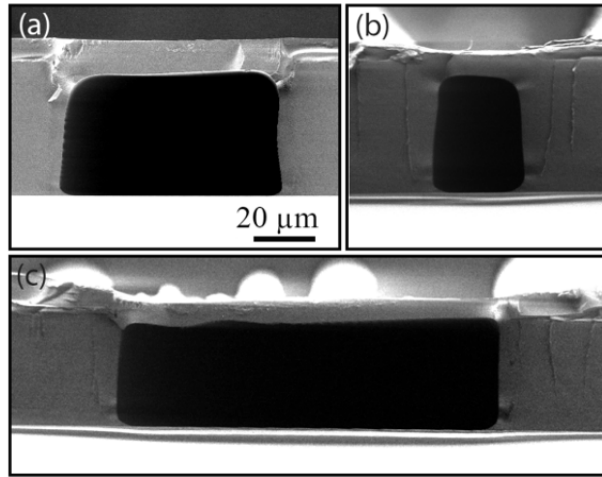


Figure 4.17: SEM pictures of cross sections of different monolithic SU-8 channels fabricated using a SU-8 layer with modified optical properties for the suspended channel top membrane. The nominal cross section areas are (a) $100 \times 50 \mu\text{m}^2$, (b) $50 \times 50 \mu\text{m}^2$ and (c) $200 \times 50 \mu\text{m}^2$ with a mean channel roof thickness of 10 μm . The channel length is several centimeters. Pictures are taken in the middle of the channel.

Only standard photolithographic equipment is required, the process can therefore be easily implemented in any microfabrication lab facility. This versatile approach opens new options for the design of microfluidic circuits or microdevices incorporating membranes. Certain drawbacks of commonly used PDMS microfluidic devices, related to the elasticity of the material for instance, as well as certain packing and interfacing issues, may be circumvented with this new technique.

5 Kinetics of the actuated bead plug

In this chapter, the physics and the dynamics of the plug of magnetic beads is discussed. The formation of a highly confined and dynamic plug of beads extending over the cross-section of the microchannel is enabled by superposing a static and a time-varying magnetic field. The latter is generated by an electromagnet and focused across the microchannel using microstructured soft magnetic tips. Finite element calculations of the magnetic force distribution compare well with the experiments. Our system allows improving the exposure of superparamagnetic beads to a microfluidic flow which is of particular interest for integrated LOC applications.

5.1 Bead capture and retention

The first important step of the assay protocol is the capture of the beads in-between the two magnetic tips. During this step, the system works in a similar way as a separation system where the magnetic beads have to be extracted from the liquid medium [151-154]. Beads are brought in proximity of the magnetic tips by the fluid flow where they are captured by the magnetic force. To control the number of beads for an assay, all the beads passing through the tips have to be captured.

5.1.1 Forces acting on a magnetic bead in a flow

Finite Element Method simulation was performed with Comsol multiphysics 3.4™. This technique was used to calculate the magnetic field distribution, forces on the beads and flow velocity. Both two-dimensional (2D) and tri-dimensional (3D) simulations were used during this work to gain a better understanding of the actuation principle. As discussed in Chapter 2, the force acting on superparamagnetic beads was calculated using the following equation:

$$\vec{F}_{mag} = (\vec{m}_{sat} \cdot \nabla) \vec{B} \quad (5.1)$$

$m_{sat} = \rho M_{sat} V = 1.78 \cdot 10^{-14} \text{ Am}^2$. $M_{sat} = 20 \text{ Am}^2/\text{kg}$ was taken from Figure 2.8 (chapter 2), $\rho = 1700 \text{ kg/m}^3$ is the density and V the volume of the particle [155]. The saturation characteristic of the material was also implemented using Vacuumschmelze® information. Figure 5.1 represents the function used to take in consideration the saturation of the magnetic tips. The relative permeability μ_r decreases down to 1 with increasing magnetic field induction (saturation is achieved for $B > 2.35 \text{ T}$).

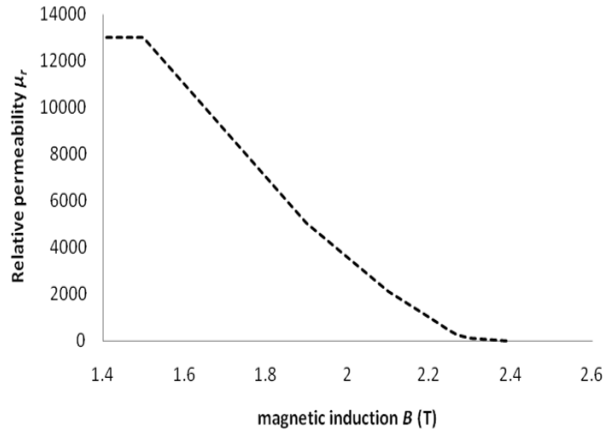


Figure 5.1: Approximated decrease of the relative permeability μ_r as a function of the magnetic field induction for the VACOFLUX 50. This function is used in Comsol multiphysics to account for the magnetic saturation of the material used for the magnetic tips.

2D simulations were used to map the force field in the microchannel. It is shown that 2D FEM simulation is sufficient to obtain qualitative information about the behavior of beads actuation. Nevertheless, a 2D FEM simulation does not give a precise estimation of the force or velocity of a bead. A 2D FEM simulation does not account the magnetic flux leakages in the vertical direction (out of the plane of the tips) and therefore does not allow a quantitative calculation of the magnetic force. 3D FEM simulations were therefore implemented in this work

to calculate quantitatively the force acting on a single bead and to take into consideration the magnetic flux leakages in 3D (section 5.3.2).

For a valuable estimation of the maximum flow rate which permits a complete capture of the beads it is important to consider the parabolic flow profile. The fluid velocity profile for a given flow rate may be estimated using a FEM simulation. Figure 5.2 shows the velocity of the liquid in a 100 μm wide microchannel using a flow rate of 5 nL/s. The maximum velocity of the liquid (in this case, 0.75 mm/s) is reached in the middle of the channel.

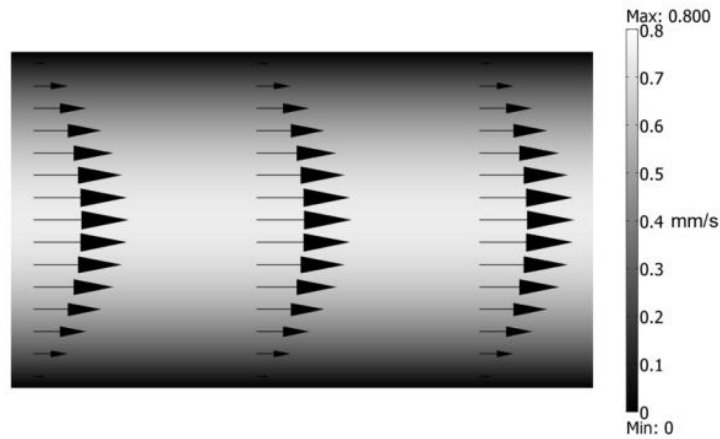


Figure 5.2. FEM simulation of the liquid flow velocity profile in a 100 μm wide microchannel using a flow rate of 5 nL/s. A maximum velocity of 0.75 mm/s is observed at the middle of the channel.

Bead release in a flow is shown in Figure 5.3. After removing the magnetic retention force, beads are released at different positions across the channel, thus they are subjected to different flow velocities. In this figure the parabolic flow profile can clearly be observed.

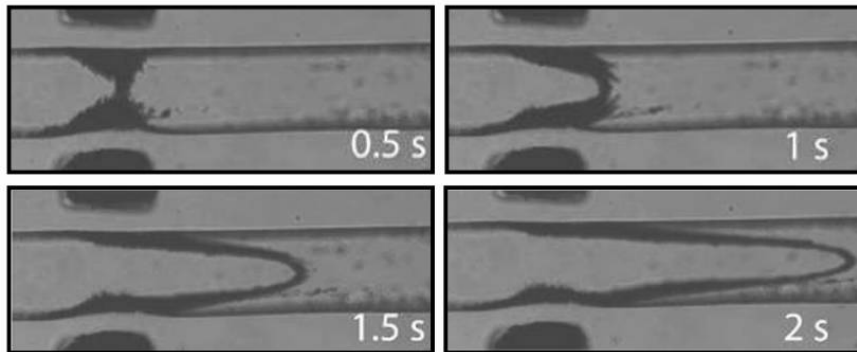


Figure 5.3: Photographs of the bead release process in a flow of 5 nL/s. The parabolic flow profile is observed during the release process of the beads.

5.1.2 Bead capture optimization

The maximum flow rate allowing a complete capture of the beads is evaluated. Beads arrive as a random dispersion in the proximity of the magnetic tips. Beads that are close to a channel side are easily deviated in the y-direction by the magnetic force and captured close to the tips at the channel wall (Figure 5.4 a). At this location the viscous drag force is low (due to the parabolic flow profile). Moreover, magnetic force components in the x-direction are high (proximity of the magnetic tips), thus the retention is more efficient. A critical situation occurs when a bead is in the middle of the channel, where the magnetic force in y-direction is low and therefore the bead is only weakly deflected (see Figure 5.4 b). In this case, the viscous drag force on the bead (x-axis) is high and may easily exceed the magnetic force and the bead can be flushed away as the maximum drag force is in the middle of the channel (Figure 5.2). Optimization of the bead capture performance is important to decrease the total assay time by increasing the maximum flow rate allowed during the capture step. Moreover, high retention forces allow for reliable and rapid exchange of the liquids and are therefore highly suitable throughout the experiment.

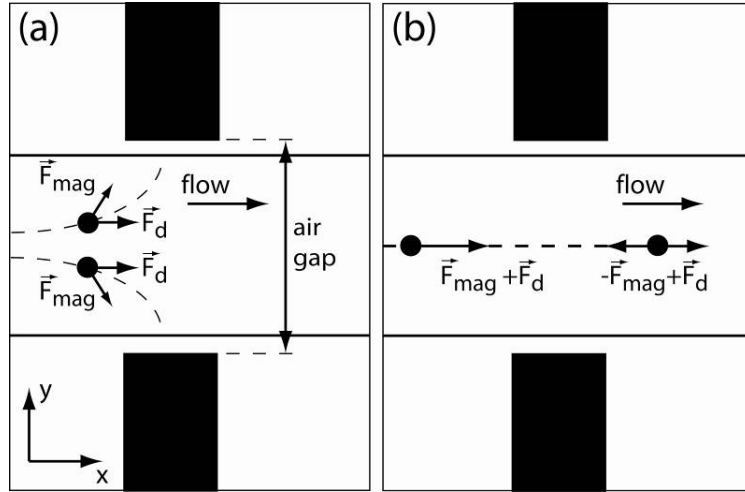


Figure 5.4: Principle of the bead capture with the viscous drag force \vec{F}_d and the magnetic force \vec{F}_{mag} acting on the bead. (a) Beads are deviated by the magnetic force and captured towards the tips. (b) Due to the symmetric field configuration, beads close to the middle of the channel experience only a weak $F_{mag,y}$ (in y-direction). Upstream of the magnetic tips $F_{mag,x}$ and $F_{d,x}$ are positive, whereas downstream of the tips, the magnetic force $F_{mag,x}$ becomes negative and has to overcome the drag force to retain the beads.

The magnetic force \vec{F}_{mag} in the middle of the channel (Figure 5.4 b) was calculated by FEM simulation in order to assess and improve the capture efficiency of the system. All simulations were done assuming that the beads are saturated ($B \cong 100$ mT) [133]. Figure 5.5

shows the influence of the air gap between the magnetic tips on the force $F_{mag,x}$. Using this FEM calculation it is possible to estimate the following dependence of the force magnitude $F_{mag,x}$ as a function of the air gap length l_{gap} .

$$F_{mag,x} \approx \frac{1}{l_{gap}^2} \quad (5.2)$$

The larger the air gap is, the weaker is the magnetic force. In our system, the air gap was minimized using adapted technologies to reduce the channel wall thickness. A fixed air gap of $180 \mu\text{m}$ was used throughout the experiments.

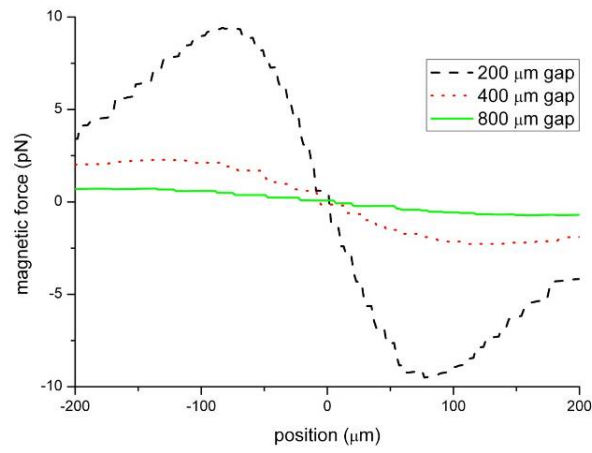


Figure 5.5: FEM calculated retention magnetic force $F_{mag,x}$ exerted on a $1 \mu\text{m}$ Dynabead bead in the middle of the channel for different air gaps between the magnetic tips. Increasing the air gap leads to a strong reduction of the magnetic force ($x=0$ is the symmetric axis of the tips).

The influence of the tip width on the magnetic force was shown to be small compared to the influence of the air gap (see Figure 5.6). Therefore a $100 \mu\text{m}$ tip was chosen to confine the beads in small volume ($< 1 \text{ nL}$). Moreover, the thin channel wall in contact to the magnetic tips is a fragile part of the chip and therefore minimizing its length improves the reliability of the chip.

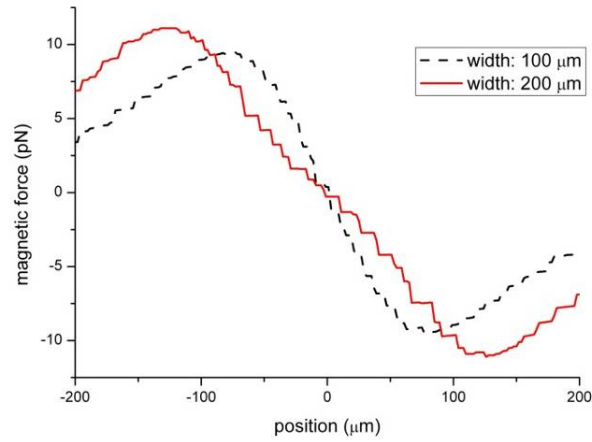


Figure 5.6: FEM calculated retention magnetic force exerted on a 1 μm Dynabead bead in the middle of the channel for different tip widths. ($x=0$ is the symmetric axis of the tips).

Combining the drag force (calculated using Figure 5.2 and eqn (2.16)) with the FEM simulated magnetic force field acting on a single bead, it is possible to estimate the upper flow rate limit for a complete bead capture. Figure 5.7 a shows the magnetic force field without flow in the microchannel. Adding the drag force calculated by FEM simulation (flow rate of 5 nL/s, Figure 5.2) results in a non-symmetrical force field (see Figure 5.7 b). In this situation, at any location of the microchannel, the magnetic force is sufficiently high to capture all the beads. Increasing the flow rate up to 10 nL/s results in the situation shown in Figure 5.7 c. In this case, the beads close to the middle of the channel might not be captured as the drag force is higher than the magnetic retention force in x-direction. Introduction of the beads in the system was therefore done at a flow rate up to 5 nL/s.

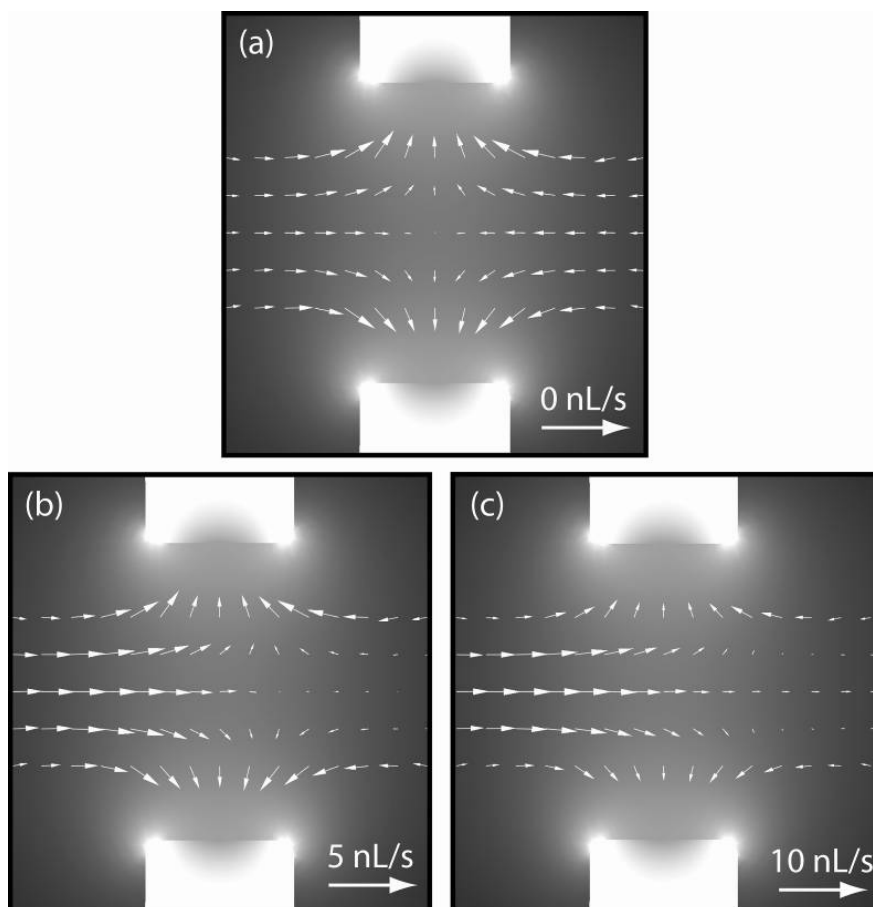


Figure 5.7: Field of FEM calculated forces exerted on a single Dynabead in the microchannel in between the magnetic tips. (a) Field of force without flow in the channel (purely magnetic). (b) Field of forces with a flow rate of 5 nL/s. The magnetic force overcomes the drag force after the tips. This configuration leads to a complete capture of the beads. (c) Field of forces with a flow rate of 10 nL/s. The magnetic force cannot overcome the drag force in the middle of the channel. A weak net force in the flow direction persists. This configuration leads to an incomplete capture of the beads.

An experiment was carried out to illustrate the total capture of the beads for a 5 nL/s flow rate. Figure 5.8 a shows that all the beads visible on the left part of the tips are captured. For a flow rate of 10 nL/s, some beads can be detected in the downstream flow (Figure 5.8 b) confirming the expected behaviour.

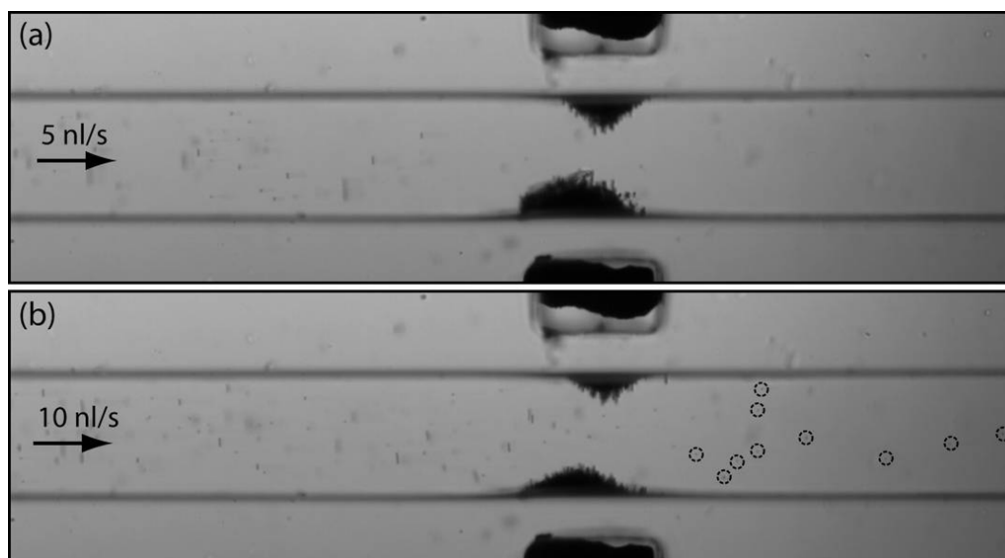


Figure 5.8: Photographs taken during bead capture. (a) Complete capture of the beads arriving from the left using a flow rate of 5 nL/s. (b) Using a flow rate of 10 nL/s leads to an incomplete capture of beads. Some beads may be observed after the retention system (dashed circles).

5.2 Bead actuation principle

An important parameter to optimize the sensitivity of an on-chip immunoassay is the number of magnetic beads compared to the number of Ag's present in the sample solution. Decreasing the number of beads is an advantage to reach a low detection limit. To allow decreasing the number of beads while keeping good Ag capture probability, a rapid cyclic motion of the beads perpendicular to the flow is of interest.

5.2.1 Bipolar configuration

As a first approach, a simple bipolar magnetic system using two soft magnetic tips without permanent magnets was tested (Figure 5.9). The 2D FEM simulation of Figure 5.9 b, shows a symmetric magnetic field with respect to the channel axis. In the experimental situation of Figure 5.9 c, a 20 Hz alternating magnetic field is applied to the tips, but no bead motion can be induced. Superparamagnetic beads are simply attracted towards the poles and form static plugs on the channel walls, even if a time-varying field is applied. Such very dense bead plugs are obviously not ideal for efficient perfusion with a liquid. Ferrimagnetic beads, having higher coercivity form rotating chains in such a bipolar field configuration [106]. In the present work, superparamagnetic beads are mandatory for release of the beads after an Ag's capture prior to detection.

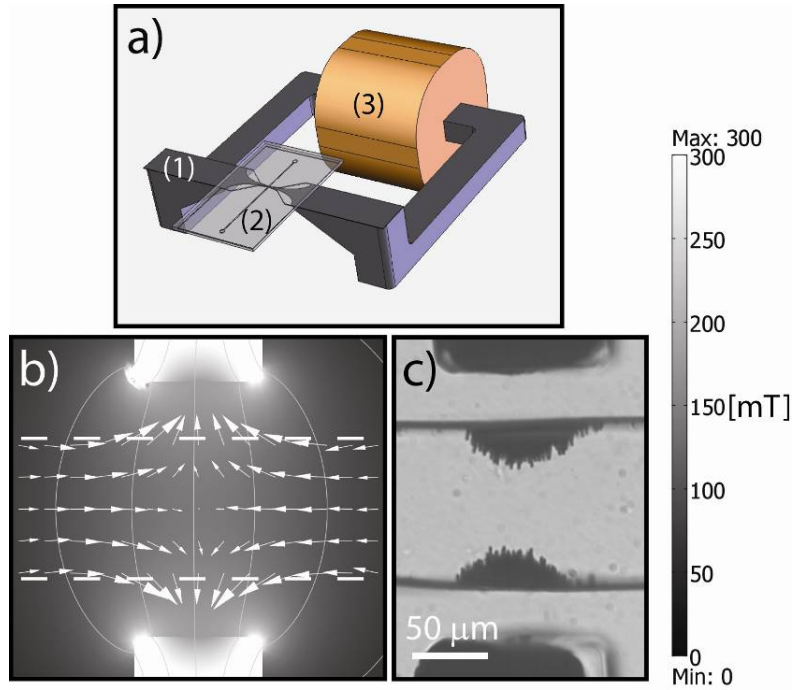


Figure 5.9: (a) Schematic view of the bipolar system with the magnetic tips (1), the microchip (2) and the external coil (3). (b) 2D FEM simulation of the magnetic induction B for a bipolar magnetic configuration (without permanent magnets). Arrows represent the force field acting on a magnetic bead. (c) Enlarged view of the region of interest in the microchannel. Two static magnetic bead plugs appear in the bipolar system even when a time varying field is applied through the tips.

5.2.2 Quadrupolar actuation system

A simple actuation system is of importance in this work to allow easy integration into the final prototype (see chapter 8). In this work, the strong magnetization of permanent magnets was used together with the tunable field produced by the electromagnet. The relatively weak magnetic field produced by the electromagnet is focused across the microchannel using magnetic tips placed in close contact to the channel (see before) while two permanent magnets are placed at several millimeters away from the magnetic tips. This configuration allows minimizing the number of microfabricated elements to only two micrometer-sized tips.

Adding two permanent magnets to the bipolar system, as schematically shown in Figure 5.10, results in a magnetic quadrupolar configuration that fundamentally changes the actuation properties. Using this configuration, it is possible to generate a cyclic motion of the beads across the channel, i.e. perpendicular to the liquid flow. In our quadrupolar magnetic system, the magnetic field produced by the permanent magnets in the region of interest is estimated to about 100 mT. Amplitude and frequency of the time-varying field between the soft magnetic tips can

be adjusted by changing the current amplitude in the coil in order to modify the dynamic behavior of the beads (see section 5.3).

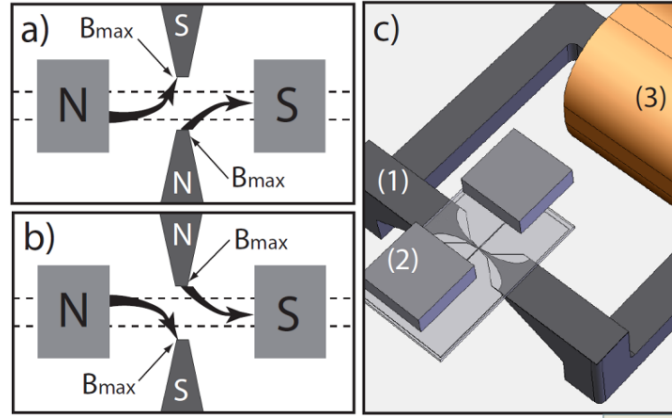


Figure 5.10: Schematic view of the active region with indication of the magnetic field, when using (a) a positive and (b) a negative coil current. (c) Microfluidic chip and magnetic actuation system: soft magnetic tips (1) are inserted in the chip from the side, while two (removable) permanent magnets are positioned on top of the channel. The time-varying field applied to the tips is generated by an external coil (3).

Symmetric magnetic field configuration

Figure 5.11 shows a 2D FEM simulation of the magnetic field induction $B \equiv |\vec{B}|$ for the quadrupolar configuration. The magnetic force field acting on a bead, calculated using equation (5.1) in the FEM simulations, is represented by arrows. By positioning the two permanent magnets symmetrically with respect to the tips, the resulting total field has point-symmetry. Beads are attracted to the corner of the magnetic tips where the field has a maximum. Inverting the coil current shifts the field maxima to the opposite tip. The magnetic force drives the beads alternatively across the channel with the frequency of the applied time varying field.

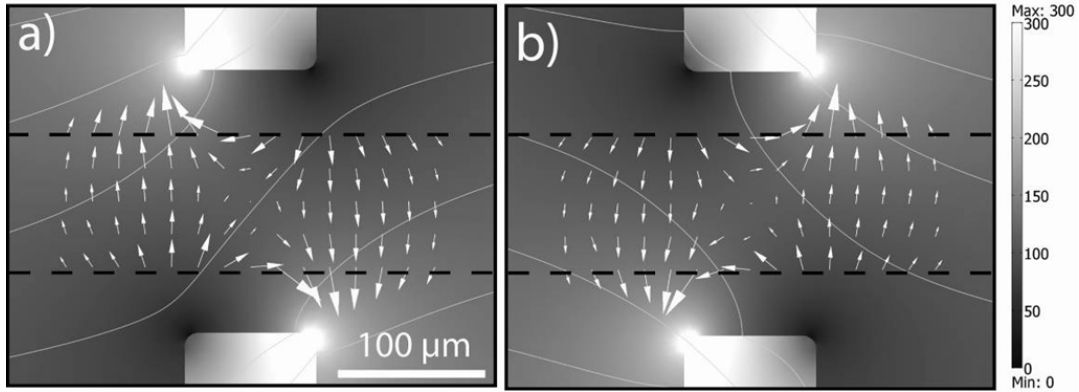


Figure 5.11: 2D FEM simulation of the symmetric quadrupolar field configuration: Magnetic field induction B for a positive (a) and negative (b) coil current (intensity in [mT]). The two permanent magnets are positioned at equal distance from the tips (symmetric configuration). Arrows represent the magnetic force field exerted on a superparamagnetic bead.

The dynamic behavior of the beads is illustrated in the photographs in Figure 5.12. The experiments show that the beads split into two distinct plugs. The two plugs cross the microchannel in opposite directions when the current polarization in the electromagnet is inverted. At low field frequencies, two dense bead plugs form temporarily on each side wall (Figure 5.12).

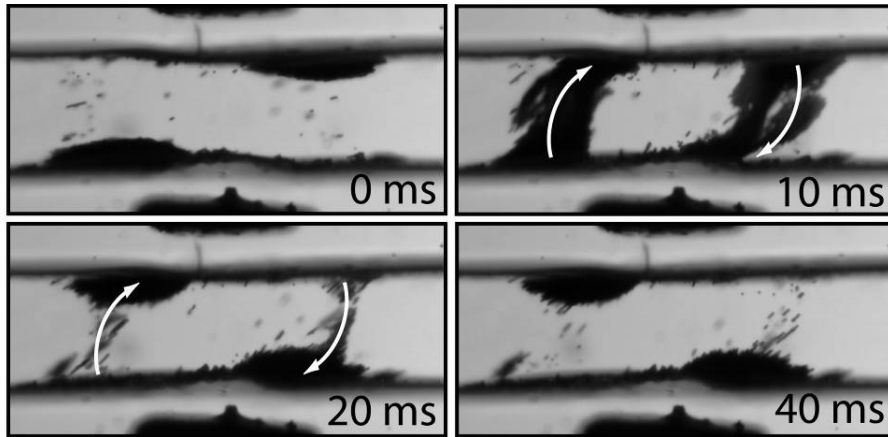


Figure 5.12: Bead plug dynamics between the magnetic tips in a symmetric quadrupolar field configuration. The sequence of photographs shows two distinct plugs of beads crossing the channel in opposite directions for a low field frequency (here 7 Hz), formation of dense plugs on the side walls is observed.

The kinetic behavior of the plugs changes significantly for higher frequencies. Figure 5.13 shows plugs actuated at 60 Hz in a symmetric quadrupolar configuration. In this case, a large portion of the beads stays in the middle of the channel. The bead chain orientation corresponds to the field lines obtained by FEM simulation (see Figure 5.11). When the current polarization is

changed, rotation of the bead chains is observed (Figure 5.13). Increasing the actuation frequency up to the limit where beads do not have time to cross completely the microchannel, results in plugs with larger cross section and higher porosity. This feature is advantageous for a better plug perfusion and higher analyte capture probability.

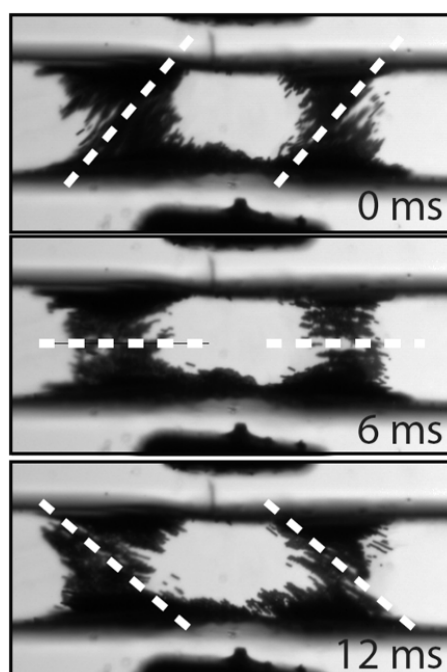


Figure 5.13: Sequence of photographs showing two distinct plugs of beads moving across the channel for an AC field frequency of 60 Hz. Chains form along the field lines and change orientation. Dashed lines represent the main orientation of the bead chains.

Asymmetric magnetic field configuration

In order to increase the sensitivity of fluorescent-based immunoassays or agglutination tests, the number of Ag's captured on the magnetic beads has to be maximized. For a given analyte concentration range, this can be achieved by minimizing the number of beads in the capture plug while keeping a high Ag capture probability. For that reason, we introduced a slightly asymmetric positioning of the permanent magnets in our system. The resulting magnetic actuation forces are higher on the left side of the tips compared to the right side (Figure 5.14 a). With this configuration, beads are confined in a single dynamic plug moving between the tips as shown in Figure 5.14b. In this way, the total number of beads for protein capture may be reduced by a factor of two without reducing significantly the capture efficiency. The asymmetric configuration will be used in the remainder of this thesis. Beads are retained in this confined volume, even in the presence of viscous drag forces imposed by a solution flow.

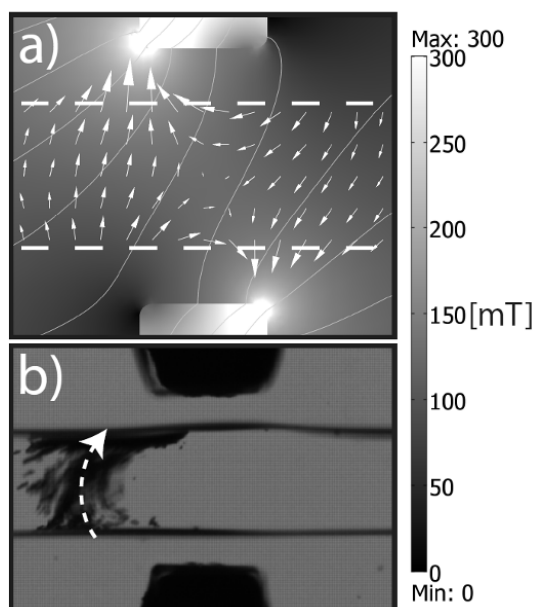


Figure 5.14: Asymmetric quadrupolar field configuration: (a) FEM simulations of field and force of the system with an asymmetric positioning of the permanent magnets with respect to the tips. In the present case, the asymmetry results in an increase of the magnetic force on the left hand side of the magnetic tips. (b) A single dynamic bead plug forms and moves in between the tips.

5.3 Analysis of the kinetic behavior of chains and clusters

Characterization of the dynamic plug of beads in the system is of importance for optimization of the beads actuation and retention efficiency. In this section, the dynamic of the plug as a function of the frequency and the field amplitude is discussed. The motion of beads starting from a single bead behavior to larger clusters in a magnetic field is studied. The importance to consider the clustering of beads in the plug dynamic is highlighted.

5.3.1 Dynamic properties of the actuated bead plug

For efficient analyte capture from a solution flow, a magnetic bead plug extending across the microchannel needs to be generated. The shape and dynamics of the bead plug formed by magnetic retention depends on the magnetic field parameters. Amplitude and frequency of the time varying field between the soft magnetic tips are modulated by changing the current in the external electromagnet. The constant magnetic induction of the permanent magnets is estimated to 100 mT in between the tips. Figure 5.15 a and b demonstrate the plug behavior for time varying field amplitudes higher than the static field (about 200 mT in the center region). Beads

are attracted towards the tip corners, where the total magnetic field has a maximum, and form two dense and diagonally opposite plugs. Changing the polarity of the coil current moves the field maxima and results in a lateral shift of the plugs along the channel walls. 2D FEM simulations show that the force acting on a bead is strongest near the tip corners (Figure 5.15 a and b).

For time-varying field amplitudes comparable to the static field strength (i.e. in the range of 100 to 150 mT), the transversal forces are higher than the lateral forces. As a consequence, the beads are no longer immobilized on a side wall of the channel, but cyclic motion across the channel occurs (Figure 5.15 c and d). This dynamic plug configuration is of particular interest for the present application. All beads are confined in the area in between the tips, while crossing from one side of the channel to the other and vice-versa, with the frequency of the applied field. Finally, if the AC field is weak compared to the permanent field, static attraction of the beads towards the channel walls near the tips is observed (Figure 5.15 e and f).

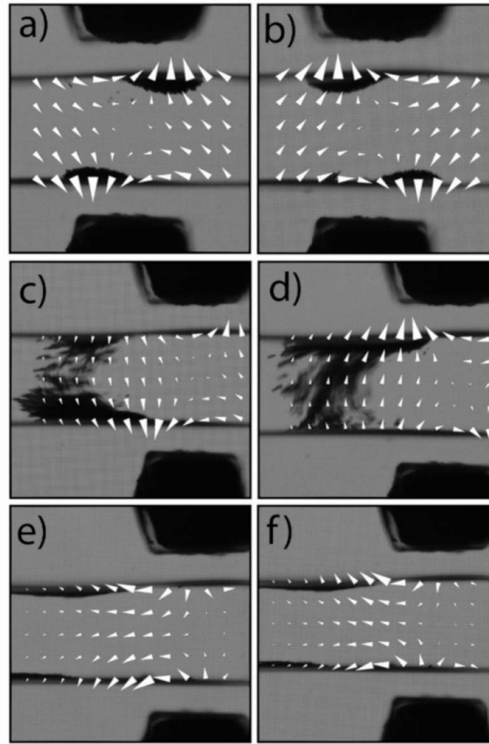


Figure 5.15: Bead plug actuation ($\approx 2 \times 10^4$ beads) in the microchannel in between the magnetic microtips. Arrows represent 2D FEM simulations of the magnetic force field. a) and b): Dense plugs form for AC field amplitudes larger than the permanent field. Alternating lateral displacement of the two plugs on the channel side walls is observed. c) and d): For comparable time-varying field and permanent field strength, beads move across the microchannel with the frequency of the applied field. A single well-confined dynamic plug is formed by a slightly asymmetric arrangement of the permanent magnets (higher forces on the left-hand side in the present case). The applied time-varying field is sinusoidal. e) and f) Time-varying field < static field with a positive (e) and negative (f) current (10 mA). Beads are permanently attracted towards the channel walls.

In Figure 5.16 a, the frequency of the time-varying field applied through the magnetic tips is 20 Hz. At this frequency, nearly all beads move from one side of the channel to the other, forming alternatively a dense plug on each side wall. Even if the bead plug extends temporarily over the whole channel cross-section, the plug motion is discontinuous. Increasing the frequency of the magnetic field to 70 Hz, results in continuous bead motion and a more uniform plug distribution Figure 5.16 (b). At this frequency not all beads may cross the channel, and a significant amount remains confined in the center region of the channel. This dynamic plug moreover extends over the whole cross-section of the microchannel. Perfusion with analyte solution of a plug showing this kinetic behavior is efficient, thus the probability for a bead to encounter a target Ag increases.

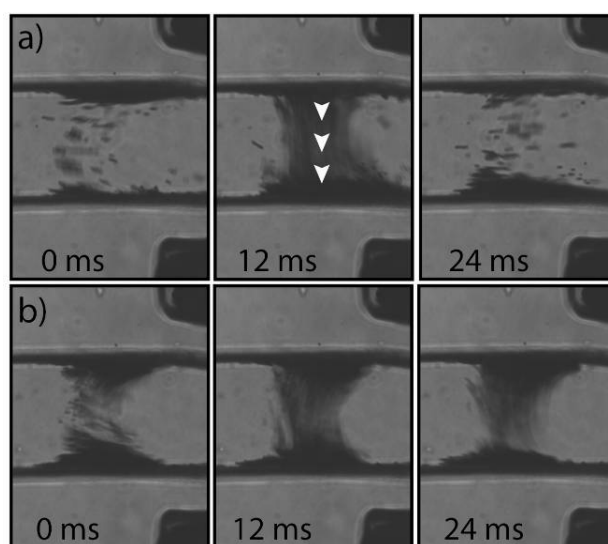


Figure 5.16: Dynamic bead plug sequences in the microchannel for two time-varying field frequencies (sinusoidal, time-varying field amplitude \cong permanent field strength). a) At 20 Hz, discontinuous displacement of the beads from one channel wall to the other with the formation of discrete plugs close to the tips; b) At 70 Hz, continuous motion of beads in the center of the channel, resulting in a more uniform plug distribution. The latter dynamic plug configuration allows efficient perfusion by the analyte solution.

5.3.2 Motion of single beads and clusters in the magnetic field

To fully understand the behavior of the beads in our device, the trajectory of a single bead was analyzed to compare its predicted behavior calculated by FEM simulation and its experimental behavior. Figure 5.17 a is a 2D FEM simulation of the magnetic actuation force superposed by two dashed curves representing the trajectories of two single beads, shown in Figure 5.17 b, c, respectively. The trajectories are obtained from a sequence of photographs obtained using a high-speed camera. The time lapse between start and end position is 105 ms and

121 ms, resp., for the sequence of Figure 5.17b and c, respectively. The trajectories of the beads are clearly parallel to the force field shown in Figure 5.17a.

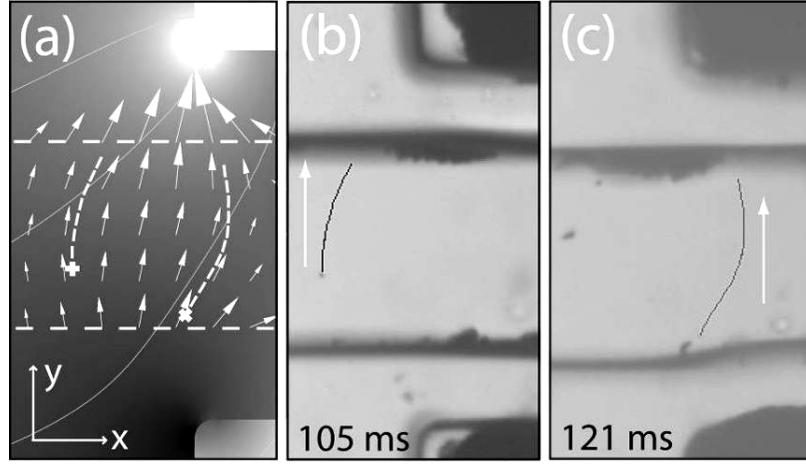


Figure 5.17: Comparison of the FEM simulated forces with the experimental trajectory of single superparamagnetic beads. (a) 2D FEM simulation of the magnetic induction. The white dashed lines indicate the experimental traces of the single beads shown in (b) and (c) (two sequences of high-speed photo recordings).

For better quantification of the force, we have performed more elaborate 3D FEM simulations and find a force $\vec{F}_{mag} = 6$ pN acting on a single bead in the middle of the channel (see Figure 5.18). A corresponding bead velocity of 0.6 mm/s can be calculated by equalizing the magnetic actuation force to the hydrodynamic drag force. We compare the thus calculated force and velocity with the experimental data, that are somewhat below theory. This difference may be attributed to effects that cannot be properly taken into account in the simulation (e.g. variation of the material properties and local saturation of the magnetic tips, incomplete saturation of the beads, etc).

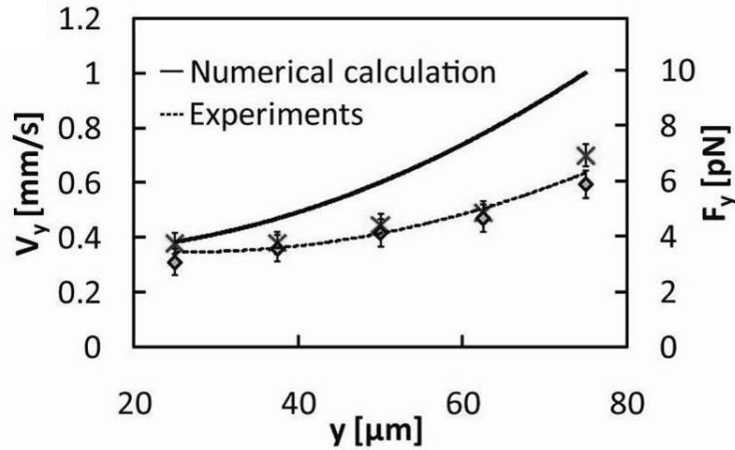


Figure 5.18: Experimental and calculated velocity (left axis) and force (right axis) of single beads along the y direction.

This experiment shows that a 2D FEM simulation is adequate to predict the qualitative behavior of single beads in the system in function of the different parameters (i.e. current, tips geometry, etc.). A 3D simulation is needed to give an acceptable approximation of the velocity of single beads.

The dynamic bead plugs shown in Figure 5.16 are not solely composed of single beads. In the presence of a magnetic field, superparamagnetic beads form chains and clusters due to the magnetic dipole interaction between the magnetic moments induced in the beads. Clustering, however, has a strong impact on the bead velocity in a given magnetic field configuration, thus the dynamic properties of the plug. It was also shown earlier that hydrodynamic interactions between beads aid the capturing of magnetic beads and may have an impact on their manipulation in a microfluidic device [156, 157].

Thus, interaction between beads in the presence of a magnetic field, in particular the formation of chains and clusters, has to be considered for a realistic description of the system. In the following, we analyze how this affects the characteristic parameters and performance of the system compared to the previously described behavior of single beads [133]. As illustrated in the image sequence in Figure 5.19 a, there is experimental evidence that the velocity increases with the number of aggregated beads. The photographs show a single bead, bead chains with different lengths and clusters moving across the microchannel in the presence of a magnetic field. The relative distance of aggregates with different size increases in time, indicating their velocity difference. These aggregates are schematically displayed in Figure 5.19b-d. Chains and clusters are oriented parallel to the magnetic field lines. We determined experimentally the mean velocity of different aggregates by analyzing image sequences taken with a fast video camera (Pixelink PL-

B741U, Ottawa, USA). Quantitative data of the velocity for single-stranded chains comprising up to 17 beads are reported in Figure 5.20 in section 5.3.3. In our system, the speed of a single bead crossing the microchannel is typically 0.4 ± 0.1 mm/s, whereas a doublet travels with a speed in the range of 0.8 ± 0.1 mm/s. Larger chains may move up to 3 times faster than single beads.

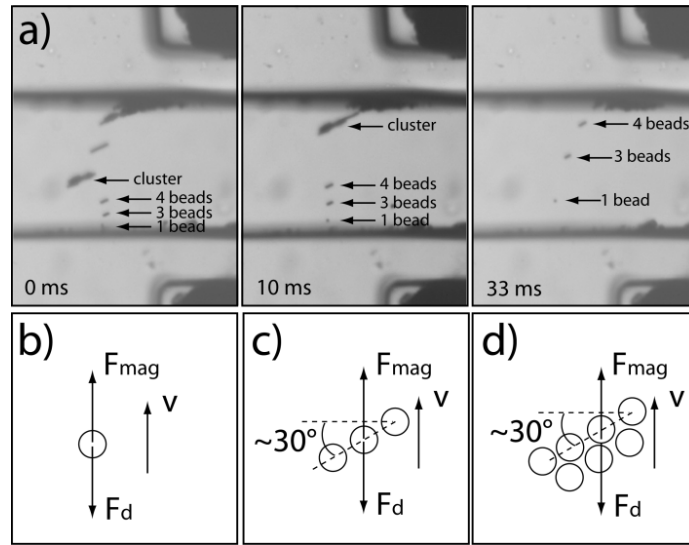


Figure 5.19: a) Sequence of photographs (time lapse 33 ms) taken with a high-speed camera showing bead aggregates of different size crossing the microchannel in the presence of a magnetic field. An increasing distance in time indicates a higher velocity of the larger aggregates. Three configurations are considered for theoretical analysis: b) a single bead, c) a single stranded chain and d) a cylindrical cluster. F_{mag} and F_d are the magnetic and the viscous drag force, respectively.

5.3.3 Theoretical models for chain and cluster motion

In literature, the magnitude of the magnetic force F_{mag} and the viscous drag force F_d are generally considered for a single bead [95, 133]. In steady state conditions, both forces are equal and the equilibrium velocity of a single bead can be derived. The particular dynamic behavior of chains or clusters in a viscous medium under the presence of a magnetic field is often not taken into account. It was shown previously that the velocity of a chain increases with the number of magnetic beads for motion parallel to its axis [117, 158]. Sedimentation of magnetic clusters with a relatively large number of beads was also discussed for motion parallel or perpendicular to the symmetry axis [159, 160]. With the dynamic plug configuration in the present device, motion perpendicular to the chain axis is of particular interest.

We consider the fluidic resistance of a cylindrical object as a general model for chains and larger clusters. An approximation for the drag force on a cylinder moving perpendicular to its axis was given as [117, 161]

$$F_{d,cylinder} \approx \frac{C_1 \pi \eta v a}{\ln\left(\frac{2a}{b}\right) + C_2} \quad (5.3)$$

where a is the length and b the radius of the cylinder, η is the viscosity of the medium and v is the velocity of the bead. It was pointed out by Derks *et al.* that the dimensionless constants C_1 and C_2 in eqn (5.3) depend on the experimental conditions [117].

Assuming that the magnetic force exerted on a chain of beads is directly proportional to the number of beads,

$$F_{mag,chain} = n F_{mag,bead} \quad (5.4)$$

where n is the number of beads in a chain (with $a=2rn$, r is the bead radius) and equalizing this force to the viscous drag force of eqn (2.16), results in the logarithmic dependence given by equation (5.5).

$$v = A \ln(n) + B \quad (5.5)$$

The fit of the experimental data based on eqn (5.5) is shown in Figure 5.20 (with $A = 0.36$ and $B = 0.43$). A similar behavior was found by Derks *et al.* for chains moving parallel to the axis in a dedicated mm-sized magnetic bead manipulator with a static magnetic field configuration [117]. Our findings show that this logarithmic law also holds for motion perpendicular to the symmetry axis and on the scale of a microchannel.

Analytical approximations for the viscous drag force for chains of 2, 3 and 4 beads have been derived by Burgers [161, 162]. These expressions take into account the distortion of the Stokes field around one bead flowing behind another bead. A frictional coefficient λ was introduced that accounts for the fluidic resistance experienced by the chain, i.e. for the increase of the drag force ($F_{d,bead} / F_{d,chain} = \lambda_n$ with $\lambda_n < 1$). As an example, the resistance coefficient for a bead pair is given by [161].

$$\lambda_2 = \frac{1}{2} \left(1 + \frac{r}{l}\right) \quad (5.6)$$

where r is the bead radius and l is the distance between the centers of the outer spheres of a chain (valid for small r/l and random chain orientations). Assuming that beads are in close contact ($r/l=0.5$), due to magnetic attraction for instance, we obtain $\lambda_2^{-1} \cong 1.33$. For saturated beads, the magnetic force is proportional to the number of beads, thus a pair of beads is expected to travel

1.5 times faster than a single bead. According to the same model, we obtain $\lambda_3^{-1} \cong 1.65$ and $\lambda_4^{-1} \cong 1.95$ for 3 and 4 beads in close contact, respectively. Chains with four beads are therefore expected to travel two times faster than single beads in a given magnetic field. It is interesting to note that the effective fluidic resistance per bead decreases when their number in the chain increases. Velocity values for 2, 3 and 4 beads have been calculated with this model and are indicated in Figure 5.20. We find that the calculated values for small chains correspond well to the logarithmic increase derived for the cylindrical model discussed above. From this result, we conclude that a simplified cylindrical model based on eqn (5.3) is a valid approach to describe the kinetics in this type of magnetic bead-based systems using the empirically determined constants $C_1=3.8$ and $C_2=-0.17$. These constants differ from the values proposed by Burgers for a cylinder ($C_1=8$ and $C_2=0.5$) due to the pearl-like shape of the chains. [161, 163] .

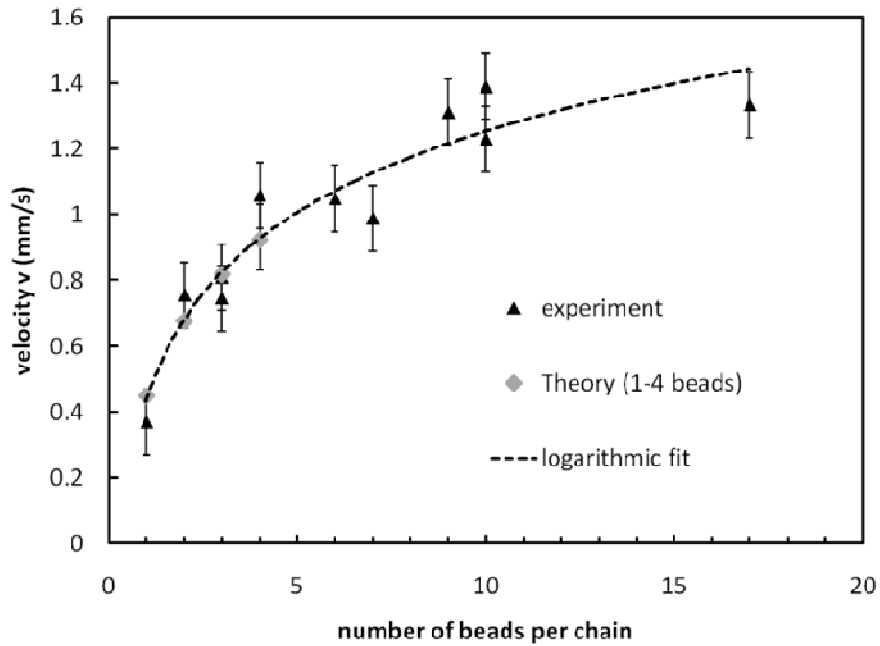


Figure 5.20: Velocity of single-stranded chains vs number of beads in the chain for motion across the microchannel in the magnetic field. Error bars are related to the pixel resolution of the camera. The fit of the experimental data derived from a cylindrical model for the chains (dashed line) shows a logarithmic increase of the velocity. Calculated values based on an analytical approximation taking into account the real shape of the chains are also indicated (for 1 to 4 beads).

6 Agglutination assay on-chip

In this chapter, one of the first agglutination assays using magnetic beads is presented using the integrated magnetic actuation system. A simple detection method based on the swelling of the released bead plug after aggregation allows for quantitative detection of the targets Ag's.

6.1 Evaluation of the capture efficiency by fluorescence measurements

Actuation of the dynamic bead plug is expected to increase the exposure of the functionalized bead surfaces to the analyte flow. Using a dynamic actuation of the beads, the capture is not limited by the intrinsic diffusion time of Ag's towards the beads. This important feature results in improved capture efficiency. This could be demonstrated in a semi-quantitative manner using fluorescent detection of fluorescein isothiocyanate FITC-conjugated anti-streptavidin (Rockland, Gilbertsville, PA, USA) captured on the streptavidin-coated beads. The principle of the test is schematically shown in Figure 6.1. Beads are first captured in-between the magnetic tips. Subsequently, a solution of (FITC)-conjugated anti-streptavidin is flushed through the plug of streptavidin-coated beads. Two cases were studied. (i) static plugs of beads immobilized on the channel wall, and (ii) a dynamic plug of beads. Subsequent fluorescent detection was always performed in a dynamic actuated plug in order to compare average signals for both capture modes (Figure 6.2 a).

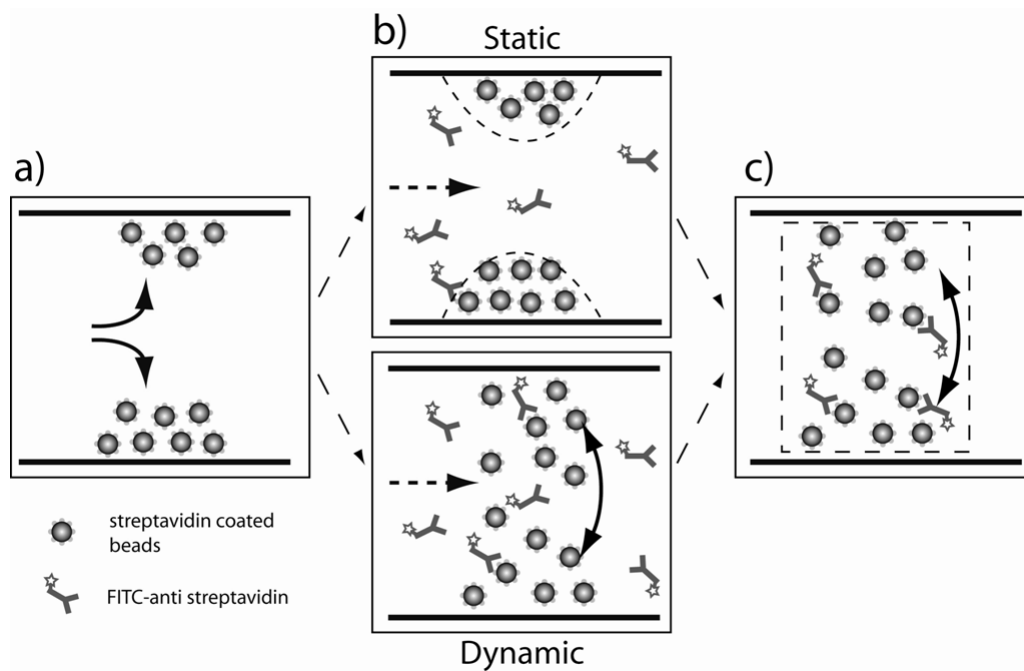


Figure 6.1: Schematic of the experiment used to assess the capture efficiency of a dynamic plug vs. static plug. (a) beads are capture and immobilized. (b) FITC conjugated anti-streptavidin is flushed through a static or a dynamic plug. (c) The fluorescent signal is detected in a dynamic plug configuration.

Perfusion with the analyte solution was either carried out with a dynamic plug (actuated at 70 Hz) or with static dense plugs (0 Hz), respectively. For the Ag capture, a volume of 250 nL analyte solution ($[5 \mu\text{g/mL}]$) was driven through the microchannel during 100 seconds. Figure 6.2b compares the two capture modes and shows an about 3-fold increase of the fluorescent signal for analyte capture in the dynamic mode. Static bead plugs on the channel side walls clearly entail weak perfusion by the analyte flow and reduced capture efficiency.

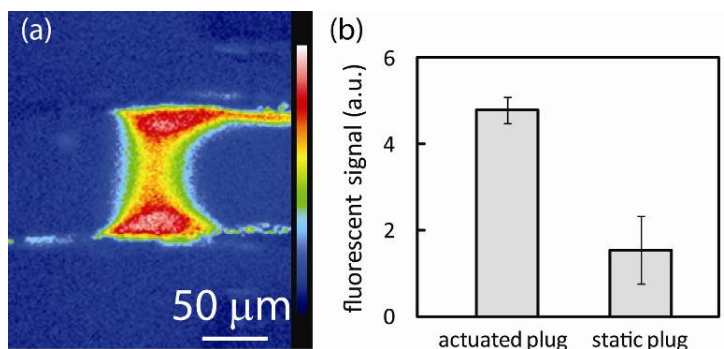


Figure 6.2: a) The fluorescent signal is recorded as mean value in the dynamic mode after capture of the analyte. b) Increase of the capture efficiency with the dynamic bead plug with respect to static plugs. FITC-conjugated anti-streptavidin capture on streptavidin coated beads is detected for both configurations.

6.2 Agglutination test protocol

6.2.1 On-chip immuno-agglutination assay principle

The principle of the on-chip agglutination assay developed in this thesis is illustrated in Figure 6.3. The assay comprises a 4-step protocol. Beads that have been grafted with specific Ab's for the capture of a selected target Ag or analyte are used for this purpose. First, a colloid of functionalized magnetic beads is injected into the microchannel and immobilized on the side walls at a well-defined location (static plugs, Figure 6.3 a). Subsequently, the analyte solution is introduced. The magnetic parameters of the system are adjusted in order to generate a cyclic motion of the beads perpendicular to the microchannel, while retaining them in a small confined volume (dynamic plug, Figure 6.3 b). Actuation of this magnetic plug allows perfusion with enhanced interaction between the analyte and the beads. Subsequent formation of aggregates is achieved by confining the beads into a dense static plug on one channel side wall for a few minutes (Figure 6.3 c). After switching off the magnetic field, the highly localized bead plug dissociates. A quantitative measure of the analyte concentration is possible by analyzing the area of the released plug after a defined lapse of time (Figure 6.3 d). No solution flow is applied during the last stage. The swelling of the bead plug is directly related to the degree of bead aggregation (size and amount of aggregates), thus to the amount of captured Ag's.

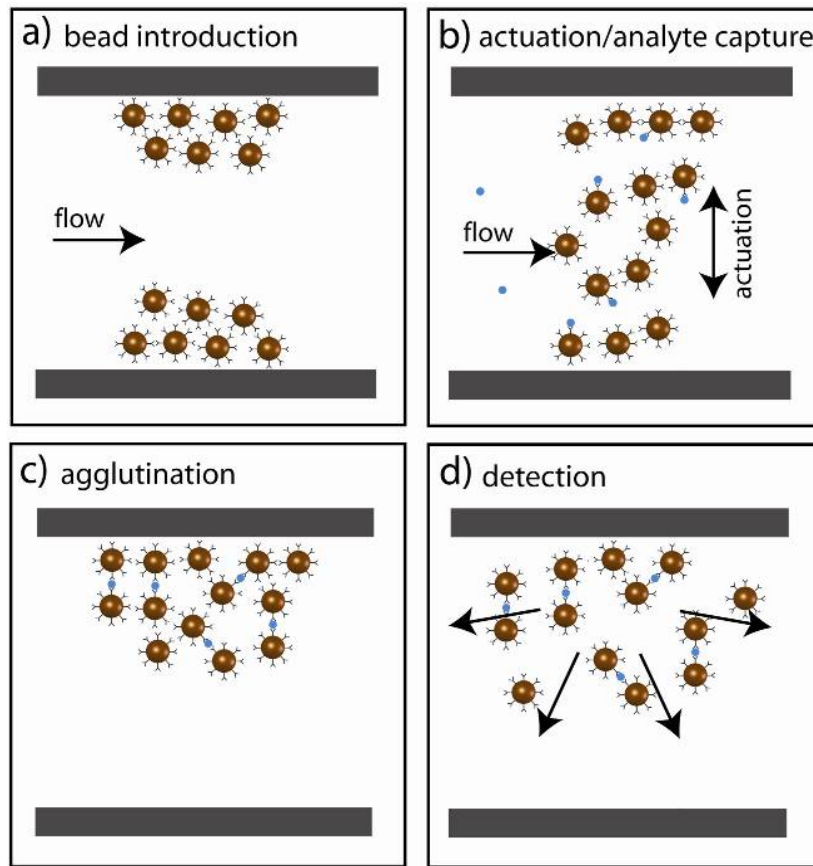


Figure 6.3: Principle of the microfluidic agglutination immunoassay: a) Functionalized magnetic beads are injected and magnetically trapped in a microchannel. b) Perfusion of the confined dynamic bead plug with the analyte solution. c) After analyte capture, beads are immobilized on one side of the channel to allow formation of aggregates. d) The magnetic field is switched off and the beads are released. The area of the released plug is a measure of the amount and size of the aggregates.

6.2.2 Model agglutination protocol

The system is placed under an inverted microscope and prefilled with 15 mM PBS (Phosphate Buffered Saline) solution. Bubbles trapped in tubes and fluidic connections are removed through a venting bypass in the chip holder. The system has to be completely bubble-free to control flow rates down to 1 nL/s in a reliable manner, i.e. without any hydraulic compliance effect. Streptavidin-coated MyOne Dynabeads® (Invitrogen, Basel, Switzerland) with a diameter of 1 μm are used throughout the experiments. 2 μL of bead solution ($[10^8 \text{ beads/mL}]$) is pipetted into the reservoir on the chip by using a microloader. At this stage, a current is applied to the external coil, resulting in a static magnetic field in between the two soft magnetic poles across the microchannel. The permanent magnets are not used at this stage. A fraction of the bead solution (200 nL) is sucked into the microchannel with a constant flow rate of 5 nL/s by

means of a high-precision syringe pump connected to the outlet (neMESYS Cetoni, Korbussen, Germany). Observation under the microscope with a fast video camera shows that, using these flow conditions and field parameters, all beads in the solution flow are attracted towards the tips and immobilized by forming a dense and localized plug on each channel side wall. The amount of captured beads is estimated to 2×10^4 beads. The surplus of the bead solution in the reservoir is removed. Fluidic handling in suction mode through the outlet allows easy solution introduction and exchange without replacing or refilling the syringe pump.

We take advantage of the strong affinity of streptavidin for biotin to develop a model assay for agglutination on-chip. In our system, the analyte (or capture Ag) is biotinylated-BSA (bBSA) (Sigma-Aldrich, Buchs, Switzerland) that may link to two streptavidin-coated beads, thus forming doublets or larger aggregates. The analyte test solution is 15 mM PBS containing bBSA concentrations in the range of 10 pg/mL to 10 ng/mL (0.15 pM to 0.15 nM). A surfactant (0.5%, Tween 20) was added to reduce non-specific agglutination. The experimental procedure for the agglutination assay starts by pipetting 2 μ L of analyte solution into the reservoir in the chip holder. The portion of the microchannel in front of the magnetic poles is prefilled with analyte solution (100 nL at 5 nL/s). Immediately afterwards, the two permanent magnets are positioned on the chip holder and the time-varying magnetic field for the formation of the dynamic bead plug is activated. Subsequently, 750 nL of analyte solution is driven through the activated bead plug at a flow rate of 1 nL/s to allow analyte capture, resulting in a total capture time of 12.5 min. Finally, the permanent magnets are removed and a static field configuration is re-established in order to attract all beads in a highly confined volume on one channel side wall. The beads are immobilized for 5 min to allow agglutination prior to detection.

Immunoassays, and in particular the detection method described in this paper, may be very sensitive to temperature. All experiments were carried out at a temperature of 32 °C, as measured by a small thermocouple probe. No additional temperature rise due to the magnetic field generator was observed in proximity of the magnetic tips.

6.2.3 Detection principle of the immuno-agglutination

We performed on-chip immuno-agglutination assays using the above described protocol for our model system. Agglutination occurs when a bBSA molecule captured on the surface of a bead binds to another bead. The suspension after agglutination is a mixture of dispersed aggregates with different size. Doublets, triplets and larger clusters are observed. In order to determine the detection limit and sensitivity, the amount of aggregation may be analyzed by

counting beads individually under a microscope [132]. We found that swelling of the released plug due to electrostatic repulsion can be used in our assay for quantitative detection of low analyte concentrations. According to the Stokes-Einstein equation, the diffusion coefficient D for spherical Brownian beads is inversely proportional to the radius r of the bead [164]. We would therefore expect that agglutinated beads will diffuse slower than single beads, as observed in our experiments. An analysis of the dynamics of the released plug reveals, however, that a simple diffusion model is not applicable. Plug swelling in the first few seconds after field removal is clearly faster than can be expected from a simple diffusion model for beads with a diameter of 1 μm . In order to clarify this phenomenon, we changed the ionic strength of the solution. In de-ionized water, swelling of the plug occurs nearly two times faster than in 15 mM PBS in the initial phase. At low ionic concentration, the Debye screening layer related to the surface charge of a bead will extend to a larger distance. Electrostatic repulsion is more important in this case [165]. We therefore speculate that electrostatic interaction of the beads is at the origin of the fast swelling of the plug during the first seconds after field removal.

The space occupied by the magnetic plug increases in time as a function of the degree of agglutination once the magnetic field is switched off (no flow in the channel). No aggregation due to magnetic forces is expected in zero-field using superparamagnetic beads. A reference test without capture analyte reveals a negligible level of non-specific agglutination in our assay. Any change in the kinetic properties of the plug can therefore safely be attributed to agglutination between beads due to Ag capture. It is not possible to distinguish to which extent the size variation of the released plug is related to direct or non-specific agglutination. However, our system presents the advantage of the ability to perform an *in situ* reference measurement just prior to exposing the bead plug to the analyte. In this way, we may reduce the effect of non-specific agglutination on the test read-out. Figure 6.4 illustrates the release of a plug after incubation with different analyte concentrations. Figure 6.4 a and Figure 6.4 b show released plugs that have been perfused by buffer solution ($[\text{bBSA}]=0$) or with a solution containing 2.5 ng/mL (35 pM) bBSA, respectively (total volume 750 nL). The photos were taken 15 s after switching off the field, when the size of the plug almost remains constant. Figure 6.4 a and b demonstrate qualitatively how the plug swelling decreases for increasing bBSA concentration, i.e. the plug area A is smaller for a higher amount of agglutinated beads. For quantitative measurements, the area of the released plug is determined using standard image processing. Grey scale photographs are converted into binary images with black pixels corresponding to regions where beads and clusters are observed. The total number of black pixels on an image is taken as a measure for the plug size. Figure 6.4 c compares the swelling of the plug as a function of time for a reference plug (i.e. after

perfusion with buffer solution, $[bBSA] = 0 \text{ ng/mL}$) and a measurement obtained after perfusion with 1.25 ng/mL (17.5 pM) bBSA. Plug area measurements have been compared after 15 s . In the case shown in Figure 6.4 c, the size of the agglutinated plug is about 75% of the reference plug. Experimental parameters are the same for all measurements (same buffer and temperature).

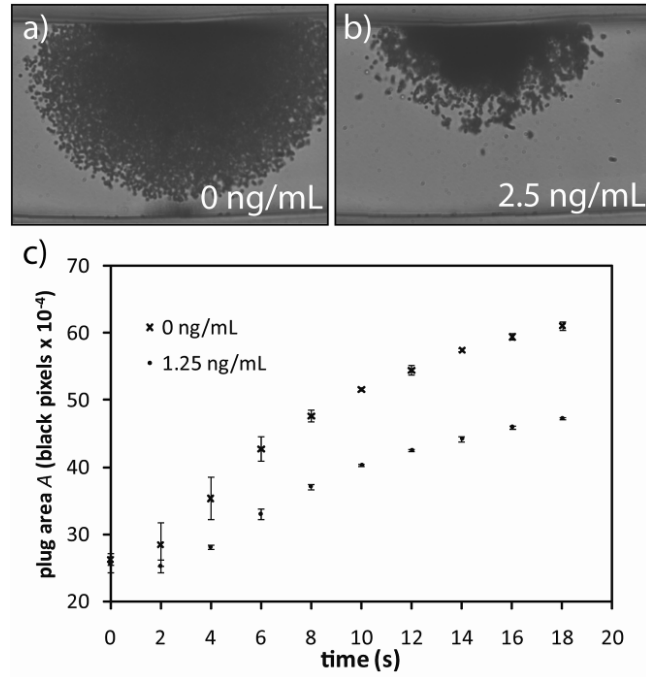


Figure 6.4: Detection of the amount of agglutination by analyzing the area of the released plug. A streptavidin-bBSA model system was used. a) and b) Photographs of the released plug after perfusion with a buffer solution ($[bBSA]=0 \text{ ng/mL}$, reference test) and an analyte solution ($[bBSA]=2.5 \text{ ng/mL}$ i.e. 35 pM), respectively. The photos are taken 15 s after switching off the field. c) Plug area as a function of time (number of black pixels after image treatment, magnetic field off at $t = 0$). Measurements have been recorded subsequently after perfusion with a reference and an analyte solution (0 ng/mL and 1.25 ng/mL bBSA, respectively). Error bars correspond to the standard deviation of three subsequent recordings.

The size of the released plug directly depends on the number of retained beads and a new batch of beads has to be introduced into the microchannel before each measurement. While the number of beads may not be exactly the same, a reference measurement in buffer solution is easily performed each time before introducing the analyte solution, without replacing the beads. Thus, exactly the same amount of beads is used for both recordings. When the plug areas are defined as A_{ref} and A_{bBSA} for the reference and the analyte measurement, respectively, considering the normalized signal $1 - A_{bBSA}/A_{ref}$ allows reliable comparison for different analyte concentrations, even if only relatively small changes at the rim of a plug have to be considered (for low bBSA concentrations). This normalization was used to establish a dose-response curve (Figure 6.5). Viscosity and ionic strength of the solution may affect the swelling of the released plug. In

practice, however, the analyte solution is washed out and replaced by buffer solution during the agglutination phase after protein capture. Detection is therefore always carried out in the same conditions for the reference and the analyte measurement.

6.3 Dose-response curve

In order to demonstrate the feasibility of a sensitive agglutination assay, we established a dose-response curve for the model assay. The signal $1 - A_{bBSA}/A_{ref}$ related to the area of the released plug was determined for different bBSA concentrations. All measurements have been recorded 15 s after switching off the magnetic field. Figure 6.5 shows the resulting dose-response curve for bBSA concentrations in the range of 0.01 ng/mL (0.15 pM) to 10 ng/mL (150 pM). This dose-response curve roughly displays a linear behavior in the low concentration range, as shown in the inset. We can safely determine a detection limit of about 200 pg/mL (≈ 3 pM). The signal for this concentration is more than three times the standard deviation above zero. Saturation occurs for concentrations higher than 5 ng/mL (70 pM), where all beads are strongly agglomerated and no swelling of the plug is observed after switching off the magnetic field.

The capture efficiency of the dynamic bead plug was evaluated by a merely geometrical consideration. With the described magnetic field configuration, the plug appears to oscillate in a nearly horizontal plane. The thickness of this plane was estimated by microscope observation to about 10 μm . Compared to the height of the microchannel (100 μm), we would therefore expect that about 10% of the analyte solution perfuses the dynamic plug, limiting the capture efficiency theoretically to a maximum of 10%.

The Ag capture efficiency may also be a function of the plug actuation frequency and the flow velocity. Both parameters have an impact on the probability that an Ag encounters a bead in the analyte flow. Agglutination tests ($[\text{bBSA}] = 1.25 \text{ ng/mL}$, flow rate of 1 nL/s) showed that the signal was the same for actuation frequencies above about 15 Hz. For frequencies of 5 Hz and below, the signal decreases by at least a factor of 3. At such low frequencies, perfusion is poor because of the temporary formation of dense plugs on the side walls of the channel. Also a test at a flow rate of 0.5 nL/s reveals an about 2-fold decrease of the signal compared to the normally used flow rate of 1 nL/s due to the reduced Ag-bead interaction.

An off-chip assay was carried out in order to compare the Ag capture efficiency with the on-chip assay. For this, test solutions with two different bBSA concentrations were prepared ($[\text{bBSA}] = 200 \text{ pg/mL}$ and 650 pg/mL , i.e. 3 pM and 10 pM). The off-chip incubation assay was performed in an Eppendorf tube with an incubation time of 12.5 min (the same as for the on-

chip assay). After off-chip incubation, the agglutinated beads were introduced into the chip for agglutination during 5 min and subsequent detection. The parameters of the on-chip assay were as described before. Signals obtained for 200 pg/mL were comparable for both assays, while for 650 pg/mL the signal obtained with off-chip incubation was about 2 times higher. However, signals obtained with this combined off-chip incubation/on-chip detection protocol are prone to large errors, mainly due to the relatively high uncertainty in the number of beads introduced into the chip. The low signal-to-noise ratio results in a deterioration of the detection limit. As explained before, errors of the full on-chip assay are much smaller, due to the possibility to perform an *in situ* reference measurement on-chip.

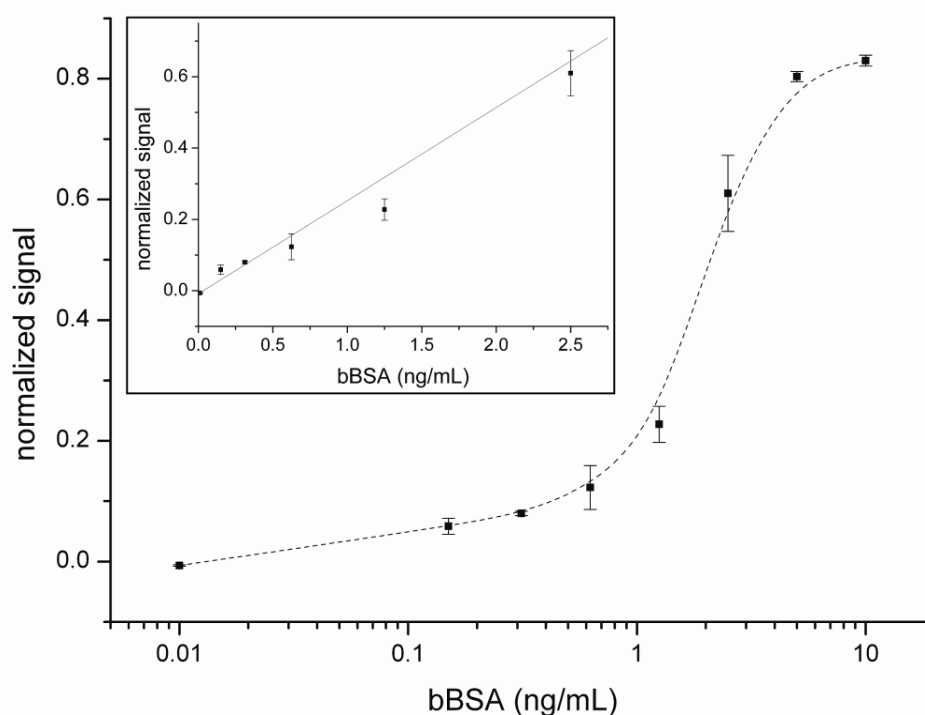


Figure 6.5: Dose-response curve for an agglutination assay on-chip using a streptavidin-bBSA model system. Analyte capture was performed with a dynamic bead plug. The signal is the normalized area of the released plug 15 s after switching off the magnetic field (1-AbBSA/Aref). Error bars correspond to the standard deviation of three nominally identical recordings. The dashed line is a guide to the eye. Inset: For low concentrations (< 3 ng/mL), a quasi-linear response is observed. A lower detection limit of about 200 pg/mL (≈ 3 pM) can be safely estimated.

An important reference related to the present assay is the work performed by Baudry et al [12]. The paper describes a magnetic bead agglutination assay with ovalbumin-IgG as biological model system. This assay was carried out in bulk format. Each sample was first incubated for 1 min and then a field was applied for 5 min. Despite this biological model system has lower

affinities, the performance of this assay appears to be somewhat better (detection limit 1 pM *vs* 3 pM, for the bulk assay in [12] *vs* the present chip-based assay, respectively). However, it was the purpose of this work to demonstrate the feasibility and potential of a full on-chip agglutination assay. The overall assay time of our chip-based assay is clearly below the duration of a typical ELISA protocol (1-2 hours). Several parameters of the system, such as the effective cross-section of the capture plug, may be further optimized to improve the performance of the described assay. The main advantages of the present on-chip assay are a reduced bead and analyte consumption, low constraints in solution handling and the possibility to perform *in situ* reference measurements.

6.4 Enhancing the capture efficiency

Up to now a quadrupolar magnetic configuration using two permanent magnets (Figure 5.10) was employed. This system is characterized by a nearly in plane configuration of the magnetic tips and permanent magnets with respect to the microfluidic channel. Due to this flat configuration, the resulting dynamic plug of beads moves in a quasi horizontal plane. The thickness of the plug was estimated to be below 10 μm using an optical microscope. Due to the relatively low filling of the microchannel cross-section, a large proportion of the Ag's are probably flowing above or below the plug without being captured. In order to increase the contact surface of the beads during actuation and increase the filling factor of the cross section, a modified system was designed and tested. The system uses a single permanent magnet placed about 5 millimeters above the microchannel resulting in a non-planar tripolar configuration. This method allows tilting the plane of actuated plug with respect to the flow as shown in Figure 6.6. The magnetic tips of the tripolar system have a reduced thickness of 50 μm and are placed in contact of the glass slide.

Using an optical microscope, it is possible to show and measure the thickness of the tilted actuated plug of beads. Figure 6.6 a schematically shows the configuration with a permanent magnet above the microchannel. in Figure 6.6 b the focal plane was adjusted to the upper part and in Figure 6.6 c to the lower part of the plug. According to the measurement, the plug is filling about 50 % of the channel cross-section.

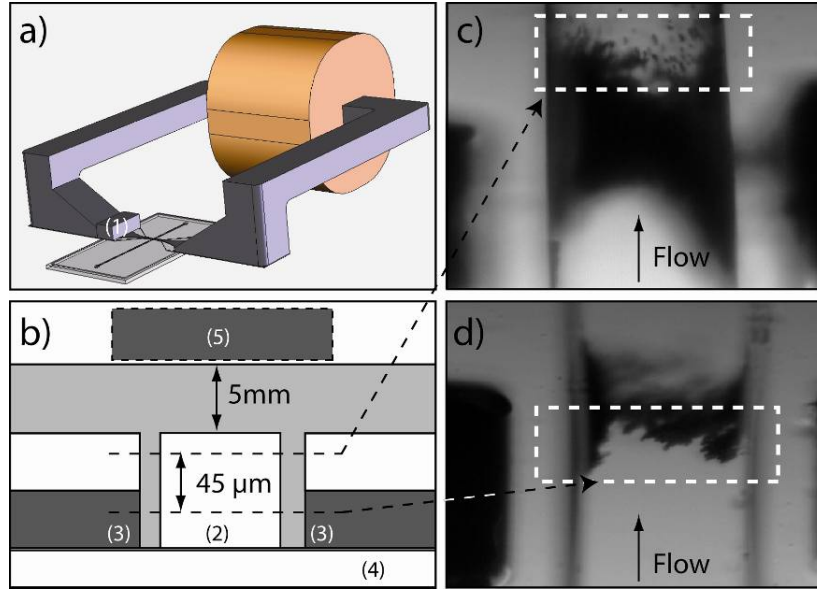


Figure 6.6: (a) 3D schematic view of the tripolar system using a single permanent magnet (1) above the microchannel used to tilt the magnetic field lines. (b) Cross sectional view of the microchannel (2), the glass slide (4), the permanent magnet (5) and magnetic tips (3) arrangement. Photographs of tilted plug with the focal plane on the upper part (c) and lower part of the bead plug.

Figure 6.7 shows a comparison between the quadrupolar and the tripolar actuation system. A nearly horizontal plug is shown in Figure 6.7 a-c corresponding to the quadrupolar configuration while in the tripolar configuration a tilted plug is observed (Figure 6.7 d-f). The dynamic behavior of the beads (velocity) in the quadrupolar and tripolar system is similar in both systems as the permanent magnetic flux density (generated by the permanent magnet) in the active region was kept constant (about 100 mT).

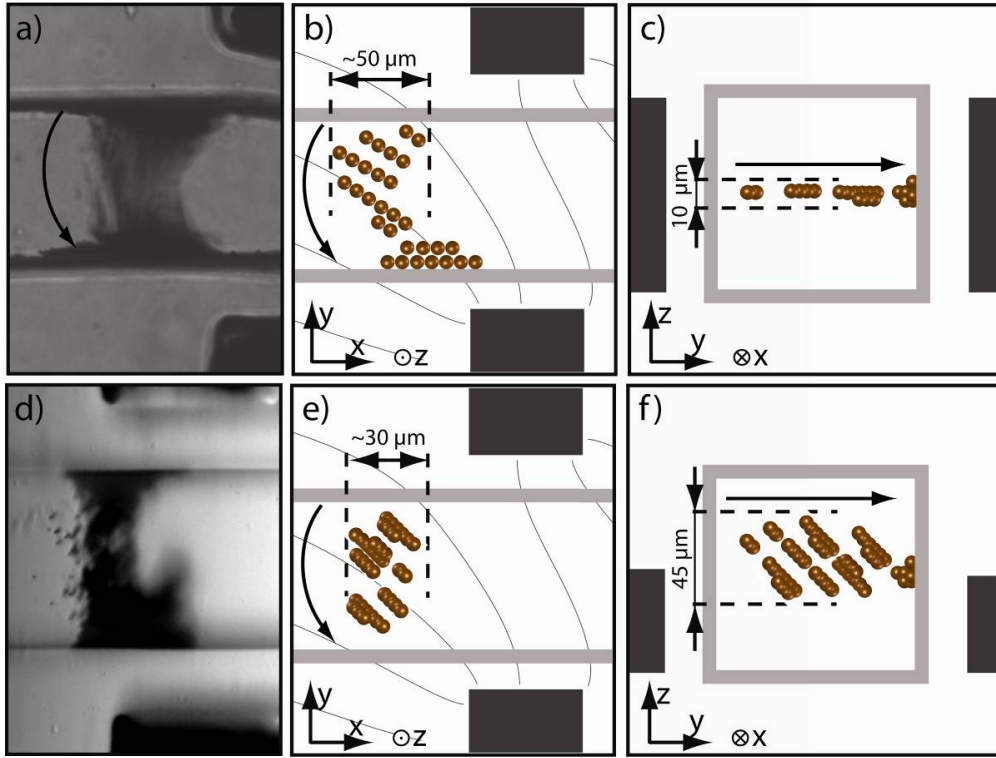


Figure 6.7: Comparison of the “flat” quadrupolar actuation system. a) Photograph from the top and b) schematic view of the actuated plug in the microchannel. c) Due to the flat arrangement of the permanent magnets and magnetic tips, the beads fill only about 10 % of the microchannel cross section. d) Photograph, (e) schematic top and (f) cross-sectional view of the actuated plug in the tripolar system. This plug actuation system uses a single permanent magnet placed above the microchannel in order to tilt the actuated plug of beads.

Experiments were performed in order to assess the increase of the capture efficiency for an agglutination assay. Figure 6.8 compares the signal of a static (Figure 5.9), a dynamic (quadrupolar system) and a dynamic tilted (tripolar configuration) plug for two bBSA concentrations (i.e. 0.6 ng/mL and 1.2 ng/mL). An about three times increase of the signal (swelling of the plug, Figure 6.4) between the dynamic and the static plug is observed. Moreover, a two times increase of the signal is observed with the tilted plug compare to the horizontal plug which indicates a better capture of the Ag’s on the beads.

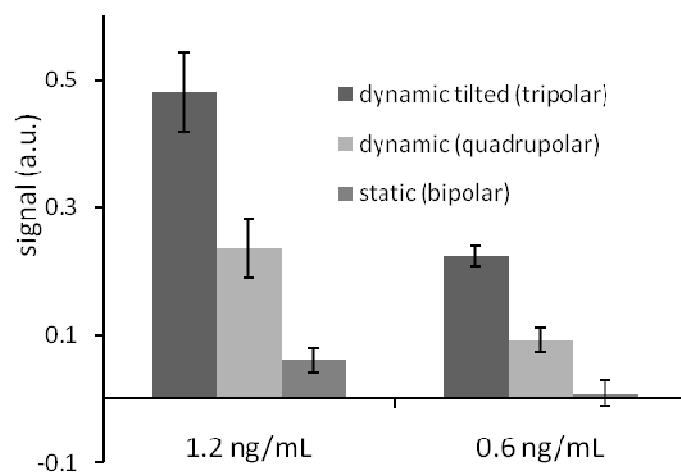


Figure 6.8: Assessment of the capture efficiency. Signal comparison (swelling of the plug, Figure 6.4) of a static (bipolar), a dynamic (quadrupolar) and a dynamic tilted (tripolar) plug for two bBSA concentrations (i.e. 0.6 ng/mL and 1.2 ng/mL). A two times increase of the signal with the tilted vs. the non-tilted plug is observed.

7 Dendritic amplification on magnetic beads

In this chapter, the feasibility of a heterogeneous on-chip assay using a fluorescence dendritic amplification scheme is demonstrated with our actuation system. The possibility to implement an on-chip dendritic amplification mechanism with a magnetic bead-based assay is verified. The lateral magnetic forces move the beads through three parallel laminar solution flows. In this way, beads may be alternatively exposed to a solution of fluorescently labeled streptavidin and a solution of biotin-conjugated anti-streptavidin, allowing a layer-by-layer dendritic amplification which generally takes up to few hours off-chip [126].

7.1 Dendritic amplification principle

The principle of a dendritic amplification mechanism is to amplify the fluorescent signal subsequently to the formation of a sandwich immunocomplex in a heterogeneous immunoassay. For this purpose, a biotinylated detection Ab is used and a dendritic structure is built onto the immunocomplex using fluorescently labeled streptavidin molecules and biotinylated Ab's. The principle of a dendritic amplification (DA) on magnetic beads is schematically illustrated in Figure 7.1 and Figure 7.2. The assay starts with the formation of a standard sandwich immunocomplex. For that purpose, beads coated with a capture Ab are introduced on-chip from inlet I-1 (Figure 7.2 a-b); subsequently a sample solution containing the Ag's is flushed through

the retained beads and Ag's bind to the beads (Figure 7.2 c). A biotinylated detection Ab is used to complete the sandwich (Figure 7.2 d). At this step, the amplification procedure may start. During the amplification, three parallel solution flows are introduced in the microchannel (see Figure 7.3 a): (I-1) buffer solution, (I-2) fluorescently labeled streptavidin (F-S) and (I-3) biotin labeled anti-streptavidin (bAS) . The buffer solution serves both to avoid diffusion between the solutions 1 and 3 and to perform washing steps during each displacement of the beads from one side of the channel to the other. In Figure 7.3 b beads are in the flow of solution 1 and therefore a molecule of F-S may bind to a molecule of bAb. Beads are then moved from solution 1 to solution 3 and several bAS (up to three) may bind to one streptavidin molecule (Figure 7.3 c). Moving the beads back from solution 3 to solution 1, F-S can bind to the bAS (Figure 7.3 d). The dendritic amplification is achieved by cyclically moving beads from solution 1 to solution 3 and vice-versa. An increasing number of F-S and bAS form a dendritic molecular structure, thus increasing the fluorescent detection signal.

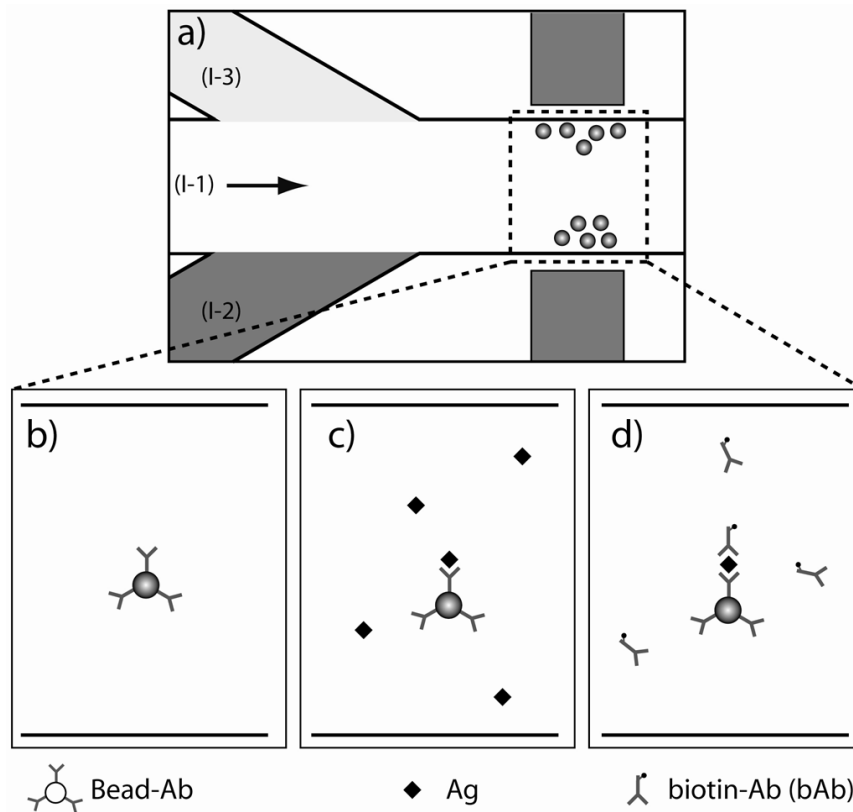


Figure 7.1: Schematic principle of the initial steps for achieving DA on-beads. (a) The protocol starts with the formation of a standard sandwich immunocomplex introducing the reactants from the open reservoir (I-1): (b) Beads coated with Ab's are introduced and retained in the microchannel. (c) The sample containing Ag's is flushed through the beads and the Ag's are captured on the bead surface. (d) Biotinylated Ab's (bAb) are then introduced and bind to the Ag's.

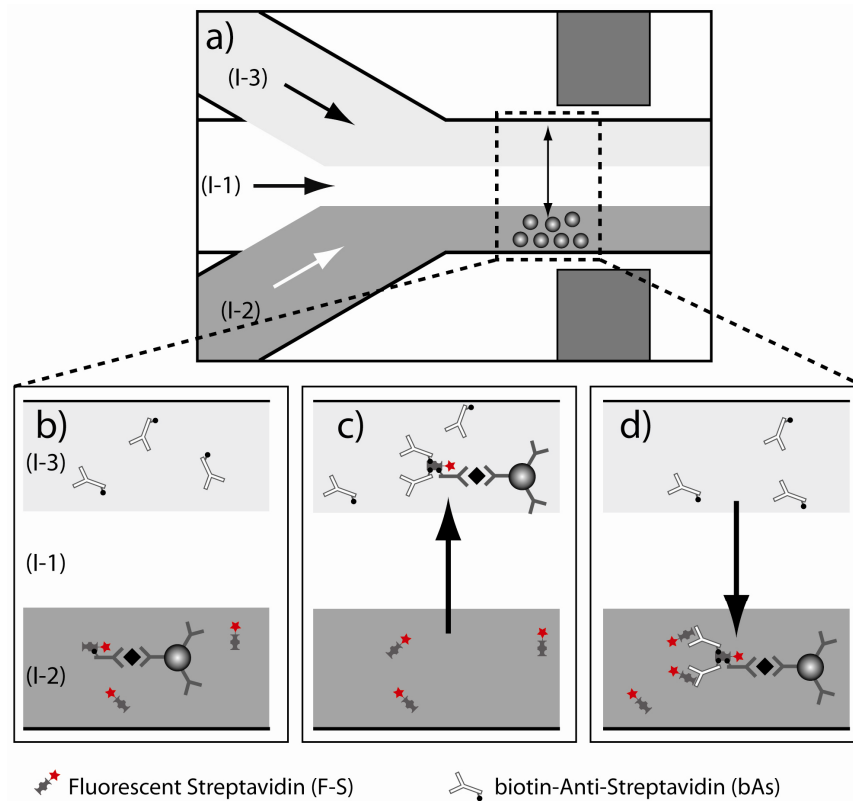


Figure 7.2: (a) The first step of the DA consists in introducing three parallel solution flows: (I-2) fluorescently labeled streptavidin (F-S), (I-1) buffer solution, and (I-3) biotin labeled anti-streptavidin (bAS). (b) Beads are in solution (1) and the F-S binds to the biotinylated Ab (bAb). (c) Beads are laterally moved to liquid (3) and up to three bAS may bind to one streptavidin molecule. (d) Beads are moved back to liquid (1) and several F-S bind to the bAS. Cyclic repetition of steps (c) and (d) results in an amplification of the fluorescent signal.

7.2 Chip design and fluidic protocol

7.2.1 Chip design

The dendritic amplification (DA) on magnetic Beads requires a microfluidic chip with three inlets to inject the different reactants involved in the DA process and one outlet. The PDMS chip for the DA was fabricated using the same technology as for the agglutination chip by adapting the design of the SU-8/silicon master. The microfluidic platform is unchanged.

The main requirement is to limit the diffusion between the three liquids before being in contact with the magnetic beads. For that reason, the intersection point of the three channels is placed close to the magnetic tips (at a distance of 200 μm) as shown in Figure 7.3.

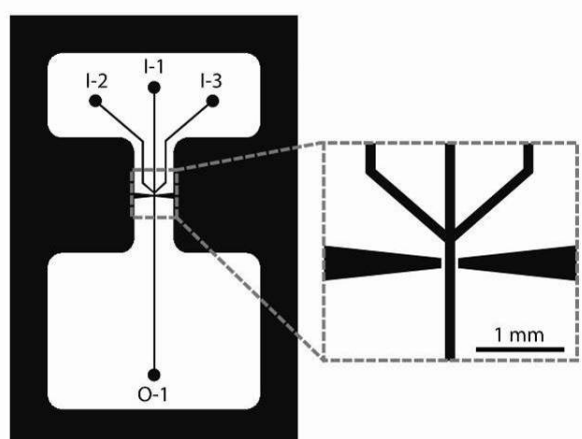


Figure 7.3: The DA-chip design consists of three inlets and a single outlet. The intersection point of the three channels is placed in proximity of the magnetic tips to reduce the interdiffusion of the three liquids.

7.2.2 Fluidic manipulation protocol

The liquid manipulation for the DA on beads is more complex than for an agglutination test, as three reactants have to be injected in parallel. A system using several open reservoirs generally results in unwanted flows because of small differences in height of the liquid. Therefore, a configuration using three syringes and a single open reservoir was chosen for the injection of the three parallel flows (see Figure 7.4). Using the chip holder describe in chapter 4, it is possible to inject liquids directly in the chip reservoirs by opening the venting holes in the chip holder. Then, when the venting holes are closed, liquids may be driven using the syringes pumps.

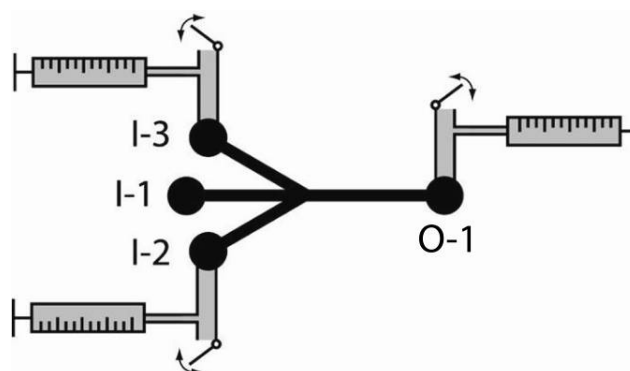


Figure 7.4: Schematic view of the liquid handling for the DA on beads. One open reservoir (I-1) is used to inject beads, sample, and detection Ab's. In DA mode, two syringes are used to push the liquid from inlets I-2 and I-3 and the third syringe is used for suction at the outlet (O-1.)

An assay starts with the complete filling of the microfluidic platform with buffer solution. The buffer is injected from the outlet while the venting holes of inlets I-2 and I-3 are open. In

the second step, beads are introduced in the open reservoir (I-1) and sucked in the microchannel from the outlet (O-1). Subsequently, sample solution, detection Ab's and buffer solution may also be introduced following the same method (see Figure 7.5 a). Before executing the DA process, the two reactants have to be introduced in the inlets I-2 and I-3. A solution of DyLight™ 649 conjugated streptavidin (Rockland Immunochemicals, Gilbertsville, USA) and a solution of biotin conjugated anti-streptavidin are injected using a pipette from the open venting holes directly in the inlet reservoirs. The open reservoir (I-1) is filled with buffer solution to separate the two reactants (Figure 7.5 b). This technique allows to fill only small on-chip reservoirs with active solution (5 nL) and filling the syringes connected to the system with buffer solution. After closing all the venting holes, the three solutions are introduced simultaneously in the channel. The two syringes connected to the inlets are set to push 1/3 of the total flow rate each while the outlet syringe is set to suck all the three liquids (see Figure 7.5 c).

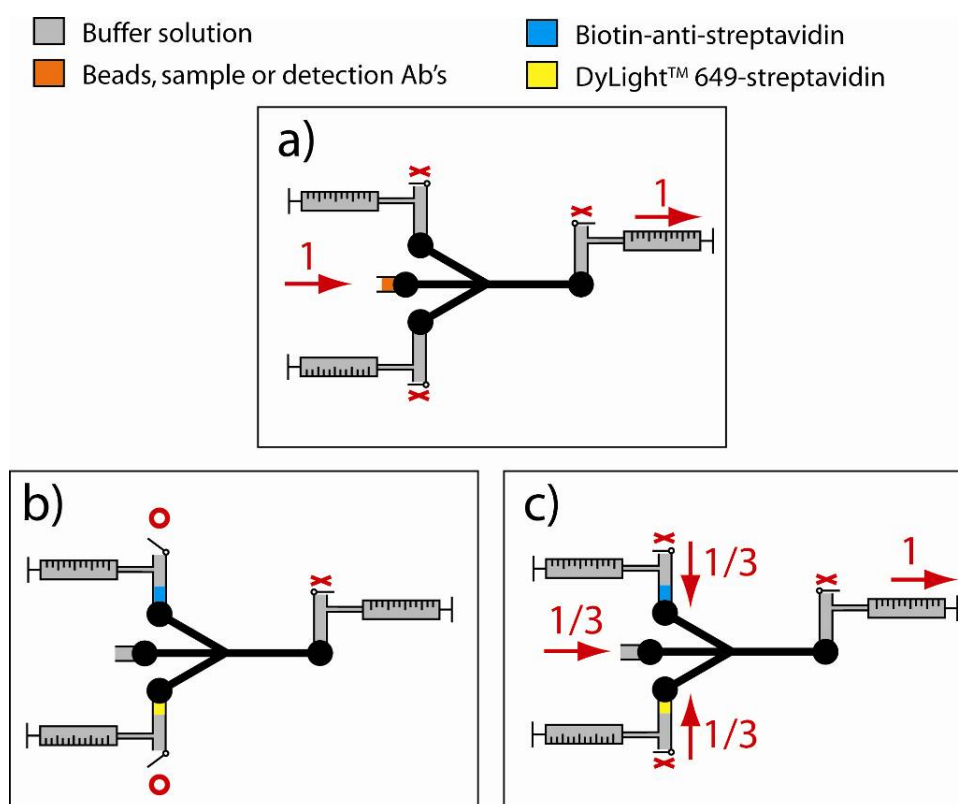


Figure 7.5: Schematic illustration of the fluidic manipulation protocol used to perform a DA on magnetic beads on-chip. Before starting an experiment, the whole system is filled with buffer solution from the outlet while the three inlets are open (I-1, I-2 and I-3). (a) The open reservoir (I-1) is filled with beads and sucked from the outlet (O-1). Successively, sample and detection Ab's are introduced and flushed through the plug of beads. (b) A solution of DyLight™ 649-conjugated streptavidin and a solution of biotin

Chapter 7 - Dendritic amplification on magnetic beads

conjugated anti-streptavidin are injected in I-2 and I-3, respectively by opening the top valve. The open reservoir (I-1) is filled with buffer (c) The three liquids are introduced in the chip by pushing the liquid from I-2 and I-3 while sucking from I-1.

For visualizing the laminar flow profiles, DyLight™ 649-conjugated streptavidin was injected in inlets I-3 (Figure 7.6 a) and I-1 (Figure 7.6 b). Focusing of the fluorescent solution is observed on the right-hand side of the channel while the non-fluorescent buffer solution stays in the 2/3 left part of the channel. To monitor the diffusion of the DyLight™ 649 conjugated streptavidin in the buffer solution, two fluorescent profiles are compared (Figure 7.6 b-c). The first profile is taken directly downstream the intersection point of the three channels and the second is taken 200 μm below, at the bead location (Figure 7.6 b). Figure 7.6 c shows that the difference between the two profiles is weak due to the short diffusion time and the three liquids are still properly separated.

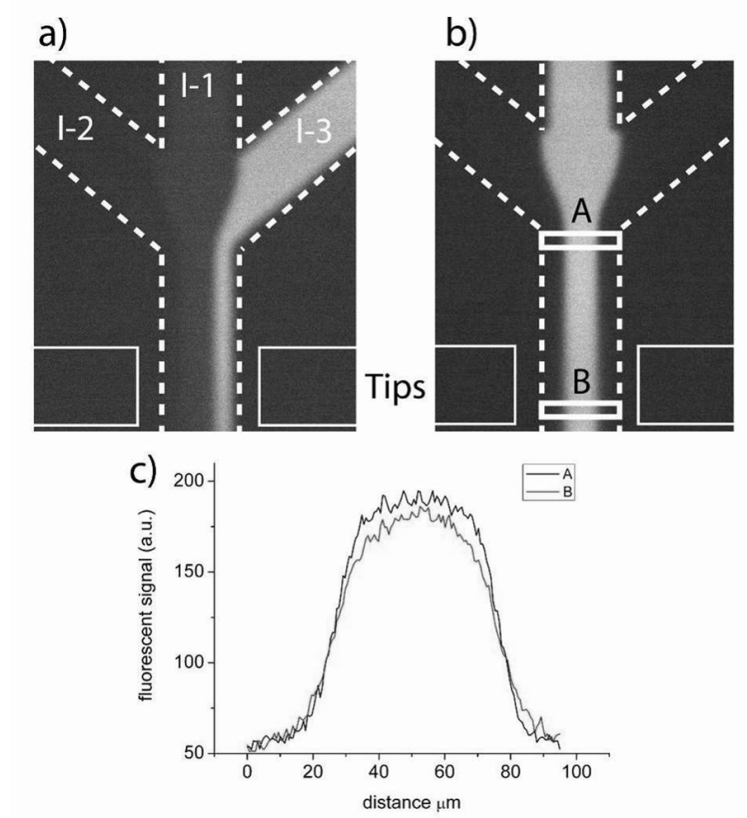


Figure 7.6: (a) Fluorescent picture of the chip with buffer in inlets I-1 and I-2 and DyLight™ 649 conjugated streptavidin in inlet I-3. The dashed lines correspond to the channel walls and the white line is the position of the magnetic tips. (b) Fluorescent picture of the chip with buffer in inlets I-2 and I-3 and DyLight™ 649-conjugated streptavidin in inlet I-1. (c) Measurement of the fluorescence intensity across the channel at the intersection point of the three channels (A) and at the beads location (B). Diffusion of the DyLight™ 649 conjugated streptavidin in the buffer solution between A and B is low.

7.3 Dendritic amplification on beads

7.3.1 Experimental protocols

For the dendritic amplification we use DyLight™ 649-conjugated streptavidin (Rockland Immunochemicals, Gilbertsville, USA) (F-S) and anti-streptavidin (rabbit) Biotin Conjugated (Rockland) (bAS). PBS buffer pH 7.4 with 0.5 % tween was used throughout the experiments. A blocking solution of PBS with 1 % BSA and 0.5 % tween was used to limit the non-specific adsorption on the beads.

Two experiments demonstrating the amplification phenomena of the fluorescent signal were carried out. Direct DA on streptavidin-coated beads and a full sandwich immunoassay followed by a DA. During experiments, beads are oscillated at 0.5 Hz resulting in a channel crossing every second. A low frequency is used to avoid mixing of the three solutions. Amplification is performed during 5 minutes and the fluorescent signal is recorded on the upper part (I-3 side) of the microchannel. The fluorescent background signal on the upper part of the channel is low as the fluorescently labeled solution is injected only in the lower part (Figure 7.5).

Signal amplification on streptavidin coated beads

As a proof-of-concept, the amplification of the fluorescent signal was first assessed directly on streptavidin-coated beads. Indeed, the fluorescent signal is visible only if both the B-AS and F-S reacts with the bead. As a negative test, anti-mouse Ab coated beads (300 nm, Ademtech, France) were used because these beads shouldn't bind to the bAS and F-S.

To perform this experiment, a solution of buffer with 0.01% beads is first introduced in the inlet I-1, 250 nL of the solution is sucked and captured in the microchannel in-between the magnetic tips (Table 7.1, step 1). A buffer solution of PBS 15 mM with 1% BSA and 0.4 % pluronic is then flushed through the beads at 5 nL/s during 50 s. The BSA is used to reduce the non-specific bindings between the Beads and the proteins in solution (Table 7.1, step 2). B-AS and F-S are introduced into inlets (I-2 and I-3). During amplification, the three solutions are flushed in the microchannel at 1 nL/s each resulting in a total flow rate of 3 nL/s in the main channel (Table 7.1, step 3).

Chapter 7 - Dendritic amplification on magnetic beads

Table 7.1: Experimental procedure for the solutions injections used to perform a signal amplification on streptavidin-coated Beads. The experiment starts with the injection of the beads (step 1, I-2). The blocking buffer is flushed through the beads (step 2, I-2). The amplification is performed by introducing B-AS (I-1), buffer (I-2) and F-S (I-3).

Steps/Inlets	I-2	I-1	I-3
1	Buffer 0 nL/s	Beads 0.01% 250 nL, 5 nL/s	Buffer 0 nL/s
2	Buffer 0 nL/s	Blocking buffer 250 nL, 3 nL/s	Buffer 0 nL/s
3	bAS 1 nL/s, 5 min	Blocking buffer 1 nL/s, 5 min	F-S 1 nL/s, 5 min

Full on-chip sandwich immunoassay with DA

A complete sandwich immunoassay using DA was also performed. For this experiment, a 150 mM PBS pH 7.4 solution added with 0.5% tween was used. Using this buffer, a better specific binding of immunocomplexes was observed compared to the PBS 15 mM previously used. 250 nL of Dynabeads® Pan Mouse IgG 0.01 % were introduced and immobilized in the microchannel (Table 7.2, Step 1). These beads are 4.5 μm in diameter and because of their size, they demonstrate a better retention stability during experiment compare to the 0.3 μm Ademtech beads. Subsequently, 250 nL of buffer solution with 1 % BSA is flushed through the beads (Table 7.2, Step 2). The sample solution containing 0 to 100 ng/mL of target Ag (Mouse IgG) is then introduced in the microchannel (Table 7.2, Step 3). The detection Ab's (bAM, 1 $\mu\text{g/mL}$, Dako, Denmark) are injected and bind to the Mouse IgG if present (Table 7.2, Step 4). A second blocking step is performed (Table 7.2, Step 5). bAS and F-S are introduced into inlets (I-2 and I-3). The three solutions are then flushed in the microchannel at 1 nL/s each resulting in a total flow rate of 3 nL/s in the main channel (Table 7.2, Step 6).

Table 7.2: Experimental procedure for the reactant injections used to perform a full on-chip sandwich immunoassay with a DA. Step 1 and step 2 are similar to the previous experiment (Table 7.1). Step 3 consists in injecting the sample solution containing 0 to 100 ng/mL of target Ag's (Mouse IgG). The biotinylated detection Ab (1 µg/mL) is then injected during step 4 and directly followed by a blocking step before the amplification (step 5). The amplification is then performed as previously by introducing B-AS (I-1), buffer (I-2) and F-S (I-3).

Steps/Inlets	I-2	I-1	I-3
1	Buffer 0 nL/s	Beads 0.01% 250 nL, 5 nL/s	Buffer 0 nL/s
2	Buffer 0 nL/s	Blocking buffer 250 nL, 3 nL/s	Buffer 0 nL/s
3	Buffer 0 nL/s	Mouse IgG, 0 – 100 ng/mL 250 nL, 3 nL/s	Buffer 0 nL/s
4	Buffer 0 nL/s	bAM, 1 µg/mL 250 nL, 3 nL/s	Buffer 0 nL/s
5	Buffer 0 nL/s	Blocking buffer 250 nL, 3 nL/s	Buffer 0 nL/s
6	bAS 100 µg/mL 1 nL/s, 5 min	Blocking buffer 1 nL/s, 5 min	F-S 10 µg/mL 1 nL/s, 5 min

7.3.2 Results of the dendritic amplification on beads

Signal amplification on streptavidin coated beads

To demonstrate the feasibility of the DA on magnetic beads, two types of beads were used for a comparison of the fluorescent signals. The first type is a streptavidin-coated bead (Dynabeads MyOne). Because of the streptavidin coating, these beads are able to bind the B-AS and thus initiate the DA process on the beads. A strong fluorescent signal has therefore been observed on the bead plug. The second bead type is coated with Anti-Mouse IgG. No binding of B-AS or F-SA is supposed to occur on these beads as there are no biotin molecules at the surface of the beads. Therefore, the fluorescent signal has to be weak (fluorescence is possible due to non-specific adsorption) in comparison to the streptavidin-coated beads.

Figure 7.7 shows qualitatively the increase of fluorescence signal on the beads with time. A clear signal is observed after five minutes of experiment on the streptavidin-coated beads, while almost no signal can be seen on the anti-mouse Ab-coated beads showing the specificity of the reaction.

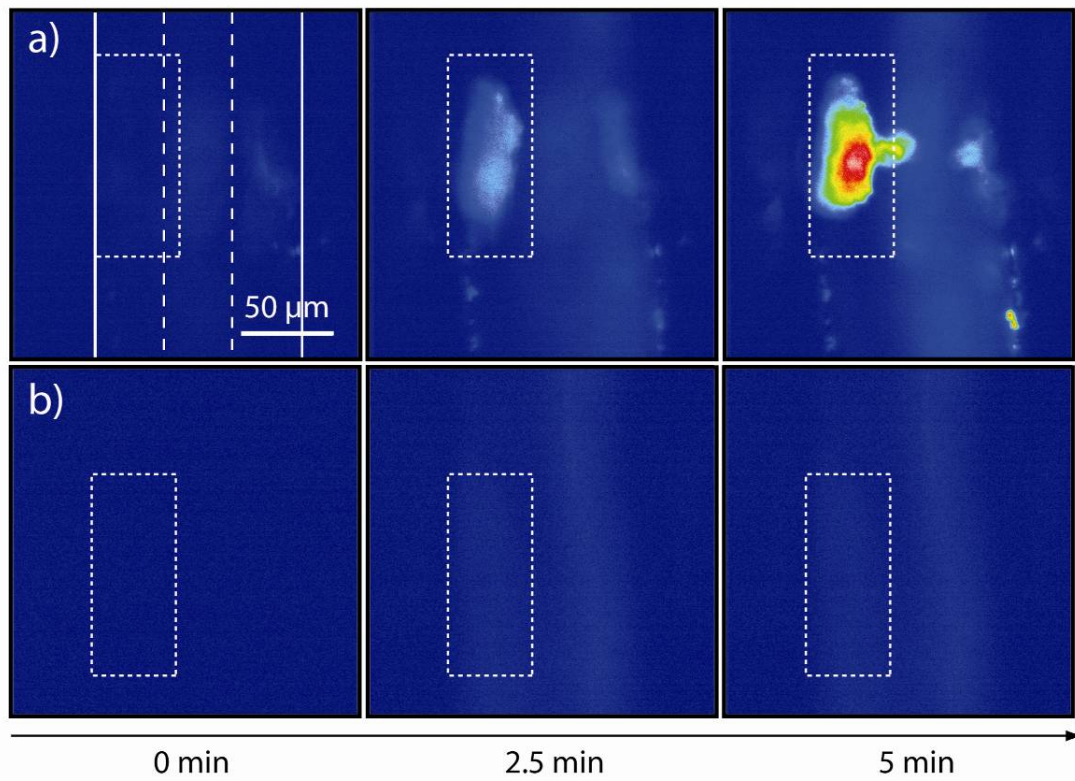


Figure 7.7: Comparison of fluorescent signal measurement on streptavidin -(positive) and anti-mouse Ab- (negative) conjugated beads. The channel walls and the three parallel flows are shown on the first picture. (a) An amplification of the fluorescent signal is observed on streptavidin-coated beads (in the rectangle) showing that the DA occurred. (b) Using anti-mouse Ab-conjugated beads, no clear fluorescent signal increase is observed on the beads because there are no binding sites to initiate the DA processes.

Figure 7.8 compares the signal increases on streptavidin-coated beads and anti-mouse Ab-coated beads. A clear amplification of the signal is seen for the streptavidin coated beads demonstrating that the amplification occurs. No significant increase of the signal is observed on the anti-mouse coated as expected.

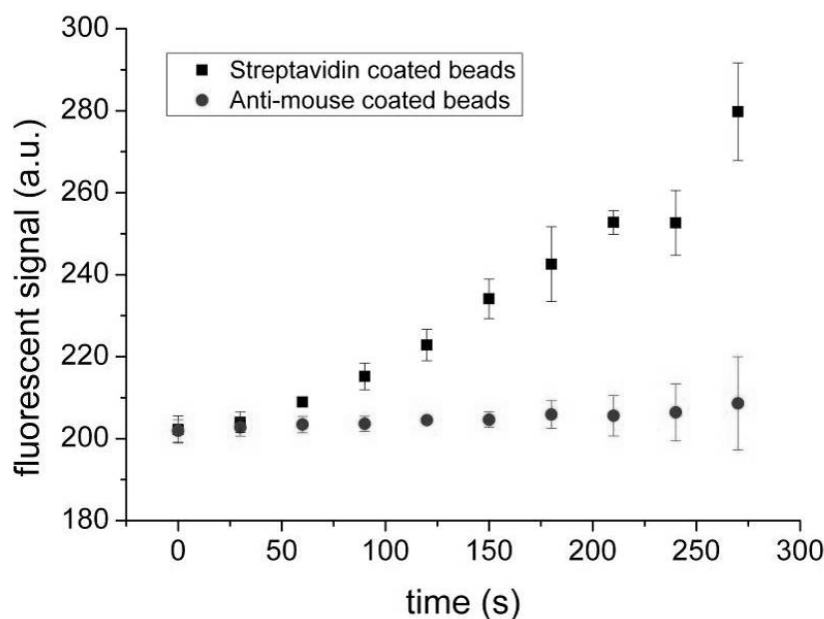


Figure 7.8: Fluorescent signal measured on the plug of beads with respect to amplification time. The fluorescent signal on streptavidin coated beads increases as the amplification takes place while no clear increase of the fluorescent signal is observed on anti-mouse Ab-coated beads. The error bars correspond to the standard deviation of three experiments.

Full on-chip sandwich immunoassay with DA

A complete sandwich immunoassay followed by a DA as described in Figure 7.1 and Figure 7.2 was also carried out. Figure 7.9 shows the fluorescent signal increase during DA for a sample at 100 ng/mL (positive) and 0 ng/mL (negative) of target Ag (Mouse IgG). The fluorescent signal of the positive test is clearly higher after five minutes of amplification than the negative test. However, a non-negligible fluorescent signal increase is also observed for the negative test. This signal increase may be explained because of the non-specific binding of the biotinylated detection Ab (B-AM) on the beads. These experiments show that because of the amplification phenomena, the signal is extremely sensitive to non-specific binding. These experiments confirm that an amplification mechanism may be used to amplify the fluorescent signal on magnetic beads.

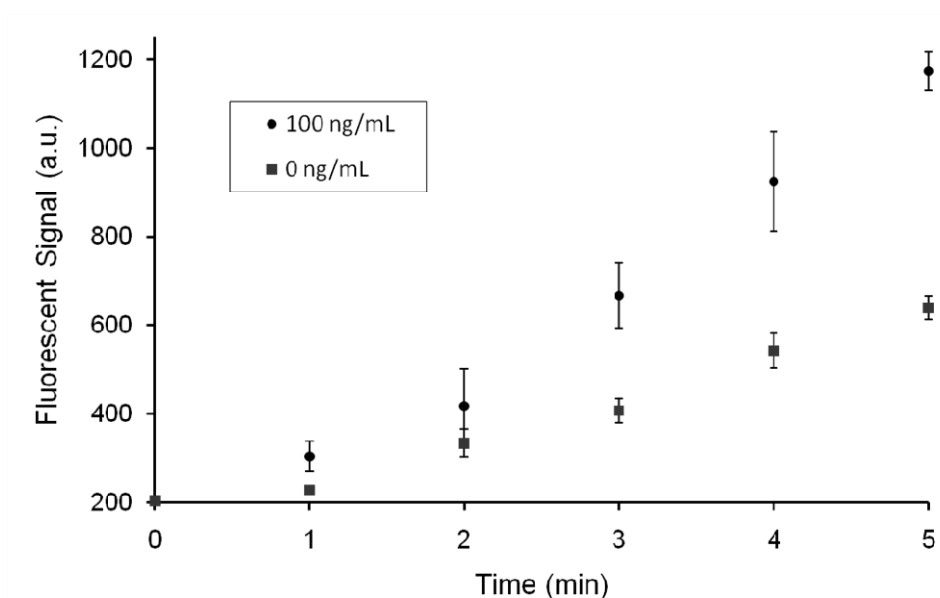


Figure 7.9: Fluorescent signal for a complete sandwich immunoassay for 100 ng/mL (positive) and 0 ng/mL (negative) of mouse IgG. The error bars correspond to the standard deviation on three measurements.

The DA amplification on magnetic beads was shown to be feasible using our magnetic actuation system. The simple approach of moving beads through three parallel flows allows for building a layer-by-layer protein structure on the beads in a very simple and straightforward manner. Increase of the fluorescent signal with time on streptavidin coated beads demonstrates the amplification mechanism. The full on-chip detection of 100 ng/mL of target Ag using a complete sandwich immunoassay and a DA was demonstrated. Further work needs to be carried out in order to decrease the unspecific binding of the detection Ab on the beads in order to optimize the detection limit of the assay.

8 Chip integration

One of the main goals of the European project *DetectHIV* [166] was the design of a biosensor platform, which allows performing a magnetic agglutination test for the detection of the HIV virus capsid protein p24 on a disposable chip. The platform comprises two different modules for the retention of magnetic beads, the enrichment of doublets prior to the detection and the detection of doublets and singlet's by light scattering. In this chapter, the design and fabrication of the final biosensor demonstrator of the *DetectHIV* project is presented. An integrated chip comprising the magnetic actuation and the optical detection system developed at the Danmarks Tekniske Universitet (DTU). The challenge of the integration was to make the fabrication process of the two systems compatible. The microfluidic platform for the DetectHIV prototype was directly adapted from the platform developed in this work.

8.1 Integrated chip

8.1.1 Magnetic and optical module

The magnetic actuation system was presented in chapter 4. It consists of a single channel with an open inlet reservoir and an outlet connected to a syringe pump. The liquids have to be driven in a pulling (suction) mode from the outlet to provide an open access for pipetting solutions and bead suspension into the inlet.

The optical detection system developed at DTU is schematically presented in Figure 8.1 a. The chip first comprises a part for 3D hydrodynamic focusing to concentrate the beads in the middle of the channel cross section prior to the detection (see Figure 8.1 a). The right part of the chip is made for the detection of the beads by light scattering (see Figure 8.1 b). The light of a laser is guided towards the chip using an integrated SU-8 waveguide. The beads crossing the laser beam modify the intensity of the scattered light. The scattered light is then measured using the two symmetric detection waveguides and a photo multiplier tube. A FEM simulation of the 3D hydrodynamic focusing is shown in Figure 8.1 c.

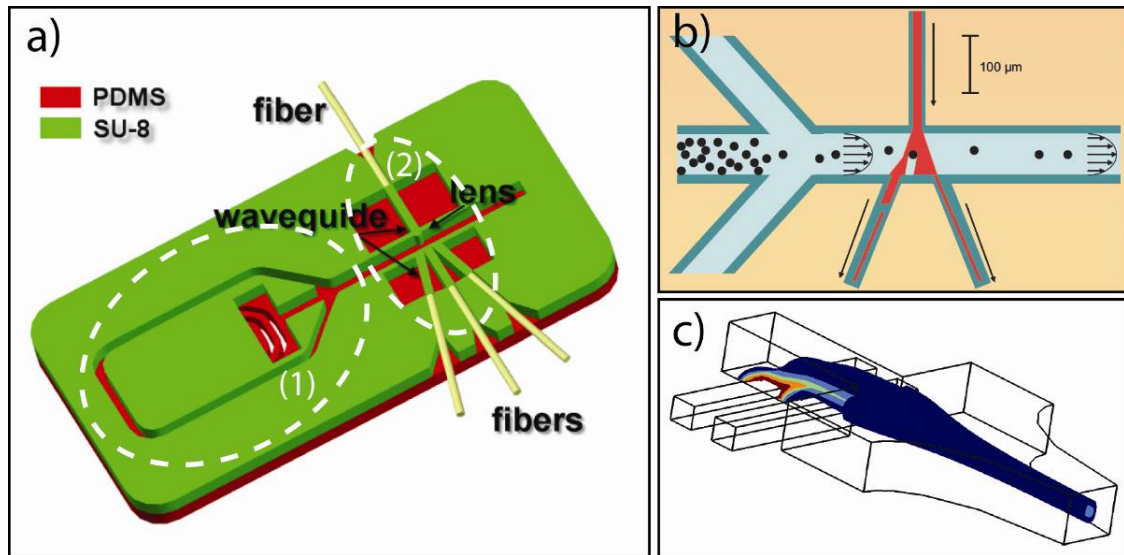


Figure 8.1: Optical detection system developed at DTU: (a) The microchip comprises a 3D hydrodynamic focusing (1) and an optical detection module (2). The setup employs a laser as incident light source. The incoming and outgoing optical fibers are aligned to the chip using structured grooves in the SU-8 layer. Scattered light is collected by on-chip waveguides and measured using a photo multiplier tube. (b) The hydrodynamically focused beads modify the intensity of the scattered light as they pass the laser beam. (c) Concentration isosurface of the focused stream obtained by numerical simulation for the 3D hydrodynamic architecture (courtesy of G.S. Zhuang, T.G. Jensen and adapted from [167])

The fluidic requirements for the optical detection system are relatively complex as five inlets are necessary to perform a fine 3D hydrodynamic focusing. Five solution flows are controlled by independent syringe pumps and stabilization of the 3D focusing flows is a critical step. For this reason, the five liquids have to be driven in pushing mode. This is a fundamental difference compared to the magnetic module and makes a straightforward integration of the two systems impossible.

To solve this problem, PDMS valves were introduced on the integrated chip to connect both modules and a hybrid system working in both pulling and pushing modes was developed in collaboration with Bertin Technologies and DTU.

8.1.2 Integrated chip design and fluidic manipulation

Figure 8.2 shows the design of the integrated chip. The chip is made of a PDMS layer and a glass slide with patterned SU-8 on top. The chip was designed to fit into a chip holder similar to the one shown in chapter 4, Figure 4.8. The main channel network is molded in the PDMS while the optical detection system is made from SU-8 (right-hand side of the chip). Three mechanical valves using pins that press on the PDMS channel are used to control the liquid directions during the experiment (see section 8.2). Two open reservoirs (R-1 and R-2) are used for the introduction of beads and sample. The six inlets (I-1 to 6) are needed to perform 3D focusing of the beads in the middle of the channel prior to the optical detection.

The meander-shaped channels are used to avoid a direct contamination between the contaminated sample and the external chip holder. The patterned SU-8 is used for the fabrication of the detection channel and the wave guides.

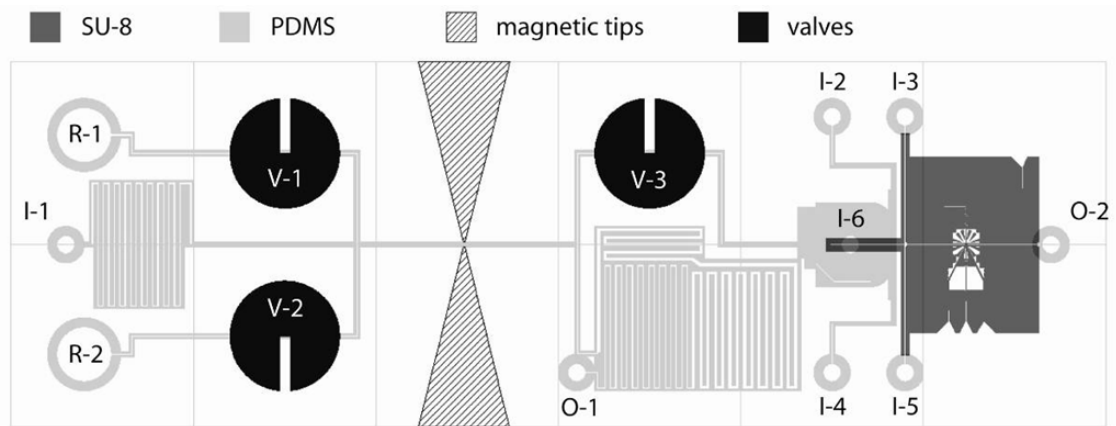


Figure 8.2: Schematic view of the integrated chip. The main fluidic channel network is molded in the PDMS layer. Two open reservoirs (R-1 and R-2) serve to introduce beads and sample solutions. Six fluidic inlets (I-1 to 6) are used to focus the beads prior to the optical detection. Serpentine structures serve to avoid the contamination of the chip holder. The optical detection system is made from SU-8. Access for the valves (V-1 to 3) and the magnetic tips is also shown.

The fluidic manipulation for the prototype is complex due to the requirement of the 3D hydrodynamic focusing. Figure 8.3 illustrates the three main steps involved in the experimental protocol. The chip is inserted in the microfluidic platform and prefilled by simultaneously

injecting buffer solution with the seven syringes (see Figure 8.3 a). The beads solution is then injected manually by pipetting in the reservoir R-1 and the reservoir R-2 is filled with the sample to be analyzed. Subsequently, the beads are sucked in the microchannel from outlet O-1 and immobilized in-between the magnetic tips (see Figure 8.3 b). Actuation of the beads is started and the sample solution is flushed through the dynamic plug (see Figure 8.3 c). At the end, the 3D hydrodynamic focusing is started and stabilized and beads are released to be analyzed through the optical detection module (see Figure 8.3 d)

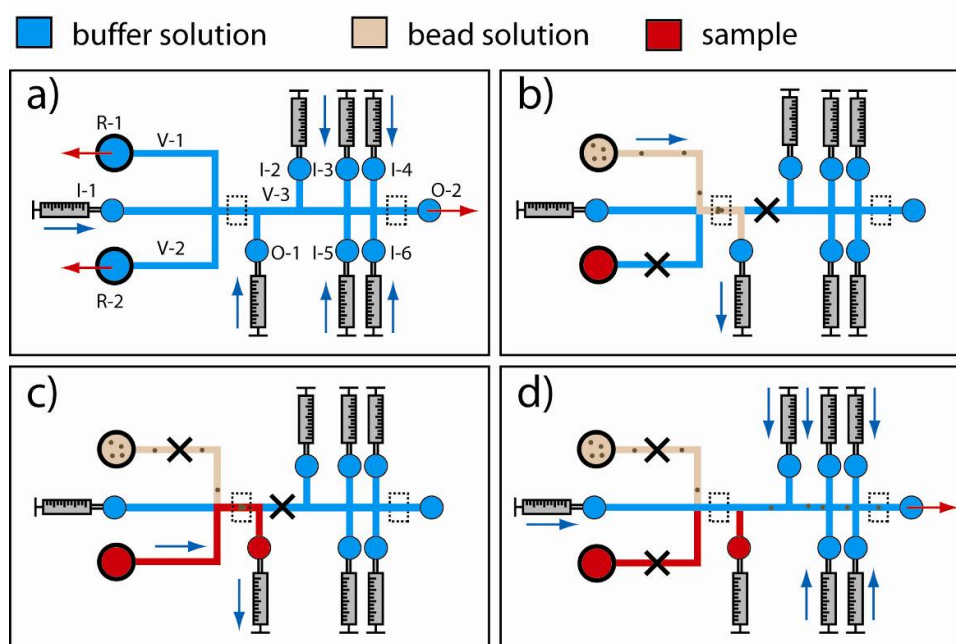


Figure 8.3: Schematic of the fluidic manipulation sequence used to complete an experiment with the integrated chip. (a) After insertion of the chip in the holder, the complete system is pre-filled with buffer solution. (b) Beads are injected in the system by sucking from outlet O-1 (valves V-2 and V-3 closed) and retained between the magnetic tips. (c) The sample solution is flushed by sucking from outlet O-1 with valves V-1 and V-3 closed. The agglutination assay is performed and (d) the doublets or aggregates are optically detected by releasing the beads through the 3D hydrodynamic focusing.

8.2 Chip and platform assembly

Fabrication of the PDMS chip is similar to the fabrication process of the magnetic actuation system. The PDMS is injected into a mold made of aluminum and PMMA. A SU-8/silicon master is placed at the bottom of the mold and is used for the casting of the channels network and microstructured parts. The fluidic accesses and open reservoirs are made using 1 mm pins and 2 mm pins in the mold, respectively. The mechanical valve accesses are made by molding a relatively thin membrane (1 mm) above the microchannel (see Figure 8.4 inset). The resulting PDMS chip is shown in Figure 8.4 b.

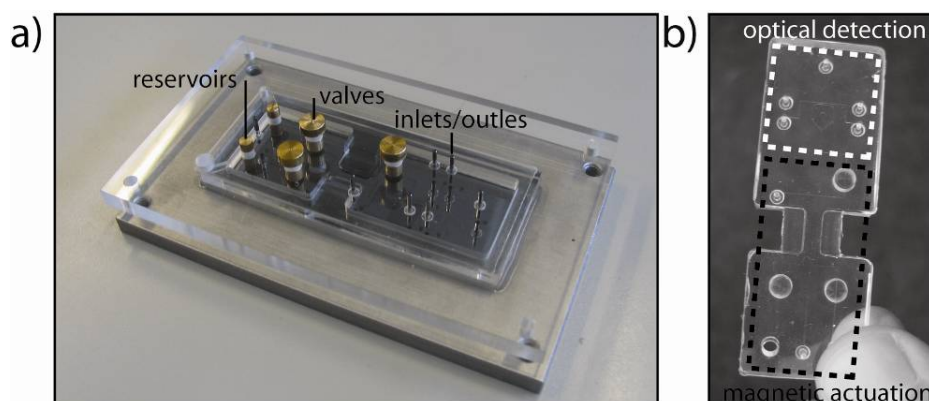


Figure 8.4: (a) Photograph of the PDMS mold. A SU-8/silicon master is used for the casting of the microstructures. Pins are used to fabricate the fluidic connections and reservoirs. (b) Photograph of the resulting PDMS chip. The lower part of the chip corresponds to the magnetic actuation system and the upper part is dedicated for the optical detection.

The final chip has to be easy to handle. Manual insertion of the magnetic poles and optical fibers has to be done during the fabrication. Clamping of the PDMS and the SU-8/glass slide is achieved by means of a PMMA case designed and fabricated by Bertin Technologies (see Figure 8.5). The magnetic tips and optical fiber are directly glued on the glass slide.

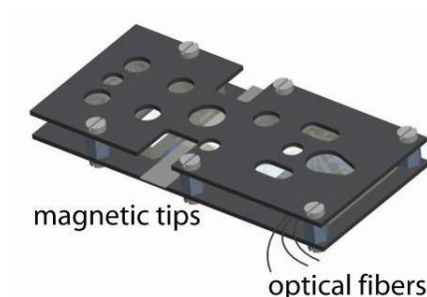


Figure 8.5: 3D schematic view of the assembled chip. The PDMS/SU-8/glass chip is clamped in a PMMA case with the magnetic tips and optical fibers glued on the glass slide (courtesy of Julien Charpentier, Bertin Technologies).

The demonstrator platform was designed and fabricated by Bertin Technologies. Figure 8.6 shows a photograph of the final demonstrator with the integrated chip. A drawer serves to slide the disposable chip in the platform, three linear motors actuate the integrated valves and a permanent magnet may be manually positioned on top of the system.

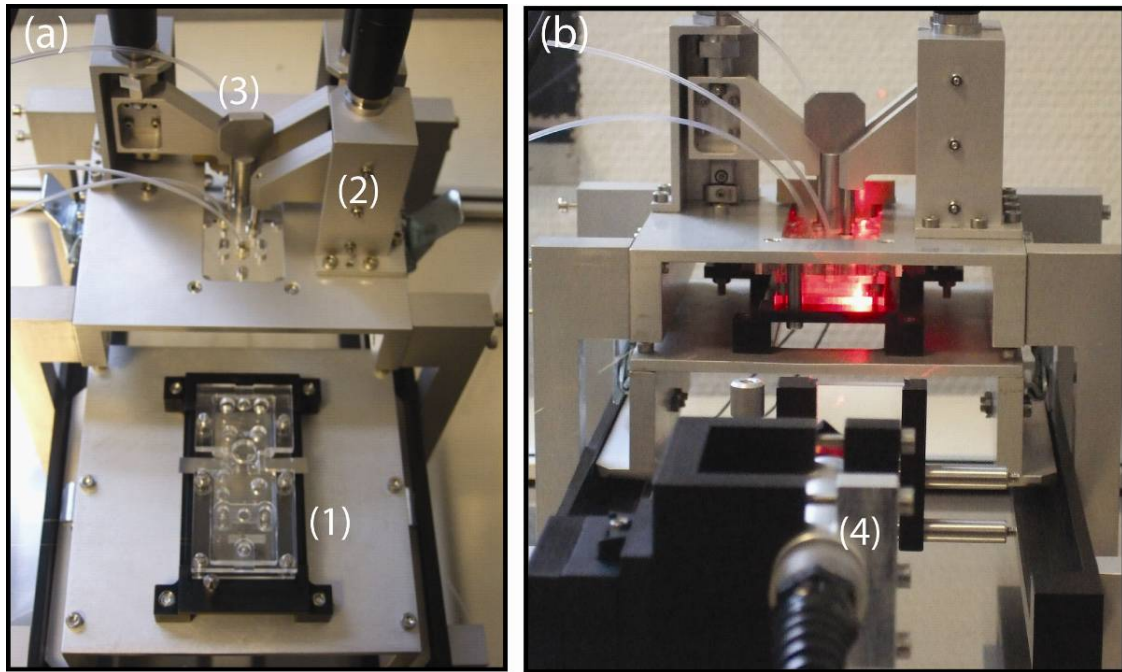


Figure 8.6: Photographs of the biosensor platform of the *DetectHIV* project with (a) the chip (1) on a drawer, before introduction in the platform and (b) with the chip in the platform ready for an experiment. Linear motors are used to actuate the valves (2) and a movable permanent magnet may be manually positioned on top of the system. A red laser is used to perform the detection by light scattering (4) (courtesy of Julien Charpentier, Bertin technologies).

This work was carried out in collaboration with Bertin Technologies and DTU. Fabrication of the PDMS part of the chip was done at EPFL and was directly adapted from the platform that was developed during this thesis. The demonstrator is ready to be tested and a model agglutination assay based on the streptavidin and biotin interaction will be first investigated.

9 Conclusion and outlook

Magnetic bead-based LOC systems are gaining interest because of the numerous advantages they offer compared to conventional systems. A major issue remains the transfer of research devices to the market because of the relatively high complexity of the majority of systems proposed in the literature. Integration of the magneto-microfluidic device developed in this thesis was an important aspect of this work. In the frame of the *DetectHIV* project, a magnetic actuation system should be implemented into a biosensor platform prototype together with an optical detection unit. We therefore focused our efforts on providing simple design rules and experimental protocols for the retention device and the dynamic manipulation of magnetic beads on-chip.

Magnetic actuation system

We have designed and fabricated an integrated system for superparamagnetic bead actuation in a microfluidic channel. The combination of permanent magnets with a single electromagnet allows simplifying the complexity of the system compared to previously existing devices. Cyclic motion of superparamagnetic beads across a microchannel may be generated by combining alternating and static magnetic fields in a magnetic quadrupolar or tripolar configuration. Micromachined magnetic tips provide the high local field strength and gradient necessary for retention and manipulation of the beads. Thanks to precise positioning and the small dimension of the soft magnetic tips, it is possible to concentrate the beads in a highly confined volume (below 1 nL) offering an efficient tool for immunoassays on-chip. We also

emphasized the importance of considering magnetic bead interactions for a thorough design of magnetic bead-based LOC devices. Indeed, in the presence of magnetic field, bead chains and clusters may form that have an impact on the kinetic properties of the dynamic plug. Moreover, we developed a fabrication process for monolithic closed SU-8 microchannels. This new approach allows for versatile chip design rules and provides a simple approach to integrate external elements, such as soft magnetic tips on microfluidic chips.

Magnetic agglutination assay

The present system may be of interest for many on-chip bio-analytical applications and in particular for magneto-microfluidic immuno-agglutination assays. Indeed, when using beads with functionalized surfaces, dynamic actuation of the magnetic bead plug increases the efficiency of analyte capture in a sample flow. Moreover, when the magnetic field is removed, the superparamagnetic nature of the beads prevents clustering and permits easy bead release from the retention system for further processing and detection downstream. Standard detection methods used for latex agglutination, such as turbidimetry, cannot be readily implemented on-chip. The detection method presented in this work, based on the swelling of the released plug, is a simple approach to quantify the amount of agglutination in a heterogeneous mixture of aggregates. We could demonstrate the performance and potential of our approach by using a streptavidin-biotin based model assay. We determined a detection limit of about 200 pg/mL (≈ 3 pM). This is several orders of magnitude lower than typical values for standard (non-magnetic) bulk assays and comparable to a previously reported magnetic assay used to detect ovalbumin-IgG in bulk format [12]. An important advantage of our chip-based assay is the possibility to strongly reduce bead and analyte solution volumes (below 1 μ l). Real testing using p24 Ag's on-chip was not yet implemented. Experiments and evaluation of p24 agglutination assays in microtiter plate format, carried out in parallel in the frame of the *DetectHIV* project, revealed problems with the colloidal stability of the anti-p24-coated bead suspensions. These biochemical issues have to be addressed in more detail before implementing the assay on-chip.

DetectHIV project and platform

The previously described device is the basis for the fully integrated microfluidic system developed in the context of the *DetectHIV* project, comprising an assay module and an optical detection module of the agglutinated beads in a flow. In collaboration with the *DetectHIV* partners Danmarks Tekniske Universitet (DTU) and Bertin Technologies, both modules have been integrated in a single disposable cartridge. For the time being, the *DetectHIV* platform and

the integrated chip have been fabricated and successfully tested for fluidic operations. It is now too early to say whether the ambitious targeted detection limit of 0.1 pg/mL for the p24 protein may be obtained. The optical detection method implemented in the integrated chip is based on a cytometric principle, i.e. on detecting and counting of beads in the flow. Light scattering will be exploited to discriminate between single beads and doublets linked by the p24 protein. This method is expected to be more sensitive for detecting a low amount of aggregated beads (ideally in the range of a few percent of doublets over singlets) compared to the simple plug swelling based method presented in this work. We may therefore expect a significant improvement of the detection limit with the final integrated biosensor system.

Dendritic amplification

Our development of a reliable magneto-microfluidic platform allowed the implementation of several applications requiring the manipulation of magnetic beads in a microfluidic channel. For instance, our magnetic actuation system allows moving beads across a microchannel comprising a parallel flow pattern of different solutions, thus the beads can be exposed to different reactants. This possibility to expose the beads repeatedly to different liquids was exploited to demonstrate the feasibility of a heterogeneous immunoassay using dendritic amplification. This resulted in the successful amplification of the fluorescent signal on streptavidin-coated beads and the detection of 100 ng/mL of a model Ag (mouse IgG). At present, the detection limit of this method is mainly limited by non-specific adsorption of the proteins. It may be expected that careful work at the protein level may help to decrease the signal of the negative test by decreasing the non-specific adsorption.

Further applications

In a similar approach, implementation of an ELISA test on-chip using three parallel reactant flows would be of interest. By using the first half of the microchannel to form the immunocomplex sandwich, it is possible to avoid non-specific adsorption on the walls of detection Ab's in the second half part of the channel where the detection is performed (see Figure 9.1). This method has a high potential to reduce the unwanted background fluorescent signal and to improve the detection of low Ag's concentration.

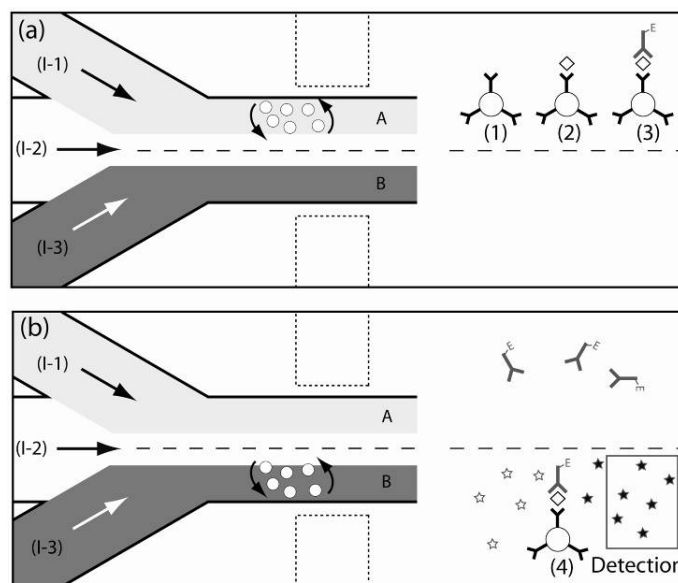


Figure 9.1: ELISA on-chip. (a) Magnetic beads are first actuated in the half part of the channel cross section (A). The immunocomplex is formed by injecting the solutions from the inlet (I-1): functionalized beads (1), sample containing Ag's (2) and enzyme conjugated detection Ab's (3). (b) After forming the immunocomplex sandwich, beads are moved to the second half part of the channel (B) where the detection takes place (4). Adsorption of detection Ab's at the surface occurs only in the half part (B) of the channel and therefore does not affect the detection signal.

The magneto-microfluidic platform was also used for the separation of magnetic beads [135] and hydromagnetic 3D focusing is presently under evaluation. These applications demonstrate the potential of our concept. This versatile method may be applied to other kinds of on-chip immunoassays in future. We think that the possibility of integrating the microfluidic agglutination assay on a disposable chip is a very promising and innovative approach for point-of-care diagnostics or for use in resource-limited settings.

References

- [1] N. T. Constantine, J. Bansal, X. Zhang, K. C. Hyams, and C. Hayes, "Enhanced chemiluminescence as a means of increasing the sensitivity of Western blot assays for HIV antibody," *Journal of Virological Methods*, vol. 47, pp. 153-164, 1994.
- [2] E. M. Lackritz, G. A. Satten, J. Aberle-Grasse, R. Y. Dodd, V. P. Raimondi, R. S. Janssen, W. F. Lewis, E. P. Notari, and L. R. Petersen, "Estimated Risk of Transmission of the Human Immunodeficiency Virus by Screened Blood in the United States," *The New England Journal of Medicine*, vol. 333, pp. 1721-1725, December 28, 1995 1995.
- [3] J.-A. Kwon, S.-Y. Yoon, C.-K. Lee, C. S. Lim, K. N. Lee, H. J. Sung, C. A. Brennan, and S. G. Devare, "Performance evaluation of three automated human immunodeficiency virus antigen-antibody combination immunoassays," *Journal of Virological Methods*, vol. 133, pp. 20-26, 2006.
- [4] S. M. Hammer, "Advances in antiretroviral therapy and viral load monitoring," *AIDS, Supplement*, vol. 10, 1996.
- [5] D. K. Owens, M. Holodniy, A. M. Garber, J. Scott, S. Sonnad, L. Moses, B. Kinosian, and J. S. Schwartz, "Polymerase Chain Reaction for the Diagnosis of HIV Infection in Adults: A Meta-Analysis with Recommendations for Clinical Practice and Study Design," *Annals of Internal Medicine*, vol. 124, pp. 803-815, May 1, 1996 1996.
- [6] J. Schupbach, "Viral RNA and p24 antigen as markers of HIV disease and antiretroviral treatment success," *International Archives of Allergy and Immunology*, vol. 132, pp. 196-209, 2003.
- [7] A. Tehe, C. Maurice, D. L. Hanson, M. Y. Borget, N. Abiola, M. Maran, D. Yavo, Z. Tomasik, J. Boni, J. Schupbach, and J. N. Nkengasong, "Quantification of HIV-1 p24 by a highly improved ELISA: An alternative to HIV-1 RNA based treatment monitoring in patients from Abidjan, Cote d'Ivoire," *Journal of Clinical Virology*, vol. 37, pp. 199-205, 2006.
- [8] J. Schupbach, J. Böni, M. Flepp, Z. Tomasik, H. Joller, and M. Opravil, "Antiretroviral treatment monitoring with an improved HIV-1 p24 antigen test: an inexpensive alternative to tests for viral RNA," *Journal of Medical Virology*, vol. 65, pp. 225-232, 2001.

- [9] C. Jennings, S. A. Fiscus, S. M. Crowe, A. D. Danilovic, R. J. Morack, S. Scianna, A. Cachafeiro, D. J. Brambilla, J. Schupbach, W. Stevens, R. Respess, O. E. Varnier, G. E. Corrigan, J. S. Gronowitz, M. A. Ussery, and J. W. Bremer, "Comparison of Two Human Immunodeficiency Virus (HIV) RNA Surrogate Assays to the Standard HIV RNA Assay," *Journal of Clinical Microbiology*, vol. 43, pp. 5950-5956, December 1, 2005 2005.
- [10] X. Cheng, D. Irimia, M. Dixon, K. Sekine, U. Demirci, L. Zamir, R. G. Tompkins, W. Rodriguez, and M. Toner, "A microfluidic device for practical label-free CD4+ T cell counting of HIV-infected subjects," *Lab on a Chip*, vol. 7, pp. 170-178, 2007.
- [11] B. Grillet, M. Gaboyard, J. Baudry, and J. Bibette, "A new magnetic agglutination assay for detection of the hepatitis B surface antigen," *Clinical Chemistry*, vol. 50, pp. A152-A152, Jun 2004.
- [12] J. Baudry, C. Rouzeau, C. Goubault, C. Robic, L. Cohen-Tannoudji, A. Koenig, E. Bertrand, and J. Bibette, "Acceleration of the recognition rate between grafted ligands and receptors with magnetic forces," *PNAS*, vol. 103, pp. 16076-16078, 2006.
- [13] J. Baudry, E. Bertrand, N. Lequeux, and J. Bibette, "Bio-specific recognition and applications: from molecular to colloidal scales," *Journal of Physics-Condensed Matter*, vol. 16, pp. R469-R480, 2004.
- [14] K. Sato, M. Tokeshi, T. Odake, H. Kimura, T. Ooi, M. Nakao, and T. Kitamori, "Integration of an immunosorbent assay system: Analysis of secretory human immunoglobulin A on polystyrene beads in a microchip," *Analytical Chemistry*, vol. 72, pp. 1144-1147, 2000.
- [15] L. G. Rashkovetsky, Y. V. Lyubarskaya, F. Foret, D. E. Hughes, and B. L. Karger, "Automated microanalysis using magnetic beads with commercial capillary electrophoretic instrumentation," *Journal of Chromatography A*, vol. 781, pp. 197-204, 1997.
- [16] M. A. M. Gijs, "Magnetic bead handling on-chip: new opportunities for analytical applications," *Microfluidics and Nanofluidics*, vol. 1, pp. 22-40, 2004.
- [17] R. M. Cornell and U. Schwertmann, *The Iron Oxides: Structure Properties, Reactions, Occurrence and Uses*. VCH, Weinheim, Germany, 2003.
- [18] "http://www.magnets.bham.ac.uk/magnetic_materials/type.htm," 2010.
- [19] S. Chikazumi and S. H. Charap, *Physics of magnetism*: Wiley New York, 1964.
- [20] U. Lehmann, "Manipulation of magnetic microparticles in liquid phases for on-chip biomedical analysis methods," EPFL, 2008.

- [21] A. Hubert and R. Schäfer, *Magnetic domains: the analysis of magnetic microstructures*: Springer Verlag, 1998.
- [22] R. C. O'Handley, *Modern magnetic materials: principles and applications*: Wiley-interscience New York, 1999.
- [23] D. L. Leslie-Pelecky and R. D. Rieke, "Magnetic properties of nanostructured materials," *Chemistry of Materials*, vol. 8, pp. 1770-1783, 1996.
- [24] T. Jonsson, P. Nordblad, and P. Svedlindh, "Dynamic study of dipole-dipole interaction effects in a magnetic nanoparticle system," *Physical Review B*, vol. 57, pp. 497-504, 1998.
- [25] A. H. Lu, E. L. Salabas, and F. Schuth, "Magnetic nanoparticles: synthesis, protection, functionalization, and application," *Angewandte Chemie*, vol. 46, pp. 1222-1245, 2007.
- [26] D. Horak, M. Babic, H. Mackova, and M. J. Benes, "Preparation and Properties of Magnetic Nano- and Microsized Particles for Biological and Environmental Separations," *Journal of Separation Science*, vol. 30, pp. 1751-1772, 2007.
- [27] "<http://www.ademtech.com/images/precision.pdf>," (February 2010).
- [28] U. Häfeli, *Scientific and Clinical Applications of Magnetic Carriers*: Kluwer Academic Publishers, 1997.
- [29] R. Becker and F. Sauter, *Electromagnetic fields and interactions*: (Dover, New York), 1982.
- [30] H. Lee, A. M. Purdon, and R. M. Westervelt, "Manipulation of biological cells using a microelectromagnet matrix," *Applied Physics Letters*, vol. 85, p. 1063, 2004.
- [31] A. C. Siegel, S. S. Shevkoplyas, D. B. Weibel, D. A. Bruzewicz, A. W. Martinez, and G. M. Whitesides, "Cofabrication of Electromagnets and Microfluidic Systems in Poly (dimethylsiloxane)," *Angewandte Chemie*, vol. 45, p. 6877, 2006.
- [32] M. K. Yapici, A. E. Ozmetin, J. Zou, and D. G. Naugle, "Development and experimental characterization of micromachined electromagnetic probes for biological manipulation and stimulation applications," *Sensors & Actuators: A. Physical*, 2008.
- [33] N. Pamme, "Magnetism and microfluidics," *Lab on a Chip*, vol. 6, pp. 24-38, 2006.
- [34] S. S. Shevkoplyas, A. C. Siegel, R. M. Westervelt, M. G. Prentiss, and G. M. Whitesides, "The force acting on a superparamagnetic bead due to an applied magnetic field," *Lab on a Chip*, vol. 7, pp. 1294-1302, 2007.
- [35] K. E. McCloskey, J. J. Chalmers, and M. Zborowski, "Magnetophoretic mobilities correlate to antibody binding capacities," *Cytometry*, vol. 40, pp. 307-315, 2000.
- [36] R. Wirix-Speetjens, W. Fyen, K. Xu, J. De Boeck, and G. Borghs, "A force study of on-chip magnetic particle transport based on tapered conductors," *IEEE Transactions on Magnetics*, vol. 41, pp. 4128-4133, 2005.

- [37] E. M. Purcell, "Life at low Reynolds number," *American Journal of Physics*, vol. 45, p. 11, 1977.
- [38] C. P. Price and D. J. Newman, *Principles and practice of immunoassay*. London: MacMillan Reference, 1997.
- [39] A. Bange, H. B. Halsall, and W. R. Heineman, "Microfluidic immunosensor systems," *Biosensors and Bioelectronics*, vol. 20, pp. 2488-2503, 2005.
- [40] E. P. Diamandis and T. K. Christopoulos, *Immunoassay*: Academic Pr, 1996.
- [41] J. R. Crowther, *ELISA: theory and practice*: Humana Press, 1995.
- [42] E. T. Maggio, *Enzyme-immunoassay*: Crc Press Boca Raton (Fla.), 1983.
- [43] J. M. Singer and C. M. Plotz, "The latex fixation test : I. Application to the serologic diagnosis of rheumatoid arthritis," *The American Journal of Medicine*, vol. 21, pp. 888-892, 1956.
- [44] G. F. Brooks, K. C. Carroll, J. S. Butel, and S. A. Morse, *Jawetz, Melnick & Adelberg's medical microbiology*: McGraw-Hill, 2007.
- [45] J. A. Molina-Bolivar and F. Galisteo-Gonzalez, "Latex immunoagglutination assays," *Journal of Macromolecular Science-Part C-Polymer Reviews*, vol. 45, p. 59, 2005.
- [46] BangsLabs, "Technote 301: Immunological applications, 1999," Bangs Labs Technotes, 1999.
- [47] A. Manz, N. Graber, and H. M. Widmer, "Miniaturized total chemical analysis systems: a novel concept for chemical sensing," *Sensors and actuators B: Chemical*, vol. 1, pp. 244-248, 1990.
- [48] T. M. Squires and S. R. Quake, "Microfluidics: Fluid physics at the nanoliter scale," *Reviews of Modern Physics*, vol. 77, p. 977, 2005.
- [49] D. J. Beebe, G. A. Mensing, and G. M. Walker, "Physics and applications of microfluidics in biology," *Annual Review of Biomedical Engineering*, vol. 4, pp. 261-286, 2002.
- [50] S. Haeberle and R. Zengerle, "Microfluidic platforms for lab-on-a-chip applications," *Lab on a Chip*, vol. 7, pp. 1094-1110, 2007.
- [51] G. M. Whitesides, "The origins and the future of microfluidics," *Nature*, vol. 442, p. 368, 2006.
- [52] P. A. Auroux, D. Iossifidis, D. R. Reyes, and A. Manz, "Micro total analysis systems. 2. Analytical standard operations and applications," *Analytical Chemistry*, vol. 74, pp. 2637-2652, 2002.

- [53] C. M. Ho and Y. C. Tai, "Micro-electro-mechanical-systems (MEMS) and fluid flows," *Annual Review of Fluid Mechanics*, vol. 30, pp. 579-612, 1998.
- [54] D. R. Reyes, D. Iossifidis, P. A. Auroux, and A. Manz, "Micro total analysis systems. 1. Introduction, theory, and technology," *Analytical Chemistry*, vol. 74, pp. 2623-2636, 2002.
- [55] B. H. Weigl, R. L. Bardell, and C. R. Cabrera, "Lab-on-a-chip for drug development," *Advanced Drug Delivery Reviews*, vol. 55, pp. 349-377, 2003.
- [56] J. P. Brody and P. Yager, "Diffusion-based extraction in a microfabricated device," *Sensors and Actuators, A: Physical*, vol. 58, pp. 13-18, 1997.
- [57] A. E. Kamholz, B. H. Weigl, B. A. Finlayson, and P. Yager, "Quantitative analysis of molecular interaction in a microfluidic channel: the T-sensor," *Analytical Chemistry*, vol. 71, pp. 5340-5347, 1999.
- [58] B. H. Weigl and P. Yager, "Microfluidics: microfluidic diffusion-based separation and detection," *Science*, vol. 283, p. 346, 1999.
- [59] A. Hatch, A. E. Kamholz, K. R. Hawkins, M. S. Munson, E. A. Schilling, B. H. Weigl, and P. Yager, "A rapid diffusion immunoassay in a T-sensor," *Nature Biotechnology*, vol. 19, pp. 461-465, 2001.
- [60] M. U. Kopp, A. J. Mello, nbsp, de, and A. Manz, "Chemical Amplification: Continuous-Flow PCR on a Chip," *Science*, vol. 280, pp. 1046-1048, May 15, 1998 1998.
- [61] A. T. Woolley, D. Hadley, P. Landre, R. A. Mathies, and M. A. Northrup, "Functional integration of PCR amplification and capillary electrophoresis in a microfabricated DNA analysis device," *Analytical Chemistry*, vol. 68, pp. 4081-4086, 1996.
- [62] D. J. Harrison, A. Manz, Z. Fan, H. Luedi, and H. M. Widmer, "Capillary electrophoresis and sample injection systems integrated on a planar glass chip," *Analytical chemistry*, vol. 64, pp. 1926-1932, 1992.
- [63] A. Manz, D. J. Harrison, E. M. J. Verpoorte, J. C. Fettingner, A. Paulus, H. Lüdi, and H. M. Widmer, "Planar chips technology for miniaturization and integration of separation techniques into monitoring systems: Capillary electrophoresis on a chip," *Journal of chromatography*, vol. 593, pp. 253-258, 1992.
- [64] K. Sato, M. Yamanaka, H. Takahashi, M. Tokeshi, H. Kimura, and T. Kitamori, "Microchip-based immunoassay system with branching multichannels for simultaneous determination of interferon," *Electrophoresis*, vol. 23, pp. 734-739, 2002.
- [65] E. Verpoorte, "Beads and chips: new recipes for analysis," *Lab on a Chip*, vol. 3, pp. 60N-68N, 2003.

- [66] C. T. Lim and Y. Zhang, "Bead-based microfluidic immunoassays: The next generation," *Biosensors and Bioelectronics*, vol. 22, pp. 1197-1204, 2007.
- [67] H. A. Stone, A. D. Stroock, and A. Ajdari, "Engineering flows in small devices," 2004.
- [68] F. Lacharme, C. Vandevyver, and M. A. M. Gijs, "Full on-chip nanoliter immunoassay by geometrical magnetic trapping of nanoparticle chains," *Analytical Chemistry*, vol. 80, pp. 2905-2910, 2008.
- [69] P. Y. Chiou, A. T. Ohta, and M. C. Wu, "Massively parallel manipulation of single cells and microparticles using optical images," *Nature*, vol. 436, pp. 370-372, 2005.
- [70] R. Tornay, T. Braschler, N. Demierre, B. Steitz, A. Finka, H. Hofmann, J. A. Hubbell, and P. Renaud, "Dielectrophoresis-based particle exchanger for the manipulation and surface functionalization of particles," *Lab on a Chip*, vol. 8, pp. 267-273, 2008.
- [71] T. Yasukawa, M. Suzuki, T. Sekiya, H. Shiku, and T. Matsue, "Flow sandwich-type immunoassay in microfluidic devices based on negative dielectrophoresis," *Biosensors and Bioelectronics*, vol. 22, pp. 2730-2736, 2007.
- [72] K. Svoboda and S. M. Block, "Biological applications of optical forces," *Annual review of biophysics and biomolecular structure*, vol. 23, pp. 247-285, 1994.
- [73] A. Ashkin, J. M. Dziedzic, and T. Yamane, "Optical trapping and manipulation of single cells using infrared laser beams," *Nature*, vol. 330, pp. 769-771, 1987.
- [74] E. Eriksson, J. Enger, B. Nordlander, N. Erjavec, K. Ramser, M. Goksör, S. Hohmann, T. Nyström, and D. Hanstorp, "A microfluidic system in combination with optical tweezers for analyzing rapid and reversible cytological alterations in single cells upon environmental changes," *Lab on a Chip*, vol. 7, pp. 71-76, 2007.
- [75] H. M. Hertz, "Standing-wave acoustic trap for nonintrusive positioning of microparticles," *Journal of Applied Physics*, vol. 78, pp. 4845-4849, 1995.
- [76] M. Wiklund and H. M. Hertz, "Ultrasonic enhancement of bead-based bioaffinity assays," *Lab on a Chip*, vol. 6, pp. 1279-1292, 2006.
- [77] R. W. Ellis and M. A. Sobanski, "Diagnostic particle agglutination using ultrasound: a new technology to rejuvenate old microbiological methods," *Journal of medical microbiology*, vol. 49, p. 853, 2000.
- [78] M. A. Grundy, W. E. Bolek, W. T. Coakley, and E. Benes, "Rapid agglutination testing in an ultrasonic standing wave," *Journal of immunological methods*, vol. 165, p. 47, 1993.
- [79] M. A. Grundy, K. Moore, and W. T. Coakley, "Increased sensitivity of diagnostic latex agglutination tests in an ultrasonic standing wave field," *Journal of immunological methods*, vol. 176, pp. 169-177, 1994.

- [80] T. Lilliehorn, M. Nilsson, U. Simu, S. Johansson, M. Almqvist, J. Nilsson, and T. Laurell, "Dynamic arraying of microbeads for bioassays in microfluidic channels," *Sensors & Actuators: B. Chemical*, vol. 106, pp. 851-858, 2005.
- [81] T. Lilliehorn, U. Simu, M. Nilsson, M. Almqvist, T. Stepinski, T. Laurell, J. Nilsson, and S. Johansson, "Trapping of microparticles in the near field of an ultrasonic transducer," *Ultrasonics*, vol. 43, pp. 293-303, 2005.
- [82] N. R. Harris, M. Hill, S. Beeby, Y. Shen, N. M. White, J. J. Hawkes, and W. T. Coakley, "A silicon microfluidic ultrasonic separator," *Sensors & Actuators: B. Chemical*, vol. 95, pp. 425-434, 2003.
- [83] M. Wiklund, S. Nilsson, and H. M. Hertz, "Ultrasonic trapping in capillaries for trace-amount biomedical analysis," *Journal of Applied Physics*, vol. 90, p. 421, 2001.
- [84] M. Wiklund, C. Günther, R. Lemor, M. Jäger, G. Fuhr, and H. M. Hertz, "Ultrasonic standing wave manipulation technology integrated into a dielectrophoretic chip," *Lab on a Chip*, vol. 6, pp. 1537-1544, 2006.
- [85] J. J. Hawkes and W. T. Coakley, "Force field particle filter, combining ultrasound standing waves and laminar flow," *Sensors & Actuators: B. Chemical*, vol. 75, pp. 213-222, 2001.
- [86] F. Petersson, A. Nilsson, C. Holm, H. Jönsson, and T. Laurell, "Continuous separation of lipid particles from erythrocytes by means of laminar flow and acoustic standing wave forces," *Lab on a Chip*, vol. 5, pp. 20-22, 2005.
- [87] M. Wiklund and H. M. Hertz, "Ultrasonic enhancement of bead-based bioaffinity assays," *Lab on a Chip*, vol. 6, pp. 1279-1292, 2006.
- [88] H. Andersson, W. van der Wijngaart, P. Enoksson, and G. Stemme, "Micromachined flow-through filter-chamber for chemical reactions on beads," *Sensors & Actuators: B. Chemical*, vol. 67, pp. 203-208, 2000.
- [89] R. D. Oleschuk, L. L. Shultz-Lockyear, Y. Ning, and D. J. Harrison, "Trapping of bead-based reagents within microfluidic systems: on-chip solid-phase extraction and electrochromatography," *Analytical Chemistry*, vol. 72, pp. 585-590, 2000.
- [90] H. Andersson, C. Jönsson, C. Moberg, and G. Stemme, "Self-assembled and self-sorted array of chemically active beads for analytical and biochemical screening," *Talanta*, vol. 56, pp. 301-308, 2002.
- [91] V. Sivagnanam, A. Sayah, C. Vandevyver, and M. A. M. Gijs, "Micropatterning of protein-functionalized magnetic beads on glass using electrostatic self-assembly," *Sensors & Actuators: B. Chemical*, vol. 132, pp. 361-367, 2008.

- [92] V. Sivagnanam, B. Song, C. Vandevyver, and M. A. M. Gijs, "On-Chip Immunoassay Using Electrostatic Assembly of Streptavidin-Coated Bead Micropatterns," *Analytical Chemistry*, vol. 81, pp. 6509-6515, 2009.
- [93] M. A. M. Gijs, F. d. r. Lacharme, and U. Lehmann, "Microfluidic Applications of Magnetic Particles for Biological Analysis and Catalysis," *Chemical Reviews*, 12/04/ 2009.
- [94] A. Rida, V. Fernandez, and M. A. M. Gijs, "Long-range transport of magnetic microbeads using simple planar coils placed in a uniform magnetostatic field," *Applied Physics Letters*, vol. 83, pp. 2396-2398, 2003.
- [95] S. Bronzeau and N. Pamme, "Simultaneous bioassays in a microfluidic channel on plugs of different magnetic particles," *Analytica Chimica Acta*, vol. 609, pp. 105-112, 2008.
- [96] M. A. Hayes, N. A. Polson, A. N. Phayre, and A. A. Garcia, "Flow-Based Microimmunoassay," *Analytical Chemistry*, vol. 73, pp. 5896-5902, 2001.
- [97] M. Slovakova, N. Minc, Z. Bilkova, C. Smadja, W. Faigle, C. Fütterer, M. Taverna, and J. L. Viovy, "Use of self assembled magnetic beads for on-chip protein digestion," *Lab on a Chip*, vol. 5, pp. 935-942, 2005.
- [98] A. L. Nel, N. Minc, C. Smadja, M. Slovakova, Z. Bilkova, J. M. Peyrin, J. L. Viovy, and M. Taverna, "Controlled proteolysis of normal and pathological prion protein in a microfluidic chip," *Lab on a Chip*, vol. 8, pp. 294-301, 2008.
- [99] N. Pamme and A. Manz, "On-chip free-flow magnetophoresis: continuous flow separation of magnetic particles and agglomerates," *Analytical Chemistry*, vol. 76, pp. 7250-7256, 2004.
- [100] S. A. Peyman, A. Iles, and N. Pamme, "Rapid on-chip multi-step (bio)chemical procedures in continuous flow - Manoeuvring particles through co-laminar reagent streams," *Chemical Communications*, pp. 1220-1222, 2008.
- [101] S. A. Peyman, A. Iles, and N. Pamme, "Mobile magnetic particles as solid-supports for rapid surface-based bioanalysis in continuous flow," *Lab on a Chip*, vol. 9, pp. 3110-3117, 2009.
- [102] L. A. Sasso and J. D. Zahn, "Continuous microfluidic biosensing with conjugated paramagnetic beads," in *ASME International Mechanical Engineering Congress and Exposition, Proceedings*, 2009, pp. 941-944.
- [103] M. Herrmann, E. Roy, T. Veres, and M. Tabrizian, "Microfluidic ELISA on non-passivated PDMS chip using magnetic bead transfer inside dual networks of channels," *Lab on a Chip*, vol. 7, pp. 1546-1552, 2007.

- [104] J. Do and C. H. Ahn, "A polymer lab-on-a-chip for magnetic immunoassay with on-chip sampling and detection capabilities," *Lab on a Chip*, vol. 8, pp. 542-549, 2008.
- [105] A. Rida and M. A. M. Gijs, "Manipulation of Self-Assembled Structures of Magnetic Beads for Microfluidic Mixing and Assaying," *Applied Physics Letters*, vol. 76, pp. 6239-6246, 2004.
- [106] A. Rida and M. A. M. Gijs, "Dynamics of magnetically retained supraparticle structures in a liquid flow," *Applied Physics Letters*, vol. 85, pp. 4986-4988, 2004.
- [107] K. Smistrup, B. G. Kjeldsen, J. L. Reimers, M. Dufva, J. Petersen, and M. F. Hansen, "On-chip magnetic bead microarray using hydrodynamic focusing in a passive magnetic separator," *Lab on a Chip*, vol. 5, pp. 1315-1319, 2005.
- [108] T. Deng, G. M. Whitesides, M. Radhakrishnan, G. Zabow, and M. Prentiss, "Manipulation of magnetic microbeads in suspension using micromagnetic systems fabricated with soft lithography," *Applied Physics Letters*, vol. 78, p. 1775, 2001.
- [109] C. S. Lee, H. Lee, and R. M. Westervelt, "Microelectromagnets for the control of magnetic nanoparticles," *Applied Physics Letters*, vol. 79, p. 3308, 2001.
- [110] U. Lehmann, S. Hadjidj, V. K. Parashar, C. Vandevyver, A. Rida, and M. A. M. Gijs, "Two-dimensional magnetic manipulation of microdroplets on a chip as a platform for bioanalytical applications," *Sensors & Actuators: B. Chemical*, vol. 117, pp. 457-463, 2006.
- [111] U. Lehmann, C. Vandevyver, V. K. Parashar, and M. A. Gijs, "Droplet-based DNA purification in a magnetic lab-on-a-chip," *Angewandte Chemie* vol. 45, p. 3062, 2006.
- [112] U. Lehmann, S. Hadjidj, V. K. Parashar, C. Vandevyver, A. Rida, and M. A. M. Gijs, "Two-dimensional magnetic manipulation of microdroplets on a chip as a platform for bioanalytical applications," *Sensors and Actuators B: Chemical*, vol. 117, pp. 457-463, 2006.
- [113] T. G. Kang, M. A. Hulsen, P. D. Anderson, J. M. J. den Toonder, and H. E. H. Meijer, "Chaotic mixing induced by a magnetic chain in a rotating magnetic field," *Physical Review E*, vol. 76, p. 66303, 2007.
- [114] I. Petousis, E. Homburg, R. Derks, and A. Dietzel, "Transient behaviour of magnetic micro-bead chains rotating in a fluid by external fields," *Lab on a Chip* vol. 7, pp. 1746-1751, 2007.
- [115] S. L. Biswal and A. P. Gast, "Micromixing with linked chains of paramagnetic particles," *Analytical Chemistry*, vol. 76, pp. 6448-6455, 2004.
- [116] R. J. S. Derks, A. J. H. Frijns, M. W. J. Prins, and A. H. Dietzel, "Self-organized twinning of actuated particles for microfluidic pumping," *Applied Physics Letters*, vol. 92, p. 024104, 2008.

- [117] R. J. S. Derks, A. Dietzel, R. Wimberger-Friedl, and M. W. J. Prins, "Magnetic bead manipulation in a sub-microliter fluid volume applicable for biosensing," *Microfluidics and Nanofluidics*, vol. 3, pp. 141-149, 2007.
- [118] V. Sivagnanam, A. Bouhmad, F. Lacharme, C. Vandevyver, and M. A. M. Gijs, "Sandwich immunoassay on a microfluidic chip using patterns of electrostatically self-assembled streptavidin-coated beads," *Microelectronic Engineering*, vol. 86, pp. 1404-1406, 2009.
- [119] F. Lacharme, C. Vandevyver, and M. A. M. Gijs, "Magnetic beads retention device for sandwich immunoassay: comparison of off-chip and on-chip antibody incubation," *Microfluidics and Nanofluidics*, pp. 1-9, 2009.
- [120] J. W. Choi, C. H. Ahn, S. Bhansali, and H. T. Henderson, "A new magnetic bead-based, filterless bio-separator with planar electromagnet surfaces for integrated bio-detection systems," *Sensors & Actuators: B. Chemical*, vol. 68, pp. 34-39, 2000.
- [121] K. S. Kim and J. K. Park, "Magnetic force-based multiplexed immunoassay using superparamagnetic nanoparticles in microfluidic channel," *Lab on a Chip*, vol. 5, pp. 657-664, 2005.
- [122] J. W. Choi, K. W. Oh, J. H. Thomas, W. R. Heineman, and H. Brian, "An integrated microfluidic biochemical detection system for protein analysis with magnetic bead-based sampling capabilities," *Lab on a Chip*, vol. 2, pp. 27-30, 2002.
- [123] M. Herrmann, T. Veres, and M. Tabrizian, "Enzymatically-generated fluorescent detection in micro-channels with internal magnetic mixing for the development of parallel microfluidic ELISA," *Lab on a Chip*, vol. 6, pp. 555-560, 2006.
- [124] F. Patolsky, A. Lichtenstein, and I. Willner, "Electrochemical Transduction of Liposome-Amplified DNA Sensing," *Angewandte Chemie* vol. 39, pp. 940-943, 2000.
- [125] F. Patolsky, K. T. Ranjit, A. Lichtenstein, and I. Willner, "Dendritic amplification of DNA analysis by oligonucleotide-functionalized Au-nanoparticles," *Chemical Communications*, vol. 2000, pp. 1025-1026, 2000.
- [126] F. Lucarelli, G. Marrazza, and M. Mascini, "Dendritic-like streptavidin/alkaline phosphatase nanoarchitectures for amplified electrochemical sensing of DNA sequences," *Langmuir*, vol. 22, pp. 4305-4309, 2006.
- [127] R. Bakalova, Z. Zhelev, H. Ohba, and Y. Baba, "Quantum Dot-Based Western Blot Technology for Ultrasensitive Detection of Tracer Proteins," *Journal of the American Chemical Society*, vol. 127, pp. 9328-9329, 2005.

- [128] R. Pei, Z. Cheng, E. Wang, and X. Yang, "Amplification of antigen-antibody interactions based on biotin labeled protein-streptavidin network complex using impedance spectroscopy," *Biosensors and Bioelectronics*, vol. 16, pp. 355-361, 2001.
- [129] H. Chen, J. H. Jiang, Y. Huang, T. Deng, J. S. Li, G. L. Shen, and R. Q. Yu, "An electrochemical impedance immunosensor with signal amplification based on Au-colloid labeled antibody complex," *Sensors & Actuators: B. Chemical*, vol. 117, pp. 211-218, 2006.
- [130] K. Hosokawa, M. Omata, and M. Maeda, "Immunoassay on a power-free microchip with laminar flow-assisted dendritic amplification," *Analytical Chemistry*, vol. 79, pp. 6000-6004, 2007.
- [131] K. Hosokawa, K. Sato, N. Ichikawa, and M. Maeda, "Power-free poly (dimethylsiloxane) microfluidic devices for gold nanoparticle-based DNA analysis," *Lab on a chip*, vol. 4, pp. 181-185, 2004.
- [132] G. Degre, E. Brunet, A. Dodge, and P. Tabeling, "Improving agglutination tests by working in microfluidic channels," *Lab on a Chip*, vol. 5, pp. 691-694, 2005.
- [133] Y. Moser, T. Lehnert, and M. A. M. Gijs, "Quadrupolar magnetic actuation of superparamagnetic particles for enhanced microfluidic perfusion," *Applied Physics Letters*, vol. 94, p. 022505, 2009.
- [134] Y. Moser, T. Lehnert, and M. A. M. Gijs, "On-chip immuno-agglutination assay with analyte capture by dynamic manipulation of superparamagnetic beads."
- [135] R. Afshar, Y. Moser, T. Lehnert, and M. A. M. Gijs, "Magnetic particle dosing and size separation in a microfluidic channel," *Sensors & Actuators: B. Chemical*, 2009.
- [136] "<http://www.vacuumschmelze.de/index.php?id=55&L=2>," 2010.
- [137] Y. Moser, T. Lehnert, and M. A. M. Gijs, "On-chip immuno-agglutination assay with analyte capture by dynamic manipulation of superparamagnetic beads," *Lab On a Chip*, vol. 9, pp. 3261 - 3267, 2009.
- [138] P. Abgrall, V. Conedera, H. Camon, A. M. Gue, and N. T. Nguyen, "SU-8 as a structural material for labs-on-chips and microelectromechanical systems," *Electrophoresis*, vol. 28, pp. 4539-4551, 2007.
- [139] B. H. Jo, L. M. Van Lerberghe, K. M. Motsegood, and D. J. Beebe, "Three-dimensional micro-channel fabrication in polydimethylsiloxane (PDMS) elastomer," *Microelectromechanical Systems, Journal of*, vol. 9, pp. 76-81, 2000.
- [140] L. Dellmann, S. Roth, C. Beuret, G. A. Racine, H. Lorenz, M. Despont, P. Renaud, P. Vettiger, and N. F. De Rooij, "Fabrication process of high aspect ratio elastic and SU-8

- structures for piezoelectric motor applications," *Sensors & Actuators: A. Physical*, vol. 70, pp. 42-47, 1998.
- [141] J. Liu, B. Cai, J. Zhu, D. Chen, Y. Li, J. Zhang, G. Ding, X. Zhao, and C. Yang, "A novel device of passive and fixed alignment of optical fiber," *Microsystem Technologies*, vol. 10, pp. 269-271, 2004.
 - [142] M. Agirregabiria, F. J. Blanco, J. Berganzo, M. T. Arroyo, A. Fullaondo, K. Mayora, and J. M. Ruano-Lopez, "Fabrication of SU-8 multilayer microstructures based on successive CMOS compatible adhesive bonding and releasing steps," *Lab on a Chip*, vol. 5, pp. 545-552, 2005.
 - [143] J. Steigert, O. Brett, C. Muller, M. Strasser, N. Wangler, H. Reinecke, M. Daub, and R. Zengerle, "A versatile and flexible low-temperature full-wafer bonding process of monolithic 3D microfluidic structures in SU-8," *Journal of Microelectromechanical Systems*, vol. 18, p. 095013, 2008.
 - [144] M. O. Heuschkel, L. Guerin, B. Buisson, D. Bertrand, and P. Renaud, "Buried microchannels in photopolymer for delivering of solutions to neurons in a network," *Sensors & Actuators: B. Chemical*, vol. 48, pp. 356-361, 1998.
 - [145] P. Abgrall, C. Lattes, V. Conedera, X. Dollat, S. Colin, and A. M. Gue, "A novel fabrication method of flexible and monolithic 3D microfluidic structures using lamination of SU-8 films," *Journal of Micromechanics and Microengineering*, vol. 16, pp. 113-121, 2006.
 - [146] P. Mali, A. Sarkar, and R. Lal, "Facile fabrication of microfluidic systems using electron beam lithography," *Lab on a Chip*, vol. 6, pp. 310-315, 2006.
 - [147] H. Yu, O. Balogun, B. Li, T. W. Murray, and X. Zhang, "Building embedded microchannels using a single layered SU-8, and determining Young's modulus using a laser acoustic," *Journal of Microelectromechanical Systems*, vol. 14, pp. 1576-1584, 2004.
 - [148] F. Ceysens and R. Puers, "Creating multi-layered structures with freestanding parts in SU-8," *Journal of Micromechanics and Microengineering*, vol. 16, pp. S19-S23, 2006.
 - [149] Y. J. Chuang, F. G. Tseng, J. H. Cheng, and W. K. Lin, "A novel fabrication method of embedded micro-channels by using SU-8 thick-film photoresists," *Sensors & Actuators: A. Physical*, vol. 103, pp. 64-69, 2003.
 - [150] I. G. Foulds and M. Parameswaran, "A planar self-sacrificial multilayer SU-8-based MEMS process utilizing a UV-blocking layer for the creation of freely moving parts," *Journal of Micromechanics and Microengineering*, vol. 16, pp. 2109-2115, 2006.

- [151] G. M. Whitesides, R. J. Kazlauskas, and L. Josephson, "Magnetic separations in biotechnology," *Trends in Biotechnology*, vol. 1, pp. 144-148, 1983.
- [152] O. Olsvik, T. Popovic, E. Skjerve, K. S. Cudjoe, E. Hornes, J. Ugelstad, and M. Uhlen, "Magnetic separation techniques in diagnostic microbiology," *Clinical microbiology reviews*, vol. 7, pp. 43-54, 1994.
- [153] V. I. Furdul and D. J. Harrison, "Immunomagnetic T cell capture from blood for PCR analysis using microfluidic systems," *Lab on a Chip*, vol. 4, pp. 614-618, 2004.
- [154] K. Smistrup, O. Hansen, H. Bruus, and M. F. Hansen, "Magnetic separation in microfluidic systems using microfabricated electromagnets--experiments and simulations," *Journal of Magnetism and Magnetic Materials*, vol. 293, pp. 597-604, 2005.
- [155] G. Fonnum, C. Johansson, A. Molteberg, S. Mrrup, and E. Aksnes, "Characterisation of Dynabeads® by magnetization measurements and Mössbauer spectroscopy," *Journal of Magnetism and Magnetic Materials*, vol. 293, pp. 41-47, 2005.
- [156] C. Mikkelsen and H. Bruus, "Fluid Dynamics Title: Microfluidic capturing-dynamics of paramagnetic bead suspensions," *Lab on a Chip*, vol. 5, pp. 1293-1297, 2005.
- [157] C. Mikkelsen, M. Fougth Hansen, and H. Bruus, "Theoretical comparison of magnetic and hydrodynamic interactions between magnetically tagged particles in microfluidic systems," *Journal of Magnetism and Magnetic Materials*, vol. 293, pp. 578-583, 2005.
- [158] V. Schaller, U. Kräling, C. Rusu, K. Petersson, J. Wipenmyr, A. Krozer, G. Wahnström, A. Sanz-Velasco, P. Enoksson, and C. Johansson, "Motion of nanometer sized magnetic particles in a magnetic field gradient," *Journal of Applied Physics*, vol. 104, p. 093918, 2008.
- [159] K. Zahn, R. Lenke, and G. Maret, "Friction coefficient of rod-like chains of spheres at very low Reynolds numbers. I. Experiment," *Journal de Physique II France*, vol. 4, pp. 555-560, 1994.
- [160] A. Meunier, "Friction coefficient of rod-like chains of spheres at very low Reynolds numbers. II. Numerical simulations," *Journal de Physique II France*, vol. 4, p. 561-566, 1994.
- [161] J. Happel and H. Brenner, *Low Reynolds Number Hydrodynamics*. Englewood Cliffs, NJ: Prentice-Hall, 1965.
- [162] J. M. Burgers, *Proc. Koninkl. Akad. Wetenschap. (Amsterdam)*, vol. 43, pp. 425, 646, 1940.
- [163] J. M. Burgers, "Geometrical considerations concerning the structural irregularities to be assumed in a crystal," *Proceedings of the Physical Society*, vol. 52, pp. 23-33, 1940.
- [164] E. L. Cussler, *Diffusion: Mass transfer in fluid systems*. Cambridge Univ Pr, 1997.

- [165] D. Lacoste, C. Brangbour, J. Bibette, and J. Baudry, "Thermal expansion within a chain of magnetic colloidal particles," *Physical Review E*, vol. 80, p. 011401, 2009.
- [166] "www.detectiv.eu," 2010.
- [167] G. S. Zhuang, T. G. Jensen, and J. P. Kutter, "Three-dimensional hydrodynamic focusing over a wide reynolds number range using a two-layer microfluidic design," in *Proceed. of the 12th International Conference on Miniaturized Systems for Chemistry and Life Sciences, μ TAS 2008 Conference*, San Diego.

Curriculum vitae

Yves Moser

Nationality: Swiss
06.09.1982
Champ-Rond 19, 1010 Lausanne
Mobile: +41 76 438 18 80
E-mail yves.moser@gmail.com



EDUCATION

2006 - Present	PhD in Microsystems and Microelectronics, EPFL
2001 - 2006	M.Sc. degree in Microengineering (Master MT, grade: 5.61/6), Micro/Nano- systems, EPFL, Lausanne

PRATICAL EXPERIENCE

2006 - Present	PhD projects: 1. Development of an on-chip immunoassay with analyte capture by dynamic manipulation of magnetic microbeads (in the frame of the DetectHIV European project: www.detecthiv.eu). 2. Design and fabrication of a miniaturized flexible temperature sensor for a biomedical application. Both projects resulted in working prototypes
2007 - Present	IT Management (40 computers), LMIS2, EPFL
2005 - 2006	Master Project: Patch-clamp microsystem: Electrophysiological characterization of cells on-chip

SPECIFIC SKILLS

Management	Central role in the frame of the DetectHIV European project (collaboration with 3 industrial partners and 3 academic institutions), IT Management. Supervision of master student projects
Microfabrication	Expert in microsystems design and fabrication: Photolithography, SU-8 and polyimide processing, dry and wet etching, metal deposition and patterning, Scanning Electron Microscopy (SEM), microfluidic devices fabrication
Magnetism	Specific knowledge in magnetism applied to superparamagnetic beads
Computer	Windows, Comsol multiphysics, Labview, Clewin, Solidworks, Pro Engineer, Visual C++, Word, Excel, Power Point, Photoshop, Illustrator, Origin, ImageJ, IT management, PC hardware
Programming Languages	Assembler, C, C++ French (mother tongue), English (Fluent, used most often at work), German (high school level)

PEER-REVIEWED PAPERS

- [1] Y. Moser, T. Lehnert, and M.A.M. Gijs. On-chip immuno-agglutination assay with analyte capture by dynamic manipulation of superparamagnetic beads. *Lab on a Chip*, 2009, 9, 3261 – 3267
- [2] Y. Moser, T. Lehnert, and M.A.M. Gijs. Quadrupolar magnetic actuation of superparamagnetic beads for enhanced microfluidic perfusion. *Applied Physics Letters*, 2009, 94, 022505
- [3] Y. Moser and M.A.M. Gijs. Miniaturised flexible temperature sensor. *Journal of Microelectromechanical Systems*, 2007, 16, 1349-1354
- [4] R. Afshar, Y. Moser, T. Lehnert, and M.A.M. Gijs. Magnetic bead dosing and size separation in a microfluidic channel. *Sensors and Actuators B: Chemical*, 2009, (in press)
- [5] Y. Moser, R. Forti, S. Jiguet, T. Lehnert and M.A.M. Gijs. Suspended SU-8 structures for monolithic microfluidic channels, *Microfluidics and nanofluidics* (submitted)
- [6] R. Afshar, Y. Moser, T. Lehnert, and M.A.M. Gijs. Three-dimensional hydro-magnetic focusing and in-flow separation of superparamagnetic beads, *Lab on a Chip* (submitted)

CONFERENCES

- [1] Y. Moser, T. Lehnert, and M.A.M. Gijs. A quadrupolar magnetic actuation system for superparamagnetic beads. *Proceedings Transducers 2009*, Denver, 1226 – 1229
- [2] R. Afshar, T. Lehnert, Y. Moser, and M.A.M. Gijs. Magnetic bead dosing, release and separation in a microfluidic chip with magnetic actuation. *Proceedings Transducers 2009*, Denver, 1238 – 1241
- [3] Y. Moser, T. Lehnert, E. Dupont, R. Afshar, and M.A.M. Gijs. Active superparamagnetic bead manipulation for immunoassays on-chip *Proceedings μ TAS 2008*, San Diego, 1372-1374
- [4] Y. Moser, T. Lehnert, R. Afshar, G. Sinicco, and M.A.M. Gijs. Active superparamagnetic bead manipulation on-chip. *Proceed. 7th International Conference on Scientific and Clinical Applications of Magnetic Carriers*, 2008, 226
- [5] R. Afshar, Y. Moser, T. Lehnert, and M.A.M. Gijs. Microfluidic chip for the separation of magnetic beads. *Digest Nanotech 2007*, Montreux
- [6] Y. Moser and M.A.M. Gijs. Miniaturized Flexible Temperature Sensor. *Proceedings Transducers '07 and Eurosensors XXI*, Lyon, France, 2007, volume 2, 2279-2282
- [7] T. Lehnert, D. Nguyen, Y. Moser, and M.A.M. Gijs. Cell sealing on glass-coated micro- and nano-apertures. *Proceedings Eurosensors XX*, 2006